Thermo-mechanical analysis of fluids using microfluidic cantilever in dynamic resonance mode

by

Rosmi Abraham

A thesis submitted in partial fulfillment of the requirements for the degree of

Doctor of Philosophy
in
Materials engineering

Department of Chemical and Materials Engineering

University of Alberta

Abstract

This thesis investigates the thermo-mechanical behavior of picograms of fluids using a suspended microchannel resonator called microfluidic cantilever operating in dynamic mode by exploring the interfacial effects of liquids on the resonance frequency. Microfluidic cantilever is a promising candidate in micro electromechanical systems (MEMS) which can provide high degree of accuracy in mass sensing, stress sensing, thermo-mechanical sensing of rare fluid samples. While characterizing fluid samples, the existing analytical model based on Euler-Bernoulli beam equation to calculate the frequency of the microfluidic cantilever does not consider the effects of surface tension and interfacial tension provided by the liquid inside the microfluidic cantilever. Hence, there exists a discrepancy between the experimental values and conventional model values. For a microfluidic cantilever with curvature, the surface stress and interfacial stress provided by the liquid inside the channel can effectively change the stiffness of the cantilever and can alter the frequency of the cantilever. An analytical model based on modified Euler Bernoulli beam equation that incorporates Young-Laplace equation to consider the effects of surface stress and the interfacial tension of fluids was proposed in this thesis. This modified model was validated by comparing the experimental values of frequencies obtained for the microfluidic cantilever filled with different alkanes with the analytical values obtained from the conventional model and the proposed modified model.

The proposed analytical model was used to measure the thermal properties of liquids quantitatively using a microfluidic cantilever irradiated with a diode laser. The thermal stress generated by the

volumetric expansion of the liquids upon photothermal heating influenced the stiffness of the cantilever and altered the resonance frequency of the microfluidic cantilever. This effect of thermal stress on the resonance frequency for different liquids was studied using the modified Euler Bernoulli beam equation. In addition to that, thermal time constant of the system was observed and the relation with the density and the heat capacity of the liquids was established. To overcome the shortcomings in using a bi-material cantilever, for the thermal characterization of liquids, such as fabrication of complicated structures and the drift in the static mode, we used a silicon nitride microfluidic cantilever filled with liquids operating in dynamic mode and analyzed the shift in the resonance frequency upon laser heating to measure the thermal properties of liquids.

As an application of the measurement of thermal properties of liquids using microfluidic cantilever, an investigation was carried out to understand the mechanical property evolution of a thermo-sensitive polymer Poly N-isopropylacrylamide (PNIPAM) as a function of temperature.
A microfluidic cantilever was used with an external heater attached to it and was operated in dynamic mode to overcome the challenges of drift and mechanical losses. Here, the thermo-mechanical property changes of PNIPAM at lower critical solution temperature (LCST) were studied by analyzing the dynamic mechanical outputs of the cantilever such as shift in frequency and quality factor. As the temperature was varied, there was conformational change for the PNIPAM aqueous solution filled inside the cantilever at LCST along with the mechanical property changes. The modulus changes of the PNIPAM at LCST altered the stiffness of the cantilever and resulted in the shift of the frequency.

Furthermore, a solution with optimum concentration of Kaolinite and PNIPAM was taken through the same thermal cycle inside the microfluidic cantilever and the coil to globule transition of PNIPAM adsorbed on Kaolinite at LCST resulted in the sedimentation of Kaolinite on the walls of the cantilever. This in turn, increased the stiffness of the cantilever changing the resonance frequency of the cantilever. The flocculation performance of the PNIPAM and Kaolinite in the microfluidic channel was compared with the macro scale flocculation experiments.

This study which uses the mechanical response of the cantilever to characterize the thermo-mechanical properties of fluids by incorporating the interfacial effects can be used to improve the precision of sensing of the portable, high thorough put devices for the in situ real-time detections of various biomolecular and chemical interactions in rare samples.

Preface

Chapter 4 of this thesis has been published as "Rosmi Abraham, Faheem Khan, Syed A. Bukhari, Qingxia Liu, Thomas Thundat, Hyun-Joong Chung, and Chun Il Kim. 2020. Effect of Surface and Interfacial Tension on the Resonance Frequency of Microfluidic Channel Cantilever, Sensors 20, 6459". Rosmi Abraham designed the experiment, developed the analytical model for the frequency calculation, performed the experiments on SEM, frequency measurements of microfluidic cantilevers with laser doppler vibrometer (LDV) and wrote the paper. Faheem Khan helped with the fabrication of devices in Nanofab, Syed A. Bhukhari helped with writing the paper. Qingxia Liu and Thomas Thundat helped in revising the papers. Hyun-Joong Chung, and Chun Il Kim helped with writing and revising the paper.

Chapter 5 of the thesis has been published as "Rosmi Abraham, Yeowon Yoon, Faheem Khan, Syed A. Bukhari, Chun-il Kim, Thomas Thundat, Hyun-Joong Chung, and Jungchul Lee. 2022. Measurement of Thermal Properties of Liquid Analytes Using Microfluidic Resonators Via Photothermal Modulation, Sensors and Actuators A: Physical 347, 113994". Rosmi Abraham and Yeowon Yoon have equal contribution in this paper. Rosmi Abraham developed the analytical model, wrote, and revised the paper. Yeowon Yoon conducted the experiments with LDV, and Faheem Khan provided the devices fabricated at Nanofab. Syed A. Bhukhari helped with revising the paper. Chun-il Kim and Thomas Thundat helped in revising the paper. Hyun-Joong Chung helped in writing and revised the paper. Jungchul Lee revised the paper and is the supervisor of Yeowon Yoon.

Chapter 6 of the thesis will be submitted for publication as "Rosmi Abraham, David Liu, Daniel Dixon, Kevin Peng, Syed A. Bhukhari, Faheem Khan, Thomas Thundat and Hyun-Joong Chung. Thermomechanical characterization of phase change of PNIPAM at LCST and flocculation of Kaolinite and PNIPAM using microfluidic cantilever." Rosmi Abraham designed the experimental set up, conducted the experiments, analyzed the data and wrote the paper. David Liu helped in conducting the experiments and analyzing the data. Further, Daniel Dixon from Joao Soares's group and Kevin Peng from Ravi Narain's group at University of Alberta helped with preparation

Acknowledgements

This thesis is certainly the reflection of years of hard work and is an important accomplishment in my life made with the support of an amazing team. I thank for the support I received from several people, including family, friends, mentors, and colleagues.

First, I am indebted to my excellent supervisor, Dr. Hyun-Joong Chung for awakening the researcher in me through his guidance and training me to become an independent researcher. My discussions with him always encouraged me to push my boundaries and strive for more and think out of the box. His passion about science and creativity boosted my confidence in many folds. He was so helpful and caring during all the stressful times and his cooperation was just amazing. His caring nature and willingness to help gave me a lot of positive energy during my degree.

I would like to extend my thanks to my supervisory committee member Dr. Thomas Thundat for his valuable insights and support throughout my studies. He is not only the committee member, but also my mentor who always finds time for scientific discussions with me. Dr. Thundat taught me to observe the amazing science in nature and helped me to develop the habit of asking the right questions. I could never thank him enough for all the guidance and support provided for me through my studies. I express my sincere gratitude to Dr. Chun-il Kim for helping me to understand the theoretical part of the project, which became the backbone of the thesis and encouraged me to solve the problems in the project.

I would like to express my sincere thanks to my senior Dr. Syed A. Bhukari for helping me with the science and technical things and motivating me all the time whenever I was down. I couldn't have completed any of the experiments without the help from Dr. Faheem Khan who trained me to fabricate micro-cantilevers and provided me with the devices for all the projects and helped whenever I needed a hand on the technical side. I would like to remember Dr. Ankur Goswami who helped me in the initial days of my studies to get an idea about the method of research and made me realize how collaboration is helpful in research.

Table of Contents

List of Tables

List of figures

Chapter 1

Introduction

1.1 Introduction

A microcantilever is a one-end fixed beam vibrating at its resonance frequency. Microcantilever sensors are the most versatile candidates in MEMS which is a rapidly growing field because of its potential applications in major fields of the global economy, such as healthcare [1], energy [2], and agriculture [3], national security [4], forensics [5], environment monitoring [6] as miniaturized analytical tools and human health care applications. In all these applications, detection, speciation, and quantification of extremely small concentrations of analytes is vital. The demand for small, fast, and reliable products in society accelerates the growth of nanotechnology tremendously.

Micro cantilevers were first introduced as displacement detection probes in atomic force microscopy (AFM) for obtaining surface topographies [7]. At a later stage, they were considered as suitable sensors for detecting the changes in temperature and relative humidity [8]. These microcantilevers are displacement sensors which reacts to surface energy changes that happens because of chemical or biomolecular interactions. When the adsorption of the molecules is restricted on one side of the cantilever surface, it results in a surface stress that can be identified as a deflection. In addition to bending, the dynamic mechanical resonance frequency of the cantilever can be subjected to variations due to molecular adsorption-induced mass loading. These two outputs, cantilever bending and resonance frequency variation, can be monitored simultaneously using a variety of detection techniques [9].

Suspended beams have been used for atto-gram level mass sensing in vacuum where the mechanism of sensing was change in frequency of resonator with adhesion of a mass on the surface of the resonating device [10]. These resonators however damped heavily when immersed into a liquid environment because of viscous force. Scott Manalis group in MIT introduced an idea in 2003 when they developed a cantilever with a microchannel embedded into it [11]. They were able to characterize different liquids without reducing the quality factor of the resonator as the liquid

was inside the channel and resonator itself could vibrate in vacuum. Using this sensor, they detected a molecule in a sub nanoliter fluid volume using shifts in resonance frequency of a suspended microfluidic channel upon accumulation of molecules on the inside walls of the device. This work motivated researchers to investigate more into this technology specifically for thermomechanical characterisation of fluids.

The frequency of the cantilever is obtained analytically using the fundamental Euler Bernoulli beam equation. The conventional model considers the geometric factors, bending stiffness and the mass density of the cantilever to calculate the frequency. However, the effect from the environmental factors such as surface stress and interfacial stress provided by liquids was not accommodated in the beam equation of microfluidic cantilever which carries liquid in it. Hence there were discrepancies between the experimental values and theoretical values of the frequency of microchannel cantilevers. This discrepancy was addressed in this thesis by considering the effects of surface stress and interfacial tension of the fluid on the resonance frequency by modifying the existing Euler Bernoulli beam equation. Inspired from the study of surface stress effect on bending resonance on nanowires by He et al., the Young-Laplace equation was introduced in the Euler Bernoulli beam equation for microfluidic cantilevers with curvature in this work [12]. The modified model was validated by comparing the calculated frequencies to the experimental values obtained for different alkane filled cantilevers.

Using the proposed analytical model, a quantitative measurement of thermal properties of liquids using microfluidic cantilevers by photothermal modulation was conducted. As the temperature rises, the liquid inside the cantilever expands and creates a thermal stress on the walls of the cantilever. An analytical study was done by calculating the thermal stress which acts as surface stress on the cantilever and by obtaining the resultant frequency shift of the resonator. The analytical results were then compared to the experimental results and validated the effects of thermal stress on the resonance frequency of the cantilever.

The measurement of thermomechanical changes of the temperature responsive polymer PNIPAM was an application of the above-mentioned work. When PNIPAM phase changes at LCST, the modulus of the PNIPAM solution changes as well [13]. This affected the overall stiffness change

of the microfluidic cantilever and resulted in noticeable shift in frequency and quality factor. Furthermore, an in-situ flocculation was carried out inside the microfluidic cantilever using an optimum solution of Kaolinite and PNIPAM and the mechanical property changes of the solution during flocculation was reflected as frequency shift and quality factor variation.

1.2 Literature and background

Microcantilevers rely on their flexibility or elasticity to create some type of measurable change when exposed to external stimuli. The cantilever's reaction to an external stimulus can be referred to as mechanical stress. This stress results in a change in one of the cantilever's mechanical properties such as bending stiffness or dynamic resonance. The ability to detect the displacement of a cantilever beam with nanometer precision makes the cantilever ideal for measuring bending or frequency fluctuation. With the advantages of cantilevers such as the minuscule mass of the device and capability to attain high-quality factors, they are extremely sensitive to adsorbed mass [14], surface stress [15], resistance [16], and temperature [17] and offer potential platforms for label-free detection of trace quantities of mass for quantitative measurements [15].

Despite having many advantages, these sensors suffer from poor sensitivity and selectivity while immersed in liquid due to viscous forces thus limiting the real-time applications. Real-time applications demand more stringent conditions such as extremely high sensitivity in the case of volatile explosive detection, detection of a specific analyte in a mixture, in the presence of a liquid environment, repeatability, high dynamic range, and high measurement throughput, regeneration of surface and stability. MEMS devices with embedded microfluidic channels have gained enormous attention from researchers because of their capability to characterize liquids with extremely small amount in pico- litre volumes. Analyzing small volumes made this technology potentially very useful to understand the biological systems. The platform of suspended microchannel resonators (SMR) enabled the liquid characterization with high quality factor and low damping. These resonators were used to measure the temperature dependent density and volume contractions of ethanol-water binary mixtures for picolitre volume samples at different temperatures [18].

In quantitative studies using a microcantilever/microfluidic cantilever, the effect of surface stress on the bending resonance of the cantilever is very well discussed. There are studies that explains the effect of surface stress in the shift of frequency during an adsorption of analyte on the cantilever [19] While certain researchers state that a change in surface elasticity is the reason for variation in frequency [20] The combined effect of surface elasticity and surface stress in changing the resonance frequency was also investigated [21] and verified with experimental evidence. The conventional Euler Bernoulli beam equation for calculating the frequency of the resonators can be modified by the inclusion of surface stress and surface elasticity terms in case of microfluidic cantilevers filled with liquid with the help of Young-Laplace equation for structures with curvature [22]. This can improve the precision in calculating the frequency of the resonators while characterising the fluid samples.

The ability to measure the thermal properties of liquids using microfluidic cantilevers can be extended to characterise the phase change of picograms of polymers as a function of temperature [23]. Thermo-responsive polymers exhibit a significant change in their solubility with respect to temperature, and thus their conformation alter significantly. The most studied thermo-responsive polymer is PNIAPM which has applications in tissue engineering [24], drug delivery [25], biosensors [26], and water treatment [27]. The solutions of PNIPAM shows a fast and reversible phase transition phenomena due to its thermo-responsiveness. The coil to globule transition of PNIPAM assisted with the mechanical property change can be studied using the dynamics of microfluidic cantilever. Suspended microchannel resonators were used to study the phase transition in polymers as the change in the elastic modulus of polymers would affect the stiffness and shift in resonance frequency of the cantilever. By taking advantage of the capability of microfluidic cantilever to study thermo-mechanical property change of polymers, it is possible to investigate the phase change of PNIPAM by analysing the shift in dynamic properties of cantilever.

PNIPAM is considered as a suitable polymeric flocculant for sedimentation of clay particles in mature fine tailings (MFT). The polymeric chains adsorb on one or more sites of dispersed clay particles by hydrogen bonding and electrostatic interactions. When the temperature of the solution is raised above LCST, the flocculation of clay particles with PNIPAM occurs due to the hydrophobic nature of PNIPAM above LCST. The mechanical property change associated with

the flocculation could be studied using the stiffness change of the microfluidic cantilever filled with the flocculation solution as a function of temperature.

1.3 Technological significance of current study

Whether it is a fundamental research project in MEMS or new formulation development in pharmaceutical industry, a system requiring low volume of liquid solutions, offering fast measurements and reliable results is required. Decreasing a volume of liquid to pico-litres does not change dynamics of molecules. Therefore, by minimizing the volume of reagents by a factor of 10^4-10^5 would help reducing costs of most assays. Lab-on-a-Chip technology offers promising solutions in new drug development. Microscale analysis systems provide advantages like low sample consumption and reduced analysis time. Micro resonators, such as micro strings and microcantilevers, have been previously employed for thermal analysis (of small masses) of liquids [1]. Both techniques suffer from dissipation and low-quality factor which affects the quality and accuracy of the results.

To overcome these difficulties, a microchannel cantilever consisting of microfluidic channel integrated on top of the cantilever was developed by Faheem et al [28]. This project "microchannel resonators to characterize thermomechanical properties of fluids" combines microfluidics and micro mechanics by realizing that such devices can characterize liquid samples with a volume down to 5 pL. With the volume of the microchannel ~ 50 pL, the resonance frequency of the cantilever is ~ 50 kHz while its quality factor lies in the order of six to eight thousand. These values ensure high resolution in detecting any changes in the resonance frequency. The system works as a density meter [29], viscosity meter [30], infrared (IR) spectrometer [31]and calorimeter [32].

It has been established that adsorption on the surface of the cantilever can affect the surface stress and hence results in the bending of the cantilever [33]. Theories has been introduced to discuss the effect of adsorption on the resonance frequency shift of the cantilever as well [34]. While we quantitatively establish the relation between the experimental results with the thermophysical properties of the sample of interest, there are discrepancies in the values. This is addressed in this

thesis by using an analytical model with modified Euler Bernoulli equation which incorporates the effect of surface and interfacial tension on the resonance frequency of the cantilever.

Further, bi-material cantilevers were used to study the thermal properties of fluids, polymers and to investigate the photothermal spectroscopy of liquids in static mode. Static deflection often suffers from drag, instability of the signal. This is addressed by using a simple microfluidic cantilever, filled with liquid, and irradiated by a laser, operating in dynamic mode. The experimental results were compared and validated with the analytical model developed based on the modified Euler Bernoulli equation that incorporates the surface stress induced by volumetric expansion of liquid upon heating of the channel.

The phase change of the thermos sensitive polymer PolyN-isopropylacrylamide (PNIPAM) is assisted with the mechanical property change as well [13]. Only few studies reported the modulus change of the PNIPAM aqueous solution at lower critical solution temperature (LCST) [35]. There understanding about the mechanical property change of this solution at LCST is still under investigation. To understand the thermomechanical property, change of the PNIPAM solution with respect to the temperature, we introduced microchannel cantilever attached with a heater working in dynamic mode. The frequency shift of the cantilever is used to analyse the modulus change of the solution at LCST. Also, the flocculation studies had been done only at macro scale experiments so far [36,37]. The existing methods to identify the flocculation of clay particles in presence of a thermo-sensitive polymer is by looking at the turbidity, sedimentation and so on. Here, we are using a microfluidic channel to study the flocculation of pico litres of Kaolinite and PNIPAM. Further, the mechanical property evolution of the solution of PNIPAM and Kaolinite is investigated using the same microfluidic cantilever during flocculation inside the cantilever at LCST.

1.4 Outline of the thesis

The main aim of this dissertation is the study of thermomechanical change of liquids inside the microchannel cantilever by analysing the frequency shift of the cantilever.

The summarized objectives of this thesis are:

1. Investigation of the effect of surface tension and interfacial tension on the natural resonance frequency of microfluidic cantilevers filled with alkanes.

2. Measurement of the thermal properties of liquids by photothermal modulation of microfluidic cantilevers.

3. The detection of the mechanical property change associated with the phase change of a temperature responsive PNIPAM polymer and the in- situ flocculation of clay particles inside the cantilever PNIPAM by observing the frequency shift of the microfluidic cantilever.

This contents in the thesis have been written according to article published in journal or manuscript submitted to journal. Each chapter will be initiated by giving the significant aspects of the study with experimental outline, highlighted results, and procedures and important analytical or simulation work in subsequent order.

This thesis consists of 7 chapters. The organization of the thesis is as follows:

Chapter 1 (the current chapter) gives the introduction to the thesis and explains the motivation and objective of the thesis.

Chapter 2 provides the background and literature on fundamentals of microcantilevers. The effect of surface stress on the dynamics of cantilever is discussed with the help of different theories. The issues in the existing theories describing the influence of surface stress on the resonance frequency and the deflection of cantilever are provided. Along with that, existing challenges of detection in liquids are discussed in detail. Detailed theoretical knowledge has been provided to explore microcantilevers as thermal sensors. A discussion on various aspects in the literature of photothermal modulation using MEMS is provided in this chapter. A special focus on the properties of clay particles, thermo-sensitive polymer PNIPAM and flocculation is given in the last part of chapter 2.

In Chapter 3, relevant characterization or fabrication techniques employed during the work will be described. The focus will be on major techniques involved in characterization of liquid samples with suspended microchannel resonators (SMR).

Chapter 4 discusses the effect of surface tension and interfacial tension on the resonance frequency of microfluidic cantilever filled with different liquids. We used alkanes to fill the channel and the mechanical response of the resonator at its resonance frequency is studied using the modified Euler- Bernoulli equation. The influence of surface stress and interfacial tension on the walls of the cantilever is used to improve the theoretical modal and this is validated using the experimental data.

Chapter 5 describes the measurement of thermal properties of liquids using the microchannel cantilever irradiated using a diode laser. We shined a laser on the cantilever filled with liquid and studied the frequency change of the cantilever for different liquids and established a relation between the volumetric expansion of liquid inside the channel and the resonance frequency of the cantilever.

Chapter 6 illustrates the flocculation of Kaolinite in the presence of thermo-responsive polymer PNIPAM inside the microfluidic cantilever. We filled the microfluidic channel with PNIPAM and Kaolinite solution and investigated the thermomechanical change of the solution during LCST transition. The dynamic mechanical response such as frequency and quality factor are obtained by Laser Doppler Vibrometer (LDV). The flocculation of Kaolinite with PNIPAM is studied by analysing the stiffness change of the system which is reflected in the frequency shift of the cantilever.

Finally, the overall conclusions and future works of this thesis are summarized in Chapter 7.

Table 1.1 Brief summary of chapter 4 to 6

Chapter 4

Title	Effect of surface and interfacial tension on the resonance frequency of microfluidic channel cantilever.
Objective	Insert 6 different liquids inside the micro channel cantilever and understand the effect of surface tension and the interfacial tension of each liquid and cantilever substrate on the resonance frequency.
Major Findings	Successfully filled the micro channel cantilever with different liquids and frequencies were obtained for each liquid filled cantilever. An analytical model based on modified Euler-Bernoulli beam was used to compute the frequency based on surface stress and interfacial tension of liquids. The analytical results are validated with the experimental values.

Chapter 5

Title	Measurement of Thermal Properties of Liquid Analytes using Microfluidic Resonators via Photothermal Modulation.
Objective	Detect the thermal properties of the liquids inside the microchannel cantilever upon shining the laser.
Major Findings	The frequency shift of the microchannel cantilever with liquid is proportional to the volumetric expansion of the liquid. The heating time constant is inversely proportional to the product of density and heat capacity of the liquid.

Chapter 6

Title	Thermomechanical characterization of real-time flocculation of Kaolinite and PNIPAM using microfluidic cantilever.

Objective	Detect the phase change of PNIPAM polymer inside the microchannel cantilever and thermomechanical property change of the solution of PNIPAM and Kaolinite during flocculation.
Major Findings	Demonstrated the phase change of PNIPAM and flocculation as a function of temperature inside the microchannel cantilever by analysing the frequency shift.

1.5 References

[1]   M. Alvarez, L.M. Lechuga, Microcantilever-based platforms as biosensing tools, Analyst. 135 (2010) 827–836. https://doi.org/10.1039/b908503n.

[2]   A. Vyas, H. Staaf, C. Rusu, T. Ebefors, J. Liljeholm, A.D. Smith, P. Lundgren, P. Enoksson, A Micromachined Coupled-Cantilever for Piezoelectric Energy Harvesters, Micromachines (Basel). 9 (2018). https://doi.org/10.3390/MI9050252.

[3]   R.S. Patkar, M. Vinchurkar, M. Ashwin, A. Adami, F. Giacomozzi, L. Lorenzelli, M.S. Baghini, V. Ramgopal Rao, Microcantilever Based Dual Mode Biosensor for Agricultural Applications, IEEE Sens J. 20 (2020) 6826–6832. https://doi.org/10.1109/JSEN.2019.2958947.

[4]   L. Senesac, T. Thundat, Explosive Vapor Detection Using Microcantilever Sensors, Counterterrorist Detection Techniques of Explosives. (2007) 109–130. https://doi.org/10.1016/B978-044452204-7/50024-9.

[5]   K.M. Hansen, T. Thundat, Microcantilever biosensors, Methods. 37 (2005) 57–64. https://doi.org/10.1016/j.ymeth.2005.05.011.

[6]   A. Boisen, J. Thaysen, H. Jensenius, O. Hansen, Environmental sensors based on micromachined cantilevers with integrated read-out, Ultramicroscopy. 82 (2000) 11–16. https://doi.org/10.1016/S0304-3991(99)00148-5.

[7]   G. Binnig, C.F. Quate, C. Gerber, Atomic force microscope, Phys Rev Lett. 56 (1986) 930–933. https://doi.org/10.1103/PHYSREVLETT.56.930/FIGURE/1/THUMB.

[8]   T. Thundat, X.-Y. Zheng, G.Y. Chen, R.J. Warmack, Role of relative humidity in atomic force microscopy imaging, Surface Science Letters. 294 (1993) L939–L943. https://doi.org/10.1016/0167-2584(93)91119-9.

[9]   H. Etayash, T. Thundat, Microcantilever Chemical and Biological Sensors, Encyclopedia of Nanotechnology. (2015) 1–9. https://doi.org/10.1007/978-94-007-6178-0_187-2.

[10]   K.L. Ekinci, Y.T. Yang, M.L. Roukes, Ultimate limits to inertial mass sensing based upon nanoelectromechanical systems, J Appl Phys. 95 (2004) 2682–2689. https://doi.org/10.1063/1.1642738.

[11]   T.P. Burg, S.R. Manalis, Suspended microchannel resonators for biomolecular detection, Appl Phys Lett. 83 (2003) 2698. https://doi.org/10.1063/1.1611625.

[12]   J. He, C.M. Lilley, Surface stress effect on bending resonance of nanowires with different boundary conditions, Appl Phys Lett. 93 (2008). https://doi.org/10.1063/1.3050108.

[13]   D. van Duinen, H.J. Butt, R. Berger, Two-Stage Collapse of PNIPAM Brushes: Viscoelastic Changes Revealed by an Interferometric Laser Technique, Langmuir. (2019). https://doi.org/10.1021/acs.langmuir.9b03205.

[14]   L.R. Senesac, D. Yi, A. Greve, J.H. Hales, Z.J. Davis, D.M. Nicholson, A. Boisen, T. Thundat, Micro-differential thermal analysis detection of adsorbed explosive molecules using microfabricated bridges, Review of Scientific Instruments. 80 (2009) 035102. https://doi.org/10.1063/1.3090881.

[15]   M. Godin, V. Tabard-Cossa, P. Grutter, Quantitative surface stress measurements using a microcantilever, American Institute of Physics. 79 (2001) 551–553.

[16]   S. Sadat, E. Meyhofer, P. Reddy, Resistance thermometry-based picowatt-resolution heat-flow calorimeter, Appl Phys Lett. 102 (2013) 163110. https://doi.org/10.1063/1.4802239.

[17]   J.R. Serrano, L.M. Phinney, J.W. Rogers, Temperature amplification during laser heating of polycrystalline silicon microcantilevers due to temperature-dependent optical properties, Int J Heat Mass Transf. 52 (2009) 2255–2264. https://doi.org/10.1016/j.ijheatmasstransfer.2008.12.003.

[18]   M.S. Ghoraishi, J.E. Hawk, A. Phani, M.F. Khan, T. Thundat, Clustering mechanism of ethanol- water mixtures investigated with photothermal microfluidic cantilever deflection spectroscopy, Nature Publishing Group. (2016) 1–7. https://doi.org/10.1038/srep23966.

[19]   J. Lagowski, H.C. Gatos, E.S. Sproles, Surface stress and the normal mode of vibration of thin crystals: GaAs, Appl Phys Lett. 26 (1975) 493–495. https://doi.org/10.1063/1.88231.

[20]   M.J. Lachut, J.E. Sader, Effect of surface stress on the stiffness of cantilever plates, Phys Rev Lett. 99 (2007) 1–4. https://doi.org/10.1103/PhysRevLett.99.206102.

[21]   Y. Zhang, L.J. Zhuo, H.S. Zhao, Determining the effects of surface elasticity and surface stress by measuring the shifts of resonant frequencies, Proceedings of the Royal Society A: Mathematical, Physical and Engineering Sciences. 469 (2013). https://doi.org/10.1098/rspa.2013.0449.

[22]   R. Abraham, F. Khan, S.A. Bukhari, Q. Liu, T. Thundat, H.J. Chung, C. il Kim, Effect of surface and interfacial tension on the resonance frequency of microfluidic channel cantilever, Sensors (Switzerland). 20 (2020) 1–14. https://doi.org/10.3390/s20226459.

[23]   S.A. Manzoor Bukhari, M.F. Khan, A. Goswami, R. McGee, T. Thundat, Thermomechanical analysis of picograms of polymers using a suspended microchannel cantilever, RSC Adv. 7 (2017) 8415–8420. https://doi.org/10.1039/c6ra25455a.

[24]   A. Choi, K.D. Seo, H. Yoon, S.J. Han, D.S. Kim, Bulk poly(N-isopropylacrylamide) (PNIPAAm) thermoresponsive cell culture platform: toward a new horizon in cell sheet engineering, Biomater Sci. 7 (2019) 2277–2287. https://doi.org/10.1039/C8BM01664J.

[25]   C.N. Cheaburu-Yilmaz, C.E. Lupuşoru, C. Vasile, New Alginate/PNIPAAm Matrices for Drug Delivery, Polymers 2019, Vol. 11, Page 366. 11 (2019) 366. https://doi.org/10.3390/POLYM11020366.

[26]   Y. Wei, Q. Zeng, Q. Hu, M. Wang, J. Tao, L. Wang, Self-cleaned electrochemical protein imprinting biosensor basing on a thermo-responsive memory hydrogel, Biosens Bioelectron. 99 (2018) 136–141. https://doi.org/10.1016/J.BIOS.2017.07.049.

[27]   X. Xu, N. Bizmark, K.S.S. Christie, S.S. Datta, Z.J. Ren, R.D. Priestley, Thermoresponsive Polymers for Water Treatment and Collection, Macromolecules. 55 (2022) 1894–1909.

https://doi.org/10.1021/ACS.MACROMOL.1C01502/ASSET/IMAGES/MEDIUM/MA1C01502_0007.GIF.

[28]   M.F. Khan, Microchannel resonators to characterize liquid samples: Ph. D. thesis, (2012). https://books.google.com/books/about/Microchannel_Resonators_to_Characterize.html?id=l4nfngEACAAJ (accessed October 19, 2022).

[29]   S. Marquez, M. Álvarez, D. Fariña Santana, A. Homs-Corbera, C. Domínguez, L.M. Lechuga, Array of Microfluidic Beam Resonators for Density and Viscosity Analysis of Liquids, Journal of Microelectromechanical Systems. 26 (2017) 749–757. https://doi.org/10.1109/JMEMS.2017.2709944.

[30]   A.F. Payam, W. Trewby, K. Voïtchovsky, Simultaneous viscosity and density measurement of small volumes of liquids using a vibrating microcantilever, Analyst. 142 (2017) 1492–1498. https://doi.org/10.1039/c6an02674e.

[31]   N. Miriyala, Photothermal effects in micro/nano electromechanical systems, n.d.

[32]   A. Alodhayb, F. Khan, H. Etayash, T. Thundat, Review—Nanomechanical Calorimetric Infrared Spectroscopy using Bi-Material Microfluidic Cantilevers, J Electrochem Soc. 167 (2020) 037504. https://doi.org/10.1149/2.0042003jes.

[33]   G.F. Wang, X.Q. Feng, Effects of surface elasticity and residual surface tension on the natural frequency of microbeams, Appl Phys Lett. 90 (2007) 1–4. https://doi.org/10.1063/1.2746950.

[34]   G.F. Wang, X.Q. Feng, Effects of surface elasticity and residual surface tension on the natural frequency of microbeams, Appl Phys Lett. 90 (2007). https://doi.org/10.1063/1.2746950.

[35]   I. Bischofberger, V. Trappe, New aspects in the phase behaviour of poly-N-isopropyl acrylamide: Systematic temperature dependent shrinking of PNiPAM assemblies well beyond the LCST, Sci Rep. 5 (2015). https://doi.org/10.1038/srep15520.

[36]   V. Vajihinejad, S.P. Gumfekar, B. Bazoubandi, Z.R. Najafabadi, J.B.P. Soares, V. Vajihinejad, S.P. Gumfekar, B. Bazoubandi, Z. Rostami, N.B.P. Soares, Water Soluble Polymer Flocculants: Synthesis, Characterization, and Performance Assessment, Macromol Mater Eng. 304 (2019) 1800526. https://doi.org/10.1002/MAME.201800526.

[37]   M. Digital, M. Digital Scholar, S. Youn, Quantitative Understanding of Nanoparticle Flocculation in Water Quantitative Understanding of Nanoparticle Flocculation in Water Treatment, 2017. https://mds.marshall.edu/wde_faculty.

Chapter 2

Theoretical Background

2.1 Introduction

In this chapter, we will address two distinct subjects. Section 2.2 will discuss the fundamentals of MEMS- based microcantilever sensors. The basic modes of operations of microcantilever sensor, various detection mechanisms and theoretical background of the surface effects on the dynamics of the cantilever will be discussed. Furthermore, the photothermal effects of the resonance characteristics of the microfluidic cantilever with liquids will be explained in this section. This section will serve as the scientific background for chapters 4, 5 and 6.

Section 2.3 will serve as a background to understand the phase transition of the poly (N-isopropylacrylamide) (PNIPAM) and water systems with and without the presence of Kaolinite clay. The evolution of mechanical properties of the solution with respect to change in temperature and its effect on the dynamics on the cantilever will be explained in this section. Section 2.3 will serve as a scientific background for chapter 6.

2.2 MEMS-based Microcantilever Sensors: Operation Principles

MEMS-based microcantilever is a powerful miniaturized platform for physical [1], chemical [2], biological [3–6], and thermomechanical [7–9] sensing applications due to their excellence in real-time, high-throughput, multiplexed detection of a myriad of chemical and biological analytes. With the advent of atomic force microscopy (AFM), introduced in 1986 by Binning et al., a revived interest in microfabrication and a plethora of applications in MEMS has been generated[10]. At the core of an AFM is a microcantilever that works as a transducer for its numerous imaging modes like topography [11], electric potential [12], magnetic [13], and force imaging [14]. Later, the AFM cantilevers were explored as a stand-alone platform for physical and chemical sensing

pioneered by Thomas Thundat and co-workers at Oak Ridge National Laboratory (ORNL) in 1994 [15]. Microcantilevers as sensors, unlike AFM cantilevers, do not require a tip at their apex or a sample surface. The beam surfaces serve as sensors to detect the adsorption of molecules taking place on these surfaces. They have been employed as physical, chemical, and biological sensors in the field of defense, medical field, polymers, etc. The cantilever can respond to the external stimuli either by bending or by a shift in the resonance frequency [16]. The explicit factors that govern the dynamics of a micro cantilever are the stiffness and mass density of the entire cantilever system [16]. Apart from that, surface stress is also an underlying crucial parameter when it comes to either adsorption or thermal expansion, chemical reaction on the surface of the cantilever, etc. [17]. The effect of surface stress on the dynamics which includes the bending of the cantilever, and the frequency shift of the cantilever is a widely discussed topic yet comes with a handful of contradictions.

In the first part of section 2.1, we will discuss the effect of surface stress on the bending resonance of the cantilever, and the frequency shift of the cantilever. Along with that, we will discuss the modified Euler-Bernoulli beam theory developed for microfluidic cantilevers which explains the effect of surface stress on the resonance frequency shift of the cantilever. In the second part, we will consider the photothermal effects of the resonance characteristics of the microfluidic cantilever filled with different liquids.

2.2.1 Basic modes of operation and detection

Microcantilever sensors are widely used for sensing applications in air, liquid, and vacuum with two basic operation modes: a) static mode (adsorption-induced deflection) and b) dynamic mode (the resonant frequency shift of the cantilever) [16]. In static mode, the bending of the cantilever is the measured quantity while a mass is attached to it, or a force is acting on it [18]. Whereas in dynamic mode, the resonance frequency shift is monitored while the mass is adsorbed on the structure [19]. The difference in the resonance frequency is calculated for finding the amount of the adsorbed mass or any type of force acting upon it. Furthermore, there is another mode called heat mode which is similar to static mode but makes use of the bimetallic effect that leads to a bending of the biomaterial cantilever with a change in temperature [20]. Each mode is dedicated

to certain applications and varies from each other in terms of transduction and detection as in Figure 2.1.
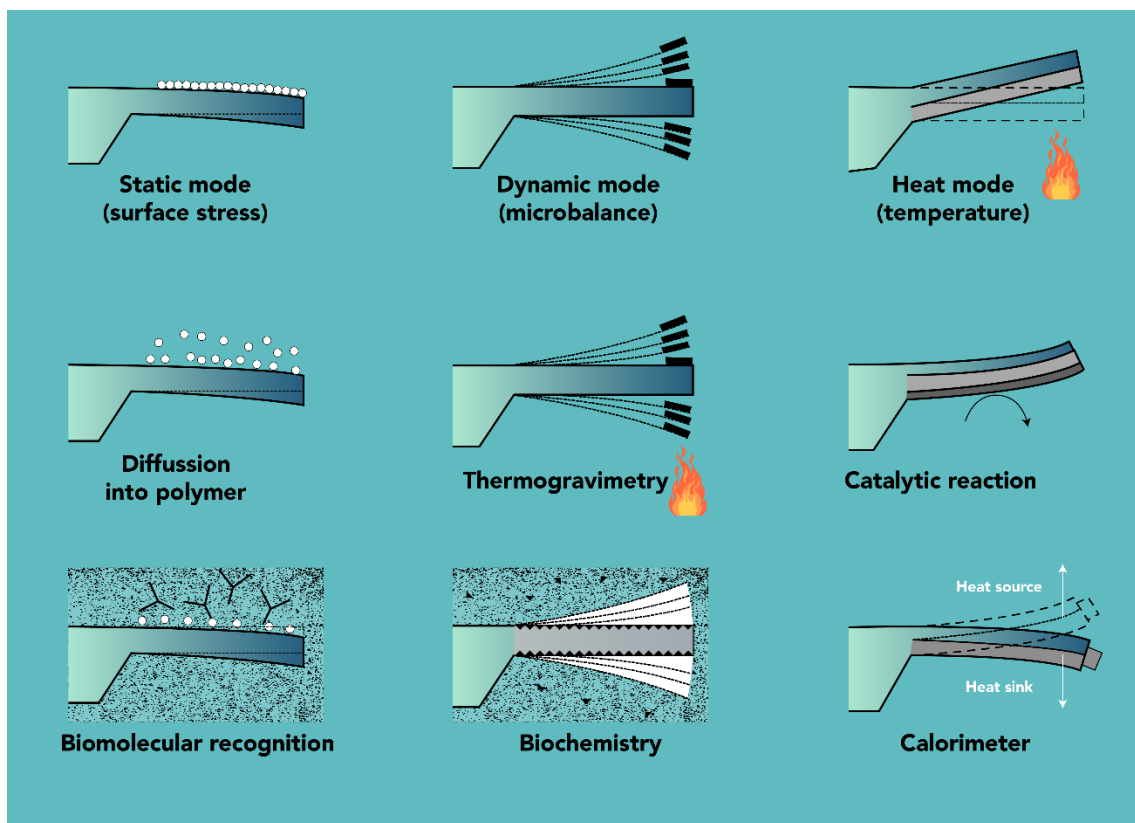
Figure 2.1: Schematic of basic modes of operations of cantilever (a) Static bending of a cantilever on adsorption of an analyte layer (b) Bending of cantilever as a result of diffusion of molecules into a polymer layer (c) Specific molecular recognition of biomolecules by receptors changes the surface stress on the upper surface of the cantilever and results in bending. (d) Frequency shift of cantilever due to mass loading (Dynamic mode) (e) Changing the temperature while a sample is attached to the apex of the cantilever allows information to be gathered on decomposition or oxidation process (f) Dynamic mode measurements in liquids yield details on mass/viscosity/adsorption changes during biochemical processes (g) In the heat mode, a bimetallic is bending due to the difference in the thermal expansion coefficients of the two materials (h) A bimetallic cantilever with a catalytically active surface bends due to heat production during a catalytic reaction (i) A tiny sample attached to the apex of the cantilever is investigated, taking advantage of the bimetallic effect Reproduced with permission from [16].

Static mode: Any type of chemical/physical/thermal reactions, occurring on the surface of the microcantilever, are obtained as mechanical property changes of the cantilever beam. In static mode, as mentioned earlier, this mechanical property change of the cantilever beam is converted

as the bending of the beam. This bending arises from a differential surface stress due to the adsorption of molecules on one side of the cantilever [7,21–25]. To serve as a physical/chemical sensor, while operating in the static mode, a specific thin sensing layer that can recognize the target molecules in adsorption processes needs to be coated only on one side of the cantilever [26]. The immobilized receptors on the cantilever surface determine the chemical/biological selectivity in the process and hence adsorption is controlled by this functionalized surface [27].

The interaction between the functionalized surface and target molecules can be physical/chemical or both and can vary from the very strong covalent bond to weak Vander Waals interaction. Adsorption of the molecules onto the functional layer generates stress at the interface between the functional and the forming molecular layer. During adsorption, the minimization of energy of the surface occurs and it leads to a decrease in surface free energy of the cantilever surface. In order to generate a differential surface stress between the two surfaces of a cantilever beam, the lower side of the cantilever is made inactive by passivation and the adsorption of molecules on a surface is restricted mostly to one side [28–32].
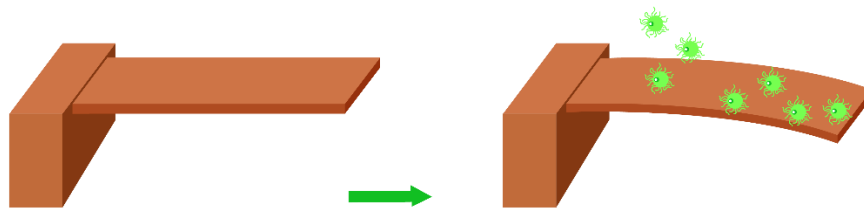
Figure 2.2: Schematic of (a) Stress-free cantilever and (b) bending of the cantilever due to the generated surface stress by interaction with analyte.

When a new molecular layer is formed on the functionalized (upper) surface of the cantilever due to the adsorption of the target molecules the cantilever experiences a downward bending due to the abovementioned surface stress [16]. When the force within the functional layer tries to keep the distance between molecules constant, the cantilever responds with bending due to its flexibility. Compressive stress is formed when the adsorbed layer of molecules produces a downward bending of the microcantilever away from its functionalized side. Tensile stress is obtained when the

cantilever bends upwards (same side of the functionalized surface). When both the upper and the lower surface of the microcantilever are exposed to surface stress changes, then the situation will be much more complex, with competing parameters such as a predominant compressive stress formation on the lower microcantilever surface might appear as tensile stress on the upper surface. For this reason, it is extremely important to properly passivate the lower surface so that, ideally, no processes take place on the lower surface of the microcantilever.
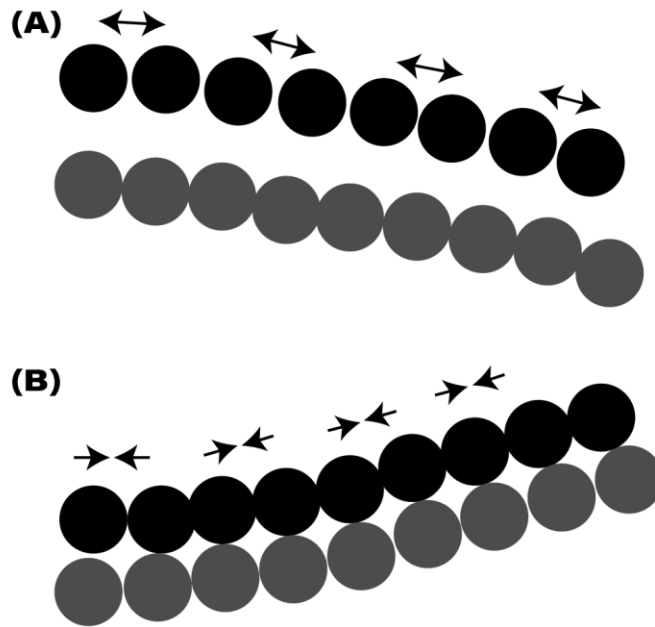
Figure 2.3: a) Compressive stress b) tensile stress on the cantilever where the functionalised surface is on the lower surface of the cantilever.

Using the Shuttleworth equation, surface stress, σ (mNm^{-1}), and surface free energy, γ (mN/m^{-1}), can be related as given

$$\sigma = \gamma + \frac{d\gamma}{d\varepsilon} \qquad (2.1)$$

where the surface strain dε is defined as the ratio of the change in surface area to the total area, dε=dA/A. Here surface free energy is considered as surface tension of the solid with units mNm^{-}

[1]. The strain contribution is neglected considering the effective bending of the cantilever to be very small compared to the length of the differential surface stress created by molecular adsorption reaches a threshold and results in cantilever bending [28].

Apart from surface stress, the flexural behavior of the microcantilever due to molecular adsorption is controlled by its spring constant k which is a function of Young's modulus (E) and cantilever dimensions. For a rectangular cantilever of length l, width w, and thickness t the spring constant is calculated as follows

$$k = \frac{3EI}{l^3} = \frac{3Ewt^3}{12l^3} = \frac{Ewt^3}{4l^3} \tag{2.2}$$

where EI is the effective modulus and $\frac{wt^3}{12}$ is the moment of inertia, I, of the cantilever. The typical value of the spring constant for silicon microcantilever of length several hundred micrometers and thickness below 1 μm varies from 0.001 to 0.1 N m^{-1}. Considering uniform surface stress ($\delta\sigma$) as the cause for cantilever bending, the shape of the deformed microcantilever can be approximated as a part of a circle of radius of curvature R given by Stoney's equation

$$\frac{1}{R} = \frac{6(1-v)}{Et^2} \delta\sigma \tag{2.3}$$

where v is the Poisson's ratio (v_{Si} = 0.24) [30]. The above equation is only valid for the case of a thin functionalization layer (much thinner than the thickness of the microcantilever). The cantilever deflection, δh, can be obtained from the above Stoney's equation that relates the difference in surface stress $\delta\sigma$ between the chemically modified surface and the untreated surface with the cantilever deflection,

$$\delta\sigma = \frac{E\delta h}{4(1-v)} \left(\frac{t}{L}\right)^2 \tag{2.4}$$

where, t and L are the thickness and the length of the cantilever, respectively. It is evident that the sensitivity of the cantilever to measure surface stresses increases with the length of the cantilever. Typically, surface stress changes of the order of 10^{-3} to 10^{-6} can be measured. The static deflection method can be operated in diverse environments such as vacuum, air and fluid.
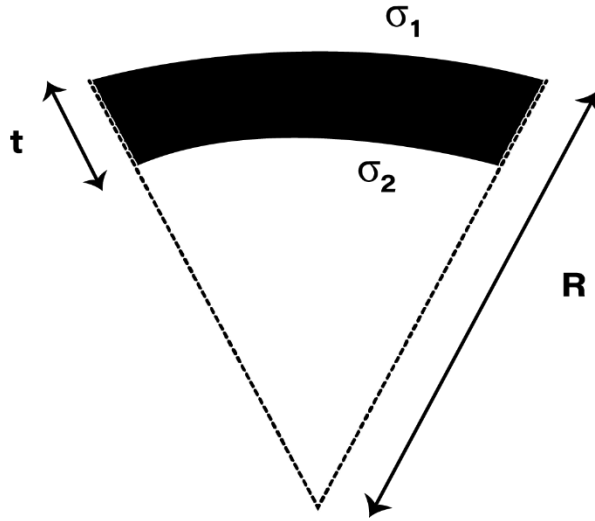
Figure 2.4: Lateral view of cantilever subject to surface stress.

The bending of simple rectangular cantilever changes according to the distribution of load on the cantilever. For distributed load,

$$h = \frac{qL^4}{8EI} \qquad (2.5)$$

For point load

$$h = \frac{pL^3}{3EI} \qquad (2.6)$$

where, h is the deflection, q and p are distributed, and point loads, respectively[5]. This mode has been used to observe antigen-antibody interactions, DNA binding and other biosensing applications [33].
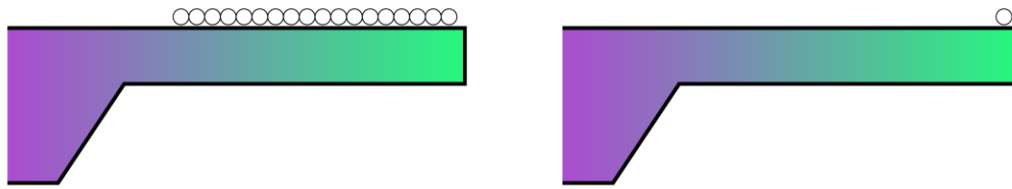
Figure 2.5: Microcantilever with a) distributed load b) point load

Dynamic mode: In the resonant mode, the cantilever is driven at its fundamental resonance frequency (or one of the harmonic frequencies), and the parameters such as frequency, quality factor, amplitude, and phase are monitored. While the static mode provides qualitative information about adsorption, the dynamic mode contributes to the quantitative information about the mass loading during adsorption [19]. The dynamic mode doesn't require the functionalization of only one cantilever surface, as the cantilever resonance frequency change depends on the total mass adsorbed on both sides.

For an oscillating cantilever, the fundamental equation for frequency is given as

$$f = \sqrt{\frac{k}{m}} \qquad (2.7)$$

where k is the spring constant and m is the effective mass. Any change in the elastic properties such as effective mass and spring constant would affect the resonant frequency of the cantilever [34]. It is evident from the equation that an increase of the cantilever mass due to analyte absorption causes a decrease in the cantilever resonance frequency. Since k is a function of EI, where E is the young's modulus and I is the moment of inertia, the decrease or increase in the elastic modulus or dimension of the cantilever would affect the frequency appropriately.

As mentioned earlier, when deflection of a cantilever provides the direct measurement of the adsorption of the molecules onto the surface of the cantilever, the quantitative information such as

the number of molecules adsorbed on the cantilever is still unknown. The surface coverage is unpredictable as molecules on the surface might be exchanged with molecules from the environment in a dynamic equilibrium. In dynamic mode, the mass change during adsorption or desorption can be determined accurately by tracking the resonant frequency shift while oscillating the microcantilever at its eigenfrequency. This method is powerful in sensing tiny mass in the range of atto-gram (10^{-18}gm) to zeptogram (10^{-21}gm) [35].

The frequency of the rectangular microcantilever at the end of the cantilever with an additional mass loading can be calculated, provided the young's modulus and thickness of the cantilever remain same, as follows

$$f = \frac{1}{2\pi}\sqrt{\frac{k}{m + \alpha\Delta m}}$$

(2.8)

The mass change on a rectangular cantilever is calculated as

$$\Delta m = \frac{k}{4\pi^2}\left(\frac{1}{f_1^2} - \frac{1}{f_0^2}\right)$$

(2.9)

where f_0 is the eigenfrequency before the mass change occurs, and f_1 the eigen frequency after the mass change [35].

Not only the mass change but also the surface stress induced by the adsorption affects the resonance frequency of the cantilever. It was found that the surface stress affects the overall stiffness of a cantilever, affecting the resonance frequency. Many models had been proposed to explain the adsorption-induced surface stress change and its resultant resonance frequency shift of a microcantilever in a vacuum or a gaseous environment. Lagowski et al. found that the resonant frequency of a microcantilever deviates significantly from those predicated by the axial load-free beam theory; they proposed that surface stress is the mechanism causing the resonant frequency shifts[36]. Subsequently, Gurtin et al. disputed Lagowski's explanation; they argued that the resonant frequency is independent of surface stress and that surface elasticity is the only

mechanism responsible for the resonant frequency shifts [37]. Later on, rigorous studies had been done to understand the effect of surface stress on the dynamics of microcantilever by Wang et al, McFarland et al, Ren et al etc.

Another important transducer parameter in the dynamic mode of operation is the mechanical quality factor which is given as

$$q = 2\frac{f_o}{\Delta f}$$

(2.10)

While operating the dynamic mode in the gas or the liquid phase, the quality factor of the resonant microcantilever is not as high as that of microcantilevers operating in vacuum [38]. This is because of the high damping of the cantilever oscillation in fluid environment is due to the high viscosity of the surrounding media. Hence, the low-quality factor Q of the oscillation makes it difficult to track of resonance frequency shift with high resolution[38]. The reduced value of the quality factor corresponds to the energy dissipation in the surrounding medium and directly affects the sensitivity and detection limit of this type of sensor.
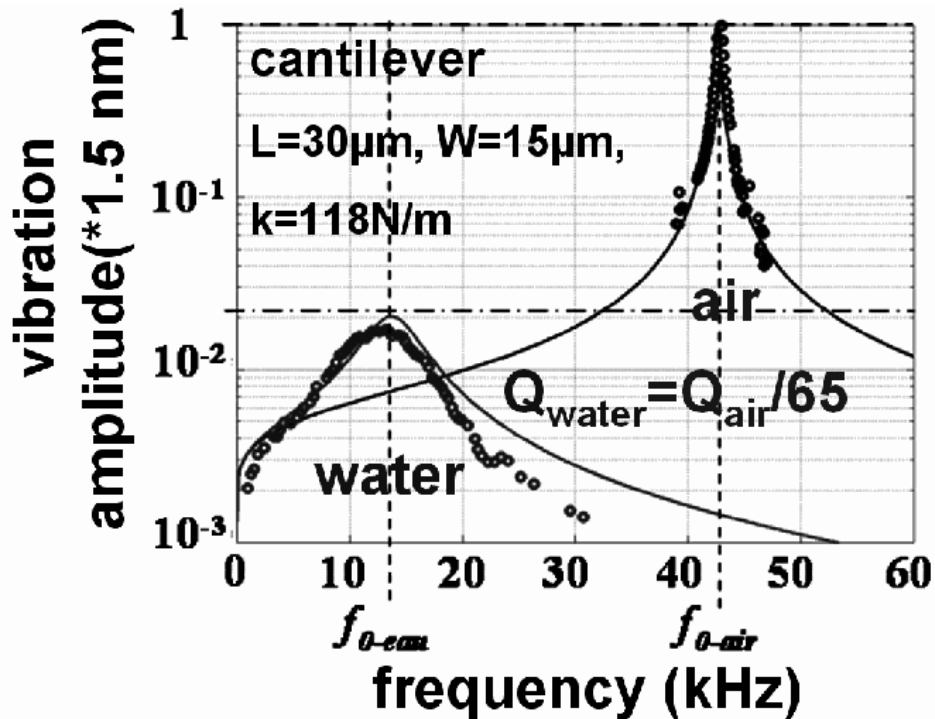
Figure 2.6: Resonance frequency of piezoelectrically-actuated cantilever in water and air. The quality factor is considerably reduced in water due to damping. Reproduced with permission from [39]

To overcome the challenge of low-quality factor and poor sensing in liquid, Manalis group came up with a microfluidic channel cantilever which has a channel on top of the microcantilever [40]. The channel can be filled with liquid of interest and the whole cantilever can be oscillated in the vacuum to achieve high-quality factor and hence a stable tracking of the resonance frequency. In order to conduct adsorption-based studies, the inner surface of the channel cantilever can be functionalized [41]. The fluid that is continuously delivering the analytes to the cantilever changes the resonance frequency of the cantilever upon binding to the complementary species that are pre-functionalized in the inner microchannel surface, without compromising on the cantilever's performance.

Sub-femtogram mass resolution is attained by shrinking the wall and fluid layer thickness to the micrometer scale and by packaging the cantilever under a high vacuum. Using this setup, weighing of a single biomolecule and nanoparticle in the fluid with a mass resolution of 300 atto-grams was demonstrated [41]. Despite a paradigm shift in sensing in a fluidic environment, these suspended microchannel cantilevers must rely on surface functionalization for selectivity, thus limiting their potential.

Heat mode: A bi-material cantilever is used for the heat mode of operation in which the bimetallic effect plays the key role in the bending of the cantilever upon a change in temperature [42]. When a material is irradiated with a specific wavelength, it can absorb photons, and a fraction of energy is converted into heat [9]. This interaction of light with a bimetallic cantilever creates heat on the cantilever surface, resulting in a bending of the cantilever. Such bimetallic-cantilever devices are capable of detecting heat flows due to an optical heating power of 100 pW, being two orders of magnitude better than in conventional photothermal spectroscopy [35].

The bi-material cantilever beam is an important microelectromechanical system structure used for thermal measurements. This kind of thermal device has greater sensitivity and smaller spatial

resolution than those of traditional thermal devices. The high sensitivity of the technique is due to the small dimensions and thermal mass of the bi-material cantilever beam in combination with current optical methods to monitor the bending with high precision [43]. In bi-material structures, a metal layer with a high coefficient of thermal expansion is deposited on a silicon or silicon nitride cantilever beam in order to achieve high sensitivity [35]. The variation in temperature results in the deflection of the bi-material cantilever beam at the free end due to the different thermal expansion coefficients of the silicon and the metal films. Consequently, bi-material cantilever beams could be used to detect very small variations in temperature.

2.2.2 Detection principles of microcantilever

Proper measurement of cantilever deflection or vibration is at the heart of acquiring precision measurements when performing cantilever-based sensing. Detection of tiny deflection of cantilever and associated structures are carried out with different sensitive displacement sensors based on the type of applications. The important transduction principle of the microcantilever is listed below.

The Optical Deflection Detection Method: The optical beam deflection method employs a laser beam of very low power of the order that does not interfere with any physical, chemical/biological activities on the surface of the microcantilever and a position-sensitive detector (PSD) [5]. The laser beam falls on the tip of the cantilever and gets reflected as the gold layer coated on the surface of the cantilever acts like a mirror with high reflectance. The reflected beam is collected by the PSD which can track the movement of the reflected laser spot from the cantilever. When the cantilever is undeformed/undeflected i.e., it is neither coated with any molecule nor under any stress, the laser beam would fall on a particular spot on the PSD. As the cantilever deflects, the position of the beam changes, which, in turn, is calculated using appropriate electronics [5]. The technique typically provides a resolution of 1 nm deflection and even sub-angstrom resolution can be achieved. Though this method provides detection of deflection in the sub-nanometer range in air/vacuum, detection in liquid cell gives spurious results due to thermal management issues from

focussed laser beam. Furthermore, the alignment system is expensive and involves great precision, which can ultimately raise the cost of the whole diagnostic kit. The portability of the detection system is also a concern regarding this system [44].
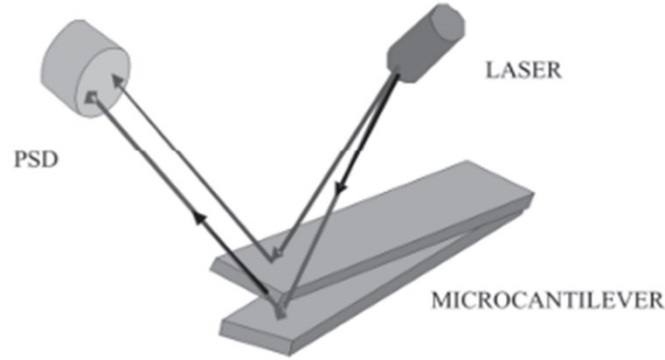
Figure 2.7: Schematic representation of a laser reflecting from a cantilever into a PSD detector. Reproduced with permission from [44]

The Piezoresistive Deflection Detection Method: When an external load creates bending in the cantilever, there are two types of stress occurred: tensile and compressive stress as mentioned in Figure 2.3. Tensile stress acts at the top of the cantilever and compressive stress occurs at the bottom of the cantilever. In order to obtain the stress change generated at the surface of the cantilever, a piezoresistive material is embedded near the top surface of the cantilever. When the cantilever deflects due to the applied mechanical stress, there will be a strain on the piezo resistor. The electrical resistance of the piezoresistive material changes according to this strain due to change in the stress of the microcantilever. The relative change in resistance as function of applied strain can be written as:

$$\frac{\Delta R}{R} = K_l K_t \delta_l \delta_t \tag{2.11}$$

where K denotes the Gage Factor, which is a material parameter[45]. The subscripts *l* and *t* refer to the longitudinal and the transversal part of the Gage Factor. The sensitivity of a piezo resistor

varies proportionally to the thickness t and the radius of curvature. The Gage Factor is proportional to Young's Modulus, E, which is the intrinsic characteristic of material. For a sensitive device, the gage factor should be of the order of 100.

The major advantage of the piezoresistive method is that the readout system can be integrated into the chip. The downside is that the deflection resolution for the piezoresistive readout system is only one nanometer compared with one Angstrom by optical detection method. Another added complication with the method is that a piezo resistor has to be embedded in the cantilever which
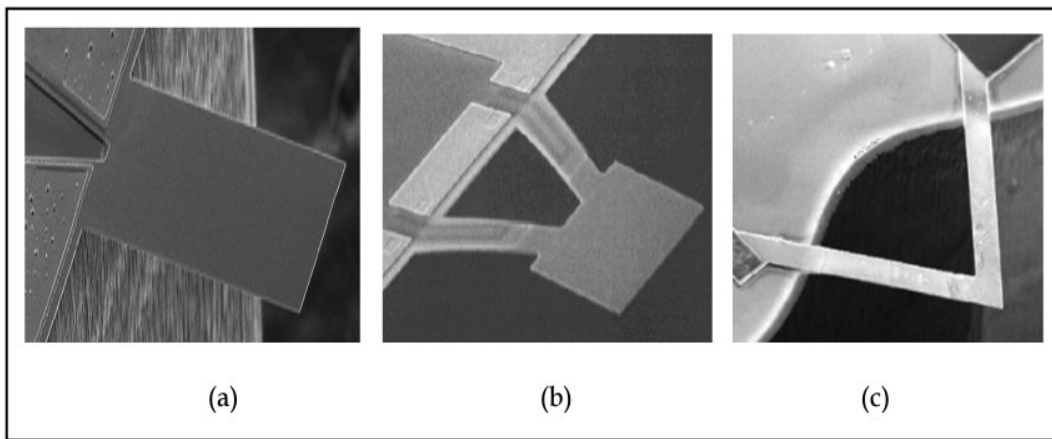
Figure 2.8: Common designs of piezoresistive MEMS cantilever available from literature studies such as rectangular shape, paddle pad and v-shape. Reproduced with permission from [45].

makes the fabrication complex. To achieve maximum sensitivity, the piezo-resistor material in the beam must be localized as close to one surface of the cantilever. The type of doping used to fabricate the piezoresistive material is also crucial in order to increase the sensitivity of piezoresistive MEMS cantilever, decreasing or making small dimension is the most popular approach in practice. However, this approach requires high precision lithography, and the equipment is very expensive, for example Micro/Nano Lithography machine [45].

The Capacitive Detection Method: The capacitive readout scheme is based on the principle that when the cantilever deflection takes place due to the adsorption of the analyte, the capacitance of a plane capacitor is changed. Here the microcantilever is one of the two capacitor plates. In a

capacitive sensing scheme, an AC voltage of frequency higher than that of the mechanical bandwidth of the cantilever is applied. The output current measured with respect to the applied voltage gives the capacitance value which is a measure of the displacement of the cantilever. The main advantages of capacitive microsensors are low-power high sensitivity, provides absolute displacement, simple structures, low temperature sensitivity and low-cost integration of the read out to the portable systems. It outdraws piezo-resistive systems because of its low power consumption. But this technique is not suitable for measuring large displacements [46]. Moreover, it does not work in electrolyte solutions due to the faradic currents between the capacitive plates. Therefore, it is limited in its sensing applications.

The Interferometry Deflection Detection Method: The interferometry method is an optical detection technique [21,22] based highly sensitive method that provides a direct and absolute measurement of the displacement of the microcantilever. This optical detection method is based on the interference of a reference laser beam with the laser beam reflected by the cantilever. The cleaved end of an optical fiber is brought close to the cantilever surface. One part of the light is reflected at the interface between fiber and surrounding media, and the other part is reflected at the cantilever back into the fiber. These two beams interfere inside the fiber, and the interference signal can be measured with a photodiode. In this method, light has to be brought close to the cantilever surface to get enough reflected light. Optical fiber few microns away from the free end of the microcantilever could measure deflection in 0.01 Å range. However, the positioning of the fibers is a difficult task. The method works well for small displacements but is less sensitive in liquids and hence, of limited use in biosensor applications [47].

2.2.3 Effect of surface stress and surface elasticity on the resonant frequency of the cantilever

Microfabricated beam cantilevers are proven to be versatile sensors, actuators, and transducers in physical, chemical, and biological applications due to their advantages of high sensitivity, enhanced reliability, fast response, reduced size, and low costs. The cantilever sensing methodologies are majorly based on the changes in physical quantities of the beam that are easily measured, such as deflection, resonance frequency, and quality factor. Therefore, it is important

to have a deeper understanding of the cantilever's response to the changes on the surface of the cantilever.

Adsorption on a functionalized surface of a microcantilever may cause mass addition, damping, and stress changes in the cantilever dynamics. The differential stress due to adsorption results in the cantilever's static bending and it was proposed as the most appealing method to detect biomolecular adsorption in liquids [48]. A shift in the resonance frequency during adsorption is often considered as a direct measure of the mass of the adsorbates on the cantilever surface by assuming that the spring constant remains fixed. Several studies such as the detection of a picogram mass of the particulates [49], and single vaccinia [50]virus using tiny cantilevers were done based on the frequency shift theory. Thundat and coworkers[51] calculated the relative number of adsorbates on the cantilever with picogram mass resolution. In many cases, however, adsorption also changes the spring constant of a microcantilever. Apart from having experimental evidence, the understanding of the influence of surface stress on the resonance frequency of a cantilever remained as minimal in the scientific community.

Surface stress can arise from several factors such as microscopic interactions of adsorbate on the surface, surface-environment interaction, or surface reconstruction. As the characteristic sizes of materials and sensors reduce to micrometers or nanometres and the surface or interface area to volume ration increases, the surface effects often play a crucial role in their mechanical behaviour [22]. There will be a difference in the physical properties and mechanical responses of surfaces with respect to the bulk of a material as the atoms on the surface layer are in a distinct local environment than the atoms in the bulk region [23]. This distinct local environment interaction of the surface layer atoms is considered as the origin of the surface elasticity and the residual surface tension for a material.

In a surface layer, the total surface stress, τ (mNm^{-1}), is given as follows

$$\tau = \sigma + C_s \varepsilon \qquad (2.12)$$

where ε is the dimensionless strain and C_s is the surface modulus (mNm^{-1}). In terms of thermodynamics, τ is a tensor that represents the reversible work to elastically stretch a pre-existing surface. τ, the total surface stress of the body arises from two factors, σ, and $C_s\varepsilon$; σ, which is strain independent, is often referred to as surface stress; C_s, which is strain dependent, is often referred to as surface elasticity. Surface elasticity is contributed by the formation of a surface layer that has different elastic properties from that of bulk. As mentioned earlier, surface layer formation depends on surface relaxation and sometimes surface reconstruction. Here, σ and C_s can be either positive or negative, which can thus either stiffen or soften a micro/nanostructure. In dynamics, the effect of the structure stiffness change (either stiffening or softening) is reflected in the shifts of the structure resonant frequencies.

With the strong evidence from more and more experimental results, it was found that surface effects significantly influence the resonance character and sensitivity of microcantilever devices. When a micromechanical cantilever is used as the detection platform for measuring the physical, chemical, or biological properties, the surface stress effect plays an important role in sensing and should be considered.

Early in 1975, it was estimated that the normal mode of vibration of GaAs thin crystals depends strongly on the surface preparation and the ambient atmosphere [36]. This phenomenon where the stiffness of the cantilever plates can be altered by varying surface stress was first reported by Lagowski [36]. This study proposed that surface stress is the reason behind the significant shift of resonant frequency of a microcantilever from those predicted by the axial load-free beam theory [36]. However, Gurtin et al. re-evaluated Lagowski's explanation by including a distributed traction over the beam surface caused by residual surface tension under bending [52]. Gurtin et al. stated that the resonant frequency is independent of surface stress (strain independent stress) and that surface elasticity is the only mechanism responsible for the resonant frequency shifts. Later, Lu et al. developed the model of Gurtin et al. to more general cases [53]. In some other studies, the surface stress was considered as an external loading and represented by a corresponding equivalent concentrated loading at the beam free end or uniformly distributed loading along the beam span [54].

The effect of surface stress is often considered as residual stress (strain independent stress), which can alter the structure bending stiffness, the morphology of the bending material, the resonant frequencies, etc. [55]. Recently, many theoretical investigations reported that both surface elasticity and surface stress influence structure stiffness [56–58]. Although the effect of surface elasticity is too small to explain the experimental observations, both surface elasticity and surface stress stand out when the structure dimensions are small as they are size dependent.

When Lagowski et al. [36] and McFarland et al. [23] explained the resonance frequency shift with the help of surface stress, they assumed zero surface elasticity in the problem. Whereas Gurtin et al. [52] explained the resonance frequency shift by implementing surface elasticity and zero surface stress. Gavan et al. were the first to introduce the two resonant frequencies of a microcantilever to determine the effects of surface elasticity and surface stress [59]. However, there were discrepancies in the fitting values in his model higher modes. Zhang et al. have developed two models to describe the effects of surface elasticity and surface stress on the frequency shift of a cylinder-like nanowire [55]. Prior to that, Wang and Feng suggested a three-layered beam model to investigate the effects of both surface elasticity and residual surface tension on microbeam vibration with the help of Young- Laplace equation [60]. The Young- Laplace equation was originally established to deal with the surface/interface tension of fluids. Gurtin et al. derived a continuum model of surface elasticity in which the Young- Laplace equation was extended to solid materials [61]. Chen et al. formulated the generalized Young- Laplace equation of curved surface in nanosized solids [62]. Wang et al had used the surface elasticity theory of Gurtin et al. and the Young- Laplace equation to investigate the effects of both surface elasticity and residual surface tension [22].

Later in 2008, He et al. approached the influence of surface stress on resonance bending nanowires by incorporating the generalized Young–Laplace equation into the Euler–Bernoulli beam theory and studying the solution for different boundary condition [63]. He explained that in small deformations, the distributed transverse force resulting from the surface stress along the nanowires longitudinal direction is considered a function of the curvature, and hence he accommodated the strain independent stress and the surface elasticity in the Euler–Bernoulli equation and validated the results [63].

For the liquid-based sensing, it is inevitable to take account of the molecular interactions on the cantilever such as the damping that adversely affects the quality factor of the cantilever. Hence microchannel cantilevers were introduced in which the liquid is kept inside the channel on the top of the plain cantilever and actuated in vacuum offering high quality factor.

The natural resonance frequency of a simple cantilever in the fundamental flexural mode is given by

$$\omega = \left(\frac{\alpha}{L}\right)^2 \sqrt{\frac{EI}{\rho A}}$$

(2.13)

where L denotes the cantilever length, $A = b \times h$ is cross-section with b and h being width and thickness, respectively. $I = bh^3/12$, E, ρ and α are geometric moment of inertia, young's modulus, mass density, and mode shape factor for the fundamental mode respectively.

This is obtained from the classical Euler–Bernoulli beam differential equation for a freely vibrating cantilever with deflection $w(x,t)$ and is given as

$$(\rho A)^* \frac{\partial^2 w(x,t)}{\partial t^2} + EI \frac{\partial^4 w(x,t)}{\partial x^4} = 0$$

(2.14)

In the case of a microchannel cantilever where a channel is placed on top of the plain beam resonator, geometrical factors will change the mechanical properties of the cantilever. The relation of frequency and mechanical parameters would change as follows

(2.15)

$$\omega = \left(\frac{\alpha}{L}\right)^2 \sqrt{\frac{(EI)^*}{(\rho A)^*}}$$

in which $(EI)^*$ and $(\rho A)^*$ are the effective modulus and effective mass respectively.

Very small changes in both mass and spring constant (EI) will affect the mechanical performance and changes the resonance frequency of the system. Changes in stiffness of the cantilever arises from various factors such as the change in dimension, material stiffness, viscosity of the liquid inside the cantilever and surface effects on the system.

In order to study the surface effects on the natural resonance frequency of microfluidic cantilever, we consider the combined effects of residual surface tension and interfacial tension. The problem is addressed on the basis of a surface layer-based theory taking into account of the origin of interfacial tension and residual surface stress.

Since the inner surface of the channel is in contact with the fluid, the system may be modelled as two homogeneous media, i.e., a bulk layer of silicon nitride in contact with a bulk layer of fluid. The Young's modulus of the channel and the fluid are denoted as E_H and E_f, respectively. The effective modulus $(EI)^*$ is then given by

$$(EI)^* = E_H I_H + E_f I_f \tag{2.16}$$

where I_H is the inertia moment of the hollow channel, and the I_f is the inertia moment of bulk fluid. Considering the effects of, σ and σ_{if} on all four walls of the channel respectively, the Young-Laplace equation on the surfaces yields

$$q_{channel}(x) = -(2\sigma \left(a + 2(b + c + g + e)\right)\frac{\partial^2 w}{\partial x^2}) \tag{2.17}$$

and

$$q_{fluid}(x) = -(4\sigma_{if}(d + g)\frac{\partial^2 w}{\partial x^2}) \tag{2.18}$$

where a, b, c, g and e are the characteristic dimension of the hollow channel. When channel is empty, σ_{if} becomes the same as σ. Here, positive $2\sigma \left(a + 2(b + c + g + e)\right)$ and $4\sigma_{if}(d + g)$ are considered as tensile stress and negative are compressive stress. In this case, since all surfaces

are exposed to surface stresses, the situation is complex and compressive stress is taken into consideration as it improves the model value towards the experimental value.

Thus, effective distributed loading can be formulated as,

$$q\,(x) = \; q_{channel}(x) + q_{fluid}(x) = -(2\sigma\,(a + 2(b + c + g + e))\frac{\partial^2 w}{\partial x^2} + 4\sigma_{if}(d + \quad \text{(2.19)}$$
$$g)\frac{\partial^2 w}{\partial x^2}$$

The equation of motion describing the motion of bending microfluidic channel incorporating the distributed transverse force in the Euler–Bernoulli beam theory is obtained as

$$(\rho A)^* \frac{\partial^2 w(x,t)}{\partial t^2} + EI^* \frac{\partial^4 w(x,t)}{\partial x^4} - q\,(x) = 0 \qquad \text{(2.20)}$$

and $(\rho A)^*$ is the effective density given as

$$(\rho A)^* = \; \rho A + \rho_f A_f \qquad \text{(2.21)}$$

in which ρ and ρ_f are the densities and A and A_f are the cross-sectional areas of the channel and fluids respectively. It is seen that both the surface elasticity and residual surface tension affect the dynamic behavior of the beam. The third term in the equation indicates that the influence of residual surface tensions is equivalent to a stretching axial loading $(2\sigma\,(a + 2(b + c + g + e))\frac{\partial^2 w}{\partial x^2} + 4\sigma_{if}(d + \; g)\frac{\partial^2 w}{\partial x^2}$ at the free end of the beam.

2.2.4 Photothermal effects on the dynamics of cantilever

A microfluidic cantilever filled with any liquid of interest can be used to characterize the thermal properties of the liquid. The analysis of the dynamics of a filled microfluidic cantilever that is irradiated by a laser of a specific wavelength can provide real-time thermomechanical property change of the liquid. The micro-fluidic cantilever can absorb the photons from the irradiating laser

leading to heat generation which in turn increases the temperature of the liquid inside the cantilever[64,65]. Hence, the mechanical property change of liquid and cantilever material caused by a rise in temperature will affect the dynamics of the system such as a change in frequency or bending of the cantilever. In this section, a theoretical understanding of photothermal excitation will be described for a bimetallic cantilever, bimetallic microfluidic cantilever, and a simple microfluidic cantilever. We will briefly discuss the effect of thermomechanical change of the fluid-cantilever system on the static bending as well as the frequency shift of the cantilever. The details about the effect of change in geometry, modulus, and density of the fluid-cantilever system upon photothermal heating on the dynamics of the system will be discussed later in this section. The thermal stress generated because of the liquid expansion inside the micro-cantilever is incorporated in the modified Euler- Bernoulli equation and the effective frequency shift is described in this section.

Basics of Photothermal Effects: The photothermal effect on the cantilever relies on the photo-induced change in the thermal state of the cantilever. When a laser with a specific wavelength is focused on the microcantilever, it has some influence on the mechanical response of the cantilever: absorption of radiation contributes to the local heating of the cantilever. This heating not only changes the temperature but also changes the thermodynamic parameters of the sample that are related to temperature.

The photothermal effect was primarily noticed in bi-material cantilevers which are made of two different materials of different thermal properties as shown in Figure 2.9. For example, silicon microcantilevers with a thin gold film on one side undergo measurable bending in response to temperature changes. This phenomenon is frequently referred to as the ''bimetallic effect''. Here, the differential stress in the cantilever is created due to dissimilar thermal expansion coefficients of the silicon substrate and the gold coating. It has been estimated that the smallest heat change that can be detected using bimaterial microcantilevers lies in the femtojoule range.
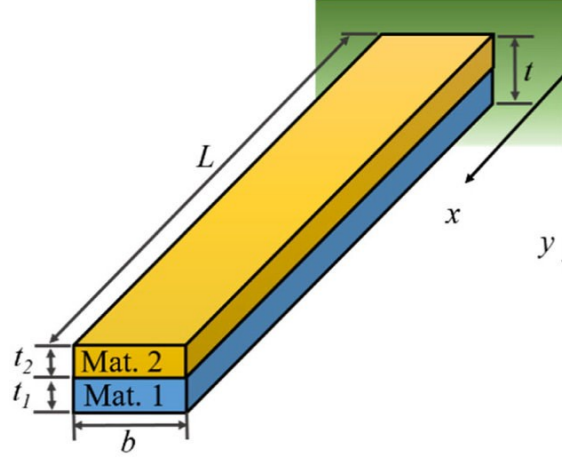
Figure 2.9: Schematic diagram of a bi-material cantilever. Reproduced with permission from [66]

When the temperature of the bi-material cantilever is increased by intrinsic or extrinsic heating, the deflection of the bi-material cantilever due to thermal stress is given by

$$\frac{d^2z}{dx^2} = 6(\alpha_1 - \alpha_2)\left(\frac{t_1+t_2}{t_2^2 K}\right)[T(x_0) - T] \qquad (2.22)$$

where

$$K = 4+6\left(\frac{t_1}{t_2}\right) + 4\left(\frac{t_1}{t_2}\right)^2 + \left(\frac{E_1}{E_2}\right)\left(\frac{t_1}{t_2}\right)^3 + \left(\frac{E_2}{E_1}\right)\left(\frac{t_2}{t_1}\right) \qquad (2.23)$$

$z(x)$ is the vertical deflection, $(T(x_0)$-T) is the temperature difference between the cantilever and ambient temperature at a location x along the length of the cantilever, α_1, α_2 and t_1 and t_2 are the coefficients of thermal expansion and the thickness of the bi-material constituents, respectively[65]. T_0 is the temperature of the cantilever at zero deflection while $T(x)$ is the temperature profile of the cantilever along its length.

Photothermal excitation of microcantilever is often non-destructive and non-contact and can be used to probe optical and thermal properties of the sample in very small areas. The use of micromachined bimorph structures as temperature sensors can be dated back to 1980's and since then they have been extensively investigated as sensitive thermal platforms. The first demonstration of this principle in bimaterial microcantilevers for temperature was done by Gimzewski et al. in a micromechanical calorimetric application to study the chemical reaction of

H2 + O2 to form H2O over a Pt-coated microcantilever [67]. They have estimated sensitivity limit of picojoule (pJ) and a temperature resolution of 10^{-5}K [67]. An energy resolution of 150 fJ and a sensitivity of 100 pW in a femtojoule calorimeter was discovered by Barnes et al. followed by the first photothermal spectroscopy application to detect dye molecules present on cantilever surface[9].Extensive research was carried out to optimize the performance and explore microcantilever platform for thermal sensing applications when Majumdar's group optimized the sensitivity limits of 40 pW and 10 fJ [68]. Thundat's group from ORNL made significant contributions in identification and detection of trace amounts of various surface adsorbed analytes such as biological warfare agents, biological species, nerve gas stimulants, organic and polymer adsorbates using microcalorimetric spectroscopy techniques [69,70]. However, detection in a liquid environment was challenging due to damping forces resulting in low-quality factor and poor signal.

Microfluidic channel-integrated cantilevers introduced by Manalis group overcome the limitations of liquid damping in the dynamic mode operation, and thus achieves unprecedented precision in thermomechanical characterization with enhanced signal stability [71]. A BMC concept was adapted for microfluidic cantilevers to study photothermal excitation of fluid-filled cantilevers as shown in Figure 2.10.
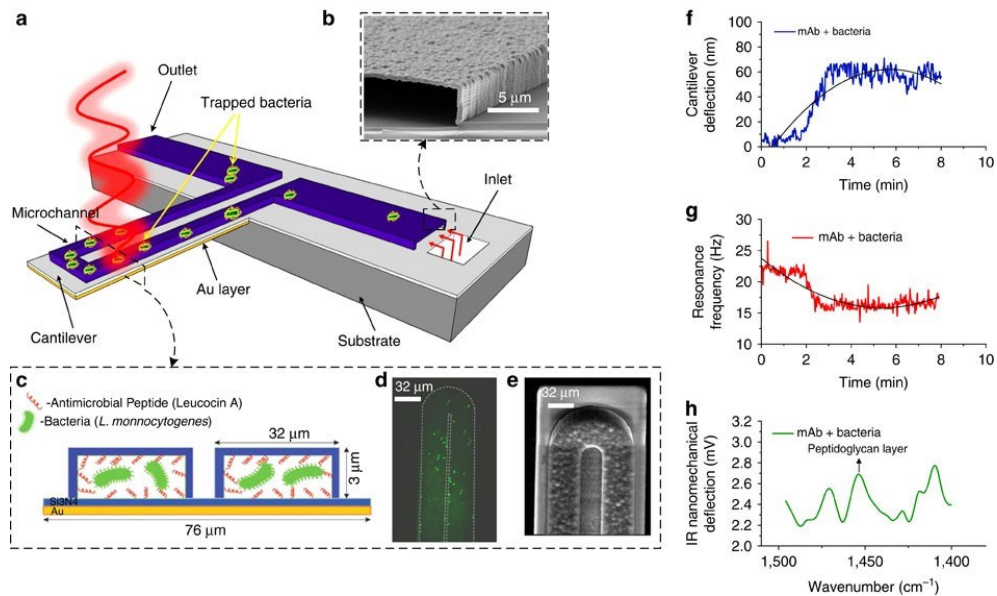
Figure 2.10: BMC filled with bacteria supported on a silicon substrate. Reproduced with permission from [72]

For the analytes in liquid states, the resonance frequency of the BMC is highly sensitive to their density. A general resonance behavior of a BMC can be described by:

$$2\pi f = wr = \sqrt{\frac{k}{m}}$$

(2.24)

where k is the spring constant and m is the mass of the cantilever. Once the liquid analyte is loaded in the BMC, the resonance frequency decreases. The total mass is given as:

$$m = m_{BMC} + m_L = V_{BMC}\rho_{BMC} + V_L\rho_L$$

(2.25)

where m_{BMC} and m_L are the mass of BMC and the liquid analyte, respectively. superscripts, V and ρ represent volume and density, respectively. Considering that V_{BMC}, ρ_{BMC} and V_L remain constant during the measurement, the density can be estimated from: $w_r = \frac{A}{\sqrt{B+\rho_f}}$ where the A and B are the calibration constants and determined from measurement of two well-known liquids [65,73].

BMC deflection is proportional to multiple factors, including the thermomechanical sensitivity of the device, the optical intensity, the irradiation time, the light absorption coefficient of a sample inside the microchannel, the thermal properties of the sample, and the difference between the thermal expansion coefficients of the constituting materials. However, the selection of the proper bi-material elements and optimization of thickness of the layers are limiting factors while considering BMC cantilevers for thermal sensitivity experiments. Also, the bending response of resonators based on static mode where the results are prone to be affected by mechanical drift and higher noise level of the photodetector have brought need of the simpler experimental model and dynamic response.

In dynamic mode, the thermal properties of the confined liquid analytes are characterized by the resonation frequency shift, whereas the shift is driven by the stress due to thermal expansion/contraction of the analyte. In explaining the thermally induced bending of BMCs with an analytical model, Tamayo et al. introduced the concept of differential surface stress [74]. In

addition, He and Lilley approached the influence of surface stress on resonance bending nanowires by incorporating the generalized Young-Laplace equation into Euler-Bernoulli beam theory and studying the solution for different boundary conditions [63] . They considered that the distributed transverse force resulting from the surface stress along the nanowires longitudinal direction is considered as a function of the curvature in small deformations. Hence, the strain-independent stress and the surface elasticity in the Euler-Bernoulli equation are accommodated by the concept of surface stress. The effect of interfacial tension on the resonance frequency of the micro-fluidic channel has been discussed with the inclusion of the Young-Laplace equation in the Euler-Bernoulli equation in a recent study. In the present work, we hypothesized that the thermal stress generated by the liquid inside the microchannel cantilever exerts transverse force acting along the longitudinal direction of the deformed beam that modulates the effective modulus of the cantilever system.

2.3 Phase Transition of PNIPAM in Water with or without Clay

In this section, materials and known phase behaviors of the PNIPAM/water/clay system are reviewed. The purpose of this review is to provide scientific background to understand the facilitated sedimentation behavior of clay particles by the aid of temperature-induced phase transformation of PNIPAM in water. Adding PNIPAM to clean up clay particles is an active area of research in the oil sands industry, where cleaning up the contaminated clay in tailing ponds is a big environmental issue. Subsections in this section includes the introductions of (i) clay particles to understand their structure and surface properties, (ii) electrical double-layer theory and (iii) mechanisms of coagulation and flocculation to understand the behavior of clay particles in the aqueous solution, (iv) phase transition of thermosensitive polymer and (v) properties that are specific to PNIPAM to understand the temperature-dependent phase transition behavior of the polymer in water.

2.3.1 Clays: Structure and Surface Properties

The major component among the fine particles in MFT is clay. Clay fines, bitumen residues and their associated effects cause the formation of MFT. Typical characteristics of clays include high

specific surface area, platelet-like morphology, and anisotropic dimensions. It is important to understand the properties of clays as they affect the bitumen recovery process and MFT dewatering [75].

The major clay minerals in MFT are kaolin and illite, but a small fraction of montmorillonite and smectite clays may also be present in clay fines [75]. Clay minerals are layered-structure materials consisting of periodically stacked tetrahedron sheets of silicon-oxygen and an octahedron sheet of aluminum-oxygen-hydroxyl as building blocks. Distinctive arrangements of the tetrahedron and octahedron sheets can result in different types of clays. Kaolinite is formed by two-layer structures, whereas illite by three-layer structures, as shown in Figure 2.11.
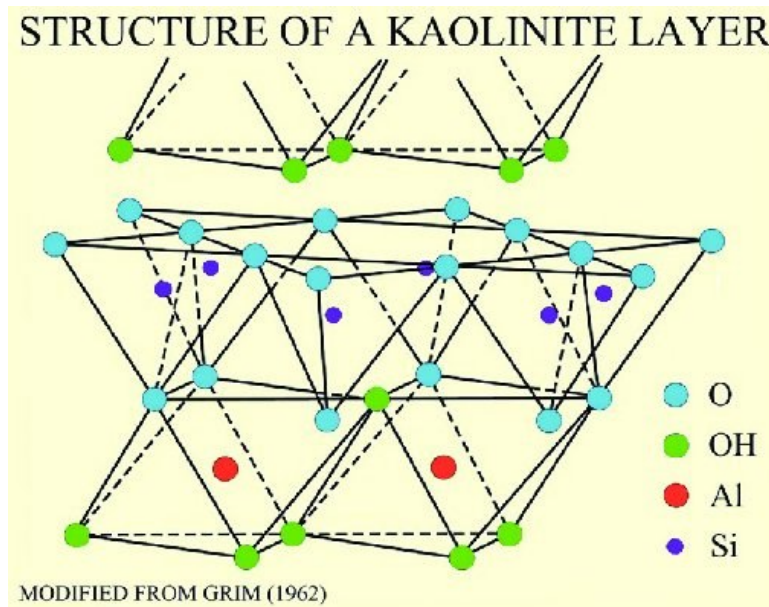
Figure 2. 11: Layer structure of kaolinite clays. Reproduced with permission from [76]

The two layers in Kaolinite are covalently bonded to each other through the oxygen atoms in the tetrahedron sheet. Throughout the mineral, there is a tetrahedral octahedral (TO) layered structure with tight packing between the layers [76]. This tight packing – like the pages of a closed book – results in Kaolinite not shrinking when dry or swelling when wet. Although Kaolinite and illite clays do not expand/swell, a small fraction of smectite clays (such as montmorillonite) in MFT undergoes significant expansion and forms a gel-like slurry due to

tetrahedral/octahedral/tetrahedral (TOT) sheet structure [75,76]. The tetrahedron and octahedron layers in Kaolinite carry permanent negative charges arising from the isomorphic substitution of higher valance cations by lower valance cations that create a charge deficiency. As MFT contains a mixture of both two- and three-layer clays, it shows strong negative zeta potential that causes colloidal stabilization [75].

2.3.2 Electrical Double Layer: (DLVO) Theory

The stability of clay dispersions is controlled largely by the colloidal interaction forces between clay mineral particles. Although MFT clays have negative charges, the water present in MFT also carries an electric charge, equal and opposite in sign to that on the MFT solids. The absolute values of charges on the clay surfaces and water are the same, and collectively form a system of charges known as the electric double layer (EDL). The EDL consists of several layers. The first layer is called the Stern layer and the electric potential at this layer is called Stern potential. The second layer of ions in solution is called the diffuse layer and the potential at the diffuse layer is called the zeta potential. A schematic for the EDL of a spherical negatively charged particle is given in Figure 2. 12. The variation of electric potential in the double layer as a function of the distance from the particle surface is shown in the embedded plot in the Figure. Ions in the diffuse layer are affected by electric interactions with the charged surface and thermal motion [75].
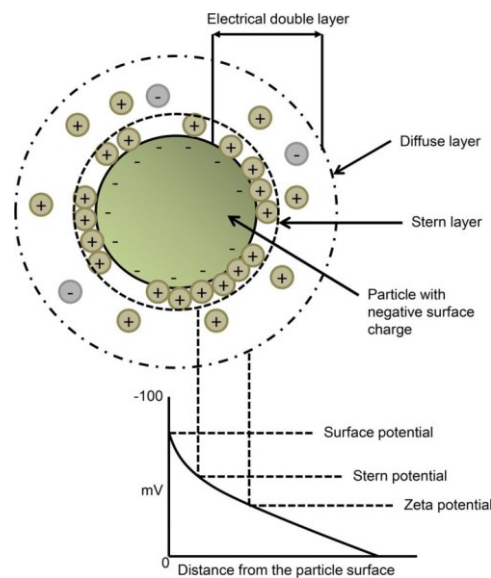
Figure 2.12: Schematic of the electric double layer and a graph of electric potential in the double layer as a function of distance from the particle surface. Reproduced with permission from [75]

According to DLVO theory, the energy of a colloidal system is the sum of attractive van der Waals energy and repulsive double layer energy as shown in Eq 2.26.

$$E = EvdW + EDL \qquad (2.26)$$

Although hydrodynamic forces are ignored in the DLVO theory, the stability of the system can be characterized based on the net interaction resulting from the attraction and repulsion between the particles. A system is considered a stable suspension if the net interaction between the particles is repulsive. If the net interaction is attractive, the system is said to be unstable and may coagulate. In the context of MFT consolidation and dewatering, the DLVO theory can help design flocculants that effectively aggregate the solids, and subsequently dewater them. Repulsive forces arising from the electrical double layer significantly contribute to the stability of MFT. An effective flocculant would compress the electrical double layer and cause MFT to sediment [75].

2.3.3 Coagulation and Flocculation Mechanisms

Coagulants (mainly multivalent inorganic cations) suppress the electrical double layer, thereby allowing van der Waals attractive forces to bring and hold particles together as shown in Figure 2.13. Hence, coagulants reduce the energy barrier that prevents particles from approaching each other. This energy barrier becomes zero at a critical coagulant concentration [75]. The critical concentration depends on valence of the electrolyte used as a coagulant. The higher the valance, the lower the coagulant concentration needed to reach the zero-energy barrier.

When an overdose of a coagulant is applied, the ions can adsorb on the clay surface and revert the net surface charge, inducing repulsive forces leading to detrimental state. The settling rate is also affected by coagulant concentration, and it decreases due to coagulant overdosing beyond a maximum. Although the addition of acid or base would result in similar behaviors, it is practically impossible to implement from a practical point of view, as it will require large amounts of acid or

base. Potassium alum, aluminum sulfate, and gypsum are frequently used as coagulants in the industry.

Flocculation refers to the macroscopic aggregation of suspended particles into loosely packed flocs by addition of a polymeric flocculant [77]. Flocs with a higher density than the surrounding medium settle rapidly and produce clear supernatants under optimal conditions. Polymeric flocculants cause finely divided particles to agglomerate and segregate into flocs as shown in Figure 2.13. Polymeric chains adsorb one or more sites of clay particles present in MFT via hydrogen bonding and electrostatic interactions. Aggregates formed by flocculation have structures that are more open than those formed by coagulation due to the high molecular weight of the polymer. Often, this open structure causes flocs to hold a large amount of water within the aggregates. In flocculation, the proper design of the architecture of the polymer molecules is very important to control adsorption and subsequent polymer configuration on the clay surfaces. An ideal case may be charged polymers with an optimum charge density because they have sufficient chain flexibility to form loops with moderate binding forces [78].
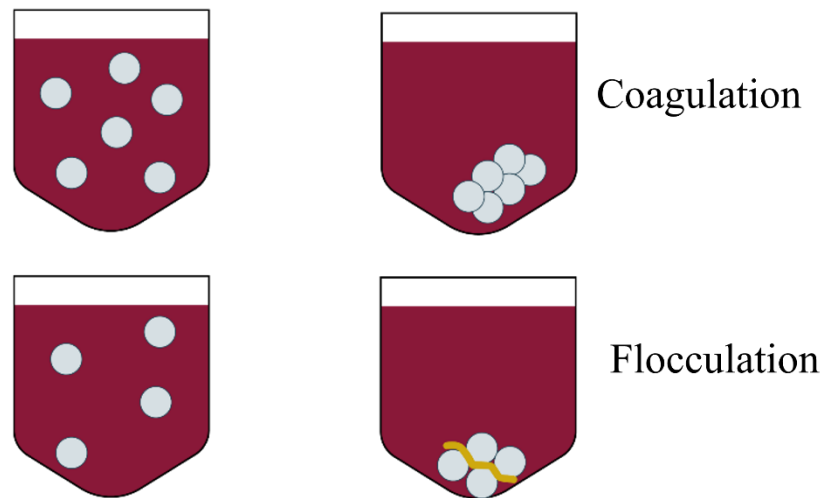
Figure 2.13: Schematic of coagulation and flocculation mechanism

2.3.4 Thermo-sensitive polymer

Stimulus-responsive polymers are polymeric materials that exhibit reversible property changes in response to a small external stimulus such as temperature, pH, ionic strength, mechanic constraints, electric field or light (UV exposure). All the stimuli driven transitions are completely reversible giving rise to switch on/off structural changes. Among different classes of stimuli-responsive polymers, thermo-responsive polymers are of special interest because of their wide applications in water treatment [79], biomedical [80] and flocculation applications [81].

Thermo-responsive polymers exhibit a drastic change in their solubility with respect to temperature, and thus their conformation alter significantly. Thermo-responsive polymers are divided into two groups based on their miscibility gap: polymers with an upper critical solution temperature (UCST) and polymers with a lower critical solution temperature (LCST) [80]. If the miscibility gap is found at a lower temperature and the polymer phase-separates above the critical temperature, the critical temperature is called a LCST of the polymer; if the solution is miscible above the critical temperature, the critical solution temperature is called UCST. In cases of atomic mixture or low molecular mixture systems, high mixing entropy facilitates the mixing between the components at high temperatures so that UCST is a common behavior. In high molecular polymer blends and polymer-water mixture systems, however, UCST behavior is rather uncommon [82–85]. In polymer-water mixture systems, the hydrogen bonding interactions between the hydrophilic segment of the polymer and the water molecules, as well as 'water shell' forming around hydrophobic segment of the polymer due to the hydrogen bonding between water molecules, tend to prevail at lower temperatures. At higher temperatures, the effect of these hydrogen bonding is weakened due to increased entropy, and thus the polymer chains tend to collapse to facilitate the LCST behavior. The temperature-dependent conformation changes of a polymer chain that exhibit LCST in water is Figure 2.14.

The transition from coil to globule confirmation of an LCST polymer is visible to the eyes because the polymer-water mixture is transparent and homogenous when the temperature is below LCST and cloudy when above LCST [80]. Hence, LCST is often referred as cloud point. The critical temperature of LCST polymers can be influenced by the nature of the side groups, chain length and molecular weight. Also, LCST is also affected by three external factors such as salt

concentration, co-solvents and surfactants due to the additives, which will alter the hydrogen bonding interactions between polymers and solvent [80].
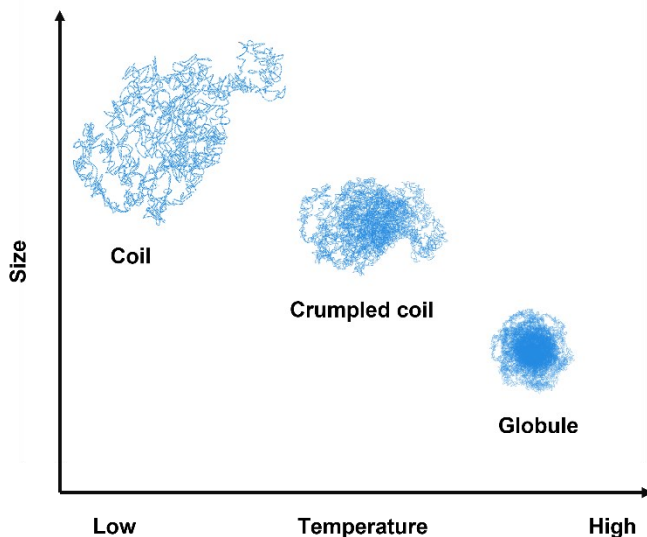
Figure 2.14: Schematic of coil to globule transition of a homopolymer in an extremely dilute aqueous solution [86]

2.3.5 PNIPAM

The most studied thermo-responsive polymer, poly (N-isopropylacrylamide) (PNIPAM), is first reported in 1950s [87] and remains as thermos responsive polymer par excellence. The versatility of PNIAPM has led to exploring applications in tissue engineering [88], drug delivery [89], biosensors [90], and water treatment [79]. The solutions of PNIPAM exhibits a fast and reversible phase transition phenomena as part of its thermo-responsiveness. In PNIPAM, the isopropyl moiety along with the carbon chain backbone is hydrophobic whereas the amide moiety is hydrophilic, as shown in Figure 2.15 [91].

PNIPAM has a lower critical solution temperature (LCST) temperature of 32 $^{\circ}$C [92]. It quickly dissolves in water at room temperature and the polymer chains are hydrated below the LCST producing a transparent solution [92]. At this temperature, PNIPAM exhibits a coil conformation due to hydrogen bonding between the hydrophilic group and water [87]. Near the LCST, the

hydrophilicity of the polymer starts to decrease; the hydrogen bonding weakens and the hydrophobic interaction between the adjacent groups dominates.
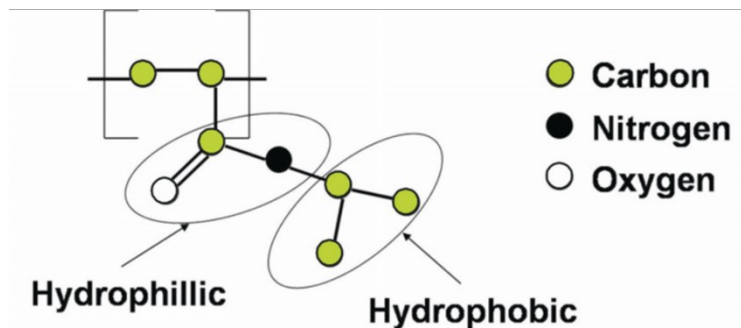
Figure 2.15 Structure of PNIPAM with hydrophobic and hydrophilic ends. Reproduced with permission from [94]

This results in release of water molecules leading to the compression of the whole polymer network and PNIPAM taking a globular conformation. Hence, a minute increase in temperature above LCST results in the chain collapse creating an abrupt and reversible change in refractive index of the solution [92]. This change is directly associated with the coil-globule phase transition of PNIPAM due to the release of polymer-bound water molecules into bulk water [86].

When the globules aggregate into larger particles, they scatter light in the visible range [92]. The polymer solution which was initially clear becomes turbid. During cooling to temperatures below LCST, the hydrophilicity of the polymer increases again, resulting in an uptake of water molecules and an expansion of the polymer network. For a single PNIPAM particle, the compression and expansion result in a decrease or increase of particle size during the coil-to-globule or globule-to-coil transition process, respectively [93]. The variation in hydrodynamic radius and radius of gyration of PNIPAM is presented in on of the pioneer studies by Wu et al and is given in Figure 2.16 [86]. Werner et al investigated the coil-to-globule transition of highly concentrated PNIPAM particle suspensions and discovered an agglomerate formation immediately after coil to globule transformation without any addition of salt or nonadsorbing polymers [93]. The detected agglomeration of the PNIPAM particles to these large agglomerates during the heating period is reversible. Optical images of PNIPAM suspension are visualized by particle vision microscope

(PVM), as shown in Figure 2.17 [93]. PVM is a probe-based in-line microscope, applied to directly visualize suspended structures (e.g., particles, droplets, or cells) within a process. The instrument can be operated in reflection or transflection mode. In addition, a relative backscatter index (RBI) can be obtained. The RBI is an area-based turbidity signal, deduced from the obtained images.
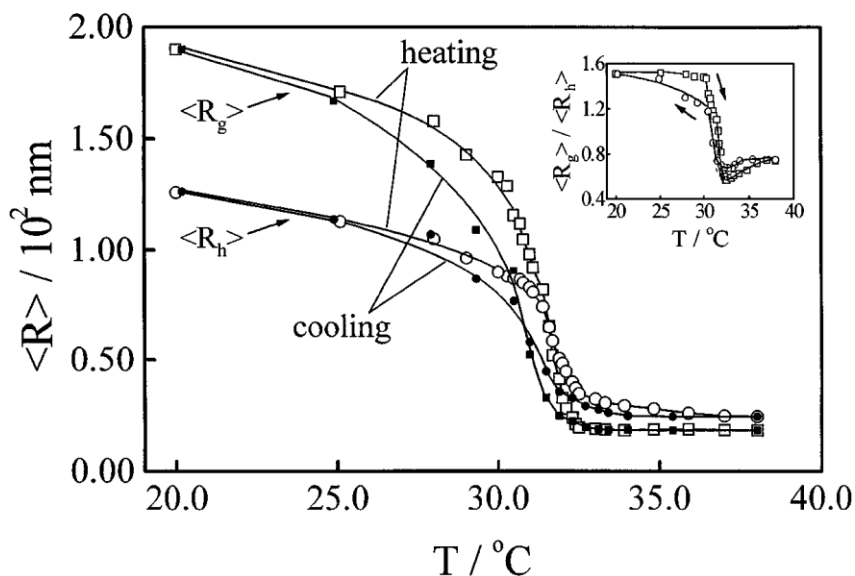
Figure 2.16: Temperature dependence of the average radius of gyration $\langle R_g \rangle$ and the average hydrodynamic radius $\langle R_h \rangle$, respectively, in the coil-to-globule (heating) and the globule to- coil (cooling) processes. Reproduced with permission from [86]
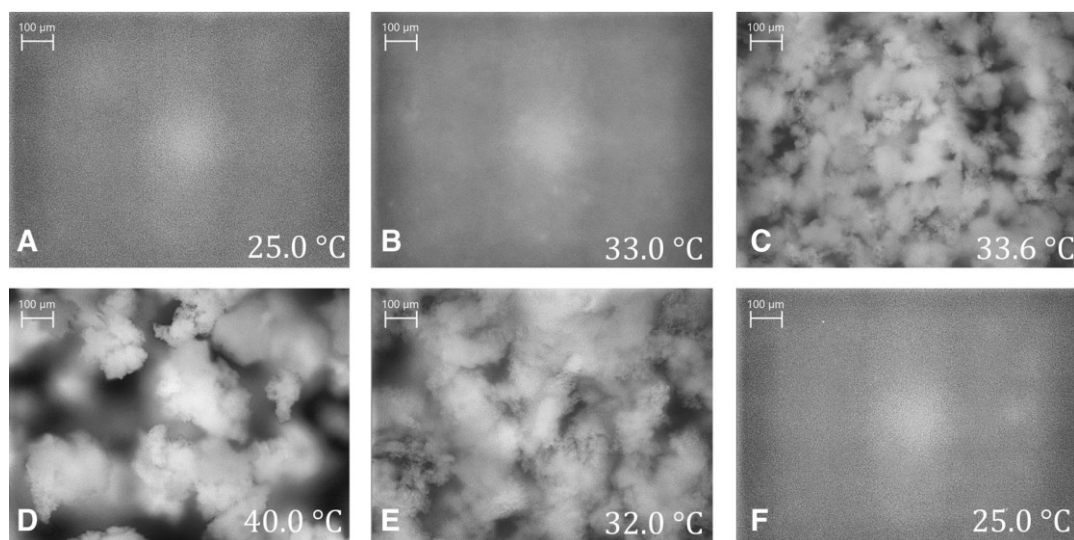
Figure 2.17: PVM images at specific temperatures of the PNIPAM suspension upon heating (A to D) and cooling (D to F). Reproduced with permission from [93]

48

2.5 References

[1] M.F. Khan, S. Schmid, Z.J. Davis, S. Dohn, A. Boisen, Fabrication of resonant micro cantilevers with integrated transparent fluidic channel, Microelectron Eng. 88 (2011) 2300–2303. https://doi.org/10.1016/J.MEE.2011.02.096.

[2] B. Guruprasad, M.G. Veena, Analysis of MEMS cantilever sensor for sensing volatile organic compounds, Micro and Nano Engineering. 16 (2022) 100143. https://doi.org/10.1016/J.MNE.2022.100143.

[3] D. Klaitabtim, A. Tuantranont, Design consideration and finite element modeling of MEMS cantilever for nano-biosensor applications, 2005 5th IEEE Conference on Nanotechnology. 1 (2005) 311–314. https://doi.org/10.1109/NANO.2005.1500758.

[4] K.S.N. Murthy, G.R.K. Prasad, N.L.N.V. Saikiran, T.V.S. Manoj, Design and simulation of MEMS biosensor for the detection of tuberculosis, Indian J Sci Technol. 9 (2016). https://doi.org/10.17485/IJST/2016/V9I31/90638.

[5] M. Chaudhary, A. Gupta, Microcantilever-based sensors, Def Sci J. 59 (2009) 634–641. https://doi.org/10.14429/DSJ.59.1569.

[6] K. Beulah Sujan, T. Shanmuganantham, Bio-MEMS cantilever sensor design and analysis for detecting multiple diseases, IEEE International Conference on Circuits and Systems, ICCS 2017. 2018-January (2018) 206–210. https://doi.org/10.1109/ICCS1.2017.8325991.

[7] M. Rahaeifard, Static behavior of bilayer microcantilevers under thermal actuation, Int J Eng Sci. 107 (2016) 28–35. https://doi.org/10.1016/J.IJENGSCI.2016.07.007.

[8] N. Inomata, M. Toda, M. Sato, A. Ishijima, T. Ono, Pico calorimeter for detection of heat produced in an individual brown fat cell, Appl Phys Lett. 100 (2012). https://doi.org/10.1063/1.3701720.

[9] J.R. Barnes, R.J. Stephenson, M.E. Welland, C. Gerber, J.K. Gimzewski, Photothermal spectroscopy with femtojoule sensitivity using a micromechanical device, Nature. 372 (1994) 79–81. https://doi.org/10.1038/372079A0.

[10] G. Binnig, C.F. Quate, C. Gerber, Atomic force microscope, Phys Rev Lett. 56 (1986) 930–933. https://doi.org/10.1103/PHYSREVLETT.56.930/FIGURE/1/THUMB.

[11] A. Bahri, M. Martin, C. Gergely, M. Pugnière, D. Chevalier-Lucia, S. Marchesseau, Atomic Force Microscopy Study of the Topography and Nanomechanics of Casein Micelles Captured by an Antibody, Langmuir. 33 (2017) 4720–4728. https://doi.org/10.1021/ACS.LANGMUIR.7B00311/ASSET/IMAGES/MEDIUM/LA-2017-00311S_0008.GIF.

[12] L.J.C. Jeuken, AFM Study on the Electric-Field Effects on Supported Bilayer Lipid Membranes, Biophys J. 94 (2008) 4711. https://doi.org/10.1529/BIOPHYSJ.107.122887.

[13] D. Vokoun, S. Samal, I. Stachiv, Magnetic Force Microscopy in Physics and Biomedical Applications, Magnetochemistry. 8 (2022). https://doi.org/10.3390/magnetochemistry8040042.

[14] J. Liu, X. Wang, W. Zhang, Atomic Force Microscopy Imaging Study of Aligning DNA by Dumbbell-like Au-Fe 3 O 4 Magnetic Nanoparticles, Langmuir. 34 (2018) 14875–14881. https://doi.org/10.1021/ACS.LANGMUIR.8B01784/SUPPL_FILE/LA8B01784_SI_001.PDF.

[15] T. Thundat, R.J. Warmack, G.Y. Chen, D.P. Allison, Thermal and ambient-induced deflections of scanning force microscope cantilevers, Appl Phys Lett. 64 (1998) 2894. https://doi.org/10.1063/1.111407.

[16] D. Aruna Mastani, D. Anitha, MEMS Microcantilevers Sensor Modes of Operation and Transduction Principles, 2014. http://www.ijces.com/.

[17] A.W. McFarland, M.A. Poggi, M.J. Doyle, L.A. Bottomley, J.S. Colton, Influence of surface stress on the resonance behavior of microcantilevers, Appl Phys Lett. 87 (2005).

[18] M.Z. Ansari, C. Cho, Deflection, frequency, and stress characteristics of rectangular, triangular, and step profile microcantilevers for biosensors, Sensors. 9 (2009) 6046–6057. https://doi.org/10.3390/S90806046.

[19] J. Mouro, R. Pinto, P. Paoletti, B. Tiribilli, Microcantilever: Dynamical Response for Mass Sensing and Fluid Characterization, Sensors 2021, Vol. 21, Page 115. 21 (2020) 115. https://doi.org/10.3390/S21010115.

[20] D. Ramos, J. Mertens, M. Calleja, J. Tamayo, Study of the origin of bending induced by bimetallic effect on microcantilever, Sensors. 7 (2007) 1757–1765. https://doi.org/10.3390/S7091757.

[21] M. Godin, V. Tabard-Cossa, P. Grutter, Quantitative surface stress measurements using a microcantilever, American Institute of Physics. 79 (2001) 551–553.

[22] J. Wang, Z. Huang, H. Duan, S. Yu, X. Feng, G. Wang, W. Zhang, T. Wang, Surface stress effect in mechanics of nanostructured materials, Acta Mechanica Solida Sinica. 24 (2011) 52–82. https://doi.org/10.1016/S0894-9166(11)60009-8.

[23] A.W. McFarland, M.A. Poggi, M.J. Doyle, L.A. Bottomley, J.S. Colton, Influence of surface stress on the resonance behavior of microcantilevers, Appl Phys Lett. 87 (2005) 1–4. https://doi.org/10.1063/1.2006212.

[24] M.J. Lachut, J.E. Sader, Effect of surface stress on the stiffness of cantilever plates, Phys Rev Lett. 99 (2007). https://doi.org/10.1103/PhysRevLett.99.206102.

[25] P. Lu, H.P. Lee, C. Lu, S.J. O'Shea, Surface stress effects on the resonance properties of cantilever sensors, Phys Rev B Condens Matter Mater Phys. 72 (2005). https://doi.org/10.1103/PhysRevB.72.085405.

[26] Q. Ren, Y.P. Zhao, Influence of surface stress on frequency of microcantilever-based biosensors, Microsystem Technologies. 10 (2004) 307–314. https://doi.org/10.1007/s00542-003-0329-4.

[27] Q. Ren, Y.P. Zhao, Influence of surface stress on frequency of microcantilever-based biosensors, Microsystem Technologies. 10 (2004) 307–314. https://doi.org/10.1007/s00542-003-0329-4.

[28] J.Q. Zhang, S.W. Yu, X.Q. Feng, G.F. Wang, Theoretical analysis of adsorption-induced microcantilever bending, J Appl Phys. 103 (2008). https://doi.org/10.1063/1.2912727.

[29] D.W. Dareing, T. Thundat, Simulation of adsorption-induced stress of a microcantilever sensor, J Appl Phys. 97 (2005). https://doi.org/10.1063/1.1853496.

[30] G.Y. Huang, W. Gao, S.W. Yu, Model for the adsorption-induced change in resonance frequency of a cantilever, Appl Phys Lett. 89 (2006). https://doi.org/10.1063/1.2236102.

[31] G.Y. Huang, W. Gao, S.W. Yu, Model for the adsorption-induced change in resonance frequency of a cantilever, Appl Phys Lett. 89 (2006). https://doi.org/10.1063/1.2236102.

[32] G.Y. Chen, T. Thundat, E.A. Wachter, R.J. Warmack, Adsorption-induced surface stress and its effects on resonance frequency of microcantilevers, J Appl Phys. 77 (1995) 3618–3622. https://doi.org/10.1063/1.359562.

[33] K. Jiang, F. Khan, J. Thomas, P.R. Desai, A. Phani, S. Das, T. Thundat, Thermomechanical responses of microfluidic cantilever capture DNA melting and properties of DNA premelting

states using picoliters of DNA solution, Appl Phys Lett. 114 (2019). https://doi.org/10.1063/1.5092333.

[34] K. Zhang, Q. Zhu, Z. Chen, Effect of distributed mass on the node, frequency, and sensitivity of resonant-mode based cantilevers, Sensors (Switzerland). 17 (2017). https://doi.org/10.3390/s17071621.

[35] N. Miriyala, Photothermal effects in micro/nano electromechanical systems, n.d.

[36] J. Lagowski, H.C. Gatos, E.S. Sproles, Surface stress and the normal mode of vibration of thin crystals: GaAs, Appl Phys Lett. 26 (1975) 493–495. https://doi.org/10.1063/1.88231.

[37] M.E. Gurtin, X. Markenscoff, R.N. Thurston, Effect of surface stress on the natural frequency of thin crystals, Appl Phys Lett. 29 (1976) 529–530. https://doi.org/10.1063/1.89173.

[38] I. Lee, J. Lee, Quality factor and vibration amplitude based viscosity measurements using suspended microchannel resonators, (2012) 1–4.

[39] M. Faucher, B. Walter, A.S. Rollier, K. Seguini, B. Legrand, G. Couturier, J.P. Aimé, C. Bernard, R. Boisgard, L. Buchaillot, Proposition of atomic force probes based on silicon ring-resonators, TRANSDUCERS and EUROSENSORS '07 - 4th International Conference on Solid-State Sensors, Actuators and Microsystems. (2007) 1529–1532. https://doi.org/10.1109/SENSOR.2007.4300436.

[40] T.P. Burg, S.R. Manalis, Suspended microchannel resonators for biomolecular detection, Appl Phys Lett. 83 (2003) 2698–2700. https://doi.org/10.1063/1.1611625.

[41] T.P. Burg, M. Godin, S.M. Knudsen, W. Shen, G. Carlson, J.S. Foster, K. Babcock, S.R. Manalis, Weighing of biomolecules, single cells and single nanoparticles in fluid, Nature. 446 (2007) 1066–1069. https://doi.org/10.1038/nature05741.

[42] W.H. Chu, M. Mehregany, R.L. Mullen, Analysis of tip deflection and force of a bimetallic cantilever microactuator, Journal of Micromechanics and Microengineering. 3 (1993) 4–7. https://doi.org/10.1088/0960-1317/3/1/002.

[43] A. Wig, E.T. Arakawa, A. Passian, T.L. Ferrell, T. Thundat, Photothermal spectroscopy of Bacillus anthracis and Bacillus cereus with microcantilevers, Sens Actuators B Chem. 114 (2006) 206–211. https://doi.org/10.1016/j.snb.2005.04.029.

[44] L.Y. Beaulieu, M. Godin, O. Laroche, V. Tabard-Cossa, P. Grütter, A complete analysis of the laser beam deflection systems used in cantilever-based systems, Ultramicroscopy. 107 (2007) 422–430. https://doi.org/10.1016/j.ultramic.2006.11.001.

[45] K. Kurihara, Steady-State and Transient Performance Analysis of Permanent-Magnet Machines Using Time-Stepping Finite Element Technique, in: Finite Element Analysis - New Trends and Developments, InTech, 2012. https://doi.org/10.5772/48426.

[46] M.S.K. Mutyala, D. Bandhanadham, L. Pan, V.R. Pendyala, H.F. Ji, Mechanical and electronic approaches to improve the sensitivity of microcantilever sensors, Acta Mechanica Sinica/Lixue Xuebao. 25 (2009) 1–12. https://doi.org/10.1007/s10409-008-0222-6.

[47] S.K. Vashist, H. Holthofer, Microcantilevers for Sensing Applications, Http://Dx.Doi.Org/10.1177/002029401004300305. 43 (2010) 84–88. https://doi.org/10.1177/002029401004300305.

[48] H.Jü. Butt, A sensitive method to measure changes in the surface stress of solids, J Colloid Interface Sci. 180 (1996) 251–260. https://doi.org/10.1006/jcis.1996.0297.

[49] H. Sone, Y. Fujinuma, S. Hosaka, Picogram mass sensor using resonance frequency shift of cantilever, Japanese Journal of Applied Physics, Part 1: Regular Papers and Short Notes and Review Papers. 43 (2004) 3648–3651. https://doi.org/10.1143/JJAP.43.3648/XML.

[50] Y. Liu, S.M. Iqbal, Silicon-Based Novel Bio-Sensing Platforms at the Micro and Nano Scale, ECS Trans. 16 (2009) 25–45. https://doi.org/10.1149/1.3104598/XML.

[51] T. Thundat, R.J. Warmack, G.Y. Chen, D.P. Allison, Thermal and ambient-induced deflections of scanning force microscope cantilevers, Appl Phys Lett. 64 (1998) 2894. https://doi.org/10.1063/1.111407.

[52] M.E. Gurtin, X. Markenscoff, R.N. Thurston, Effect of surface stress on the natural frequency of thin crystals, Appl Phys Lett. 29 (1976) 529–530. https://doi.org/10.1063/1.89173.

[53] P. Lu, H.P. Lee, C. Lu, S.J. O'Shea, Surface stress effects on the resonance properties of cantilever sensors, Phys Rev B Condens Matter Mater Phys. 72 (2005) 085405. https://doi.org/10.1103/PHYSREVB.72.085405/FIGURES/2/MEDIUM.

[54] Y. Zhang, Q. Ren, Y.P. Zhao, Modelling analysis of surface stress on a rectangular cantilever beam, J Phys D Appl Phys. 37 (2004) 2140–2145. https://doi.org/10.1088/0022-3727/37/15/014.

[55] Y. Zhang, L.J. Zhuo, H.S. Zhao, Determining the effects of surface elasticity and surface stress by measuring the shifts of resonant frequencies, Proceedings of the Royal Society A: Mathematical, Physical and Engineering Sciences. 469 (2013). https://doi.org/10.1098/rspa.2013.0449.

[56] C.Q. Ru, A strain-consistent elastic plate model with surface elasticity, Continuum Mechanics and Thermodynamics. 28 (2016) 263–273. https://doi.org/10.1007/s00161-015-0422-9.

[57] P. Sharma, S. Ganti, N. Bhate, Effect of surfaces on the size-dependent elastic state of nano-inhomogeneities, Appl Phys Lett. 82 (2003) 535–537. https://doi.org/10.1063/1.1539929.

[58] G.F. Wang, X.Q. Feng, Effects of surface elasticity and residual surface tension on the natural frequency of microbeams, Appl Phys Lett. 90 (2007) 1–4. https://doi.org/10.1063/1.2746950.

[59] K. Babaei Gavan, H.J.R. Westra, E.W.J.M. van der Drift, W.J. Venstra, H.S.J. van der Zant, Size-dependent effective Young's modulus of silicon nitride cantilevers, Appl Phys Lett. 94 (2009) 2007–2010. https://doi.org/10.1063/1.3152772.

[60] G.F. Wang, X.Q. Feng, Effects of surface elasticity and residual surface tension on the natural frequency of microbeams, Appl Phys Lett. 90 (2007) 1–4. https://doi.org/10.1063/1.2746950.

[61] M.E. Gurtin, A. Ian Murdoch, A continuum theory of elastic material surfaces, Arch Ration Mech Anal. 57 (1975) 291–323. https://doi.org/10.1007/BF00261375.

[62] T. Chen, M. sen Chiu, C.N. Weng, Derivation of the generalized Young-Laplace equation of curved interfaces in nanoscaled solids, J Appl Phys. 100 (2006). https://doi.org/10.1063/1.2356094.

[63] J. He, C.M. Lilley, Surface stress effect on bending resonance of nanowires with different boundary conditions, Appl Phys Lett. 93 (2008). https://doi.org/10.1063/1.3050108.

[64] N. Gao, D. Zhao, R. Jia, D. Liu, Microcantilever Actuation by Laser Induced Photoacoustic Waves, Sci Rep. 6 (2016). https://doi.org/10.1038/srep19935.

[65] N. Miriyala, Photothermal effects in micro/nano electromechanical systems, n.d.

[66] M. Rahman, H. Zhao, Temperature sensing performance and calibration of bi-material layer structure: role of material property variation, Forces in Mechanics. 1 (2020) 100001. https://doi.org/10.1016/J.FINMEC.2020.100001.

[67] J.K. Gimzewski, C. Gerber, E. Meyer, R.R. Schlittler, Observation of a chemical reaction using a micromechanical sensor, 1994.

[68] J. Lai, T. Perazzo, Z. Shi, A. Majumdar, Optimization and performance of high-resolution micro-optomechanical thermal sensors, Sens Actuators A Phys. 58 (1997) 113–119. https://doi.org/10.1016/S0924-4247(96)01401-X.

[69] T. Thundat, L. Senesac, Receptor-Free Detection of Chemicals and Biomolecules Using Nanomechanical Sensors, Microscopy and Microanalysis. 13 (2007) 696–697. https://doi.org/10.1017/S1431927607079019.

[70] L.R. Senesac, D. Yi, A. Greve, J.H. Hales, Z.J. Davis, D.M. Nicholson, A. Boisen, T. Thundat, Micro-differential thermal analysis detection of adsorbed explosive molecules using microfabricated bridges, Review of Scientific Instruments. 80 (2009) 035102. https://doi.org/10.1063/1.3090881.

[71] T.P. Burg, S.R. Manalis, Suspended microchannel resonators for biomolecular detection, Appl Phys Lett. 83 (2003) 2698–2700. https://doi.org/10.1063/1.1611625.

[72] H. Etayash, M.F. Khan, K. Kaur, T. Thundat, Microfluidic cantilever detects bacteria and measures their susceptibility to antibiotics in small confined volumes, Nat Commun. 7 (2016). https://doi.org/10.1038/ncomms12947.

[73] M. Faheem Khan, S. Kim, D. Lee, S. Schmid, A. Boisen, T. Thundat, Nanomechanical identification of liquid reagents in a microfluidic channel, Lab Chip. 14 (2014) 1302–1307. https://doi.org/10.1039/c3lc51273h.

[74] D. Ramos, J. Mertens, M. Calleja, J. Tamayo, Study of the Origin of Bending Induced by Bimetallic Effect on Microcantilever, Sensors. 7 (2007) 1757–1765. www.mdpi.org/sensors.

[75] S. Prakash Gumfekar, Multifunctional Water-Soluble Polymers for Dewatering of Oil Sands Tailings, n.d.

[76] O. Rivera, O. Pavez, J.L. Kao, A. Nazer, Metallurgical characterization of kaolin from Atacama, Chile, Revista Escola de Minas. 69 (2016) 473–478. https://doi.org/10.1590/0370-44672016690005.

[77] M. Digital, M. Digital Scholar, S. Youn, Quantitative Understanding of Nanoparticle Flocculation in Water Quantitative Understanding of Nanoparticle Flocculation in Water Treatment Treatment, 2017. https://mds.marshall.edu/wde_faculty.

[78] V. Vajihinejad, S.P. Gumfekar, B. Bazoubandi, Z.R. Najafabadi, J.B.P. Soares, Water Soluble Polymer Flocculants: Synthesis, Characterization, and Performance Assessment, Macromol Mater Eng. 304 (2019) 1800526. https://doi.org/10.1002/MAME.201800526.

[79] X. Xu, N. Bizmark, K.S.S. Christie, S.S. Datta, Z.J. Ren, R.D. Priestley, Thermoresponsive Polymers for Water Treatment and Collection, Macromolecules. 55 (2022) 1894–1909.

https://doi.org/10.1021/ACS.MACROMOL.1C01502/ASSET/IMAGES/MEDIUM/MA1C01502_0007.GIF.

[80] F. Doberenz, K. Zeng, C. Willems, K. Zhang, T. Groth, Thermoresponsive polymers and their biomedical application in tissue engineering-A review, J Mater Chem B. 8 (2020) 607–628. https://doi.org/10.1039/C9TB02052G.

[81] A. Nakamura, K. Murakami, A. Nakamura, K. Murakami, The Aggregation of Bentonite Using Poly(N-isopropylacrylamide) as a Flocculant, Journal of Materials Science and Chemical Engineering. 6 (2018) 94–108. https://doi.org/10.4236/MSCE.2018.64011.

[82] Q. Zhang, R. Hoogenboom, Polymers with upper critical solution temperature behavior in alcohol/water solvent mixtures, Prog Polym Sci. 48 (2015) 122–142. https://doi.org/10.1016/J.PROGPOLYMSCI.2015.02.003.

[83] J. Lu, M. Xu, Y. Lei, L. Gong, C. Zhao, Aqueous Synthesis of Upper Critical Solution Temperature and Lower Critical Solution Temperature Copolymers through Combination of Hydrogen-Donors and Hydrogen-Acceptors, Macromol Rapid Commun. 42 (2021). https://doi.org/10.1002/MARC.202000661.

[84] H.Y. Tian, J.J. Yan, D. Wang, C. Gu, Y.Z. You, X.S. Chen, Synthesis of thermo-responsive polymers with both tunable UCST and LCST, Macromol Rapid Commun. 32 (2011) 660–664. https://doi.org/10.1002/MARC.201000713.

[85] J. Seuring, S. Agarwal, Polymers with Upper Critical Solution Temperature in Aqueous Solution, Macromol Rapid Commun. 33 (2012) 1898–1920. https://doi.org/10.1002/MARC.201200433.

[86] C. Wu, X. Wang, Globule-to-Coil Transition of a Single Homopolymer Chain in Solution, (1998).

[87] H.G. Schild, Poly(N-isopropylacrylamide): experiment, theory and application, Prog Polym Sci. 17 (1992) 163–249. https://doi.org/10.1016/0079-6700(92)90023-R.

[88] A. Choi, K.D. Seo, H. Yoon, S.J. Han, D.S. Kim, Bulk poly(N-isopropylacrylamide) (PNIPAAm) thermoresponsive cell culture platform: toward a new horizon in cell sheet engineering, Biomater Sci. 7 (2019) 2277–2287. https://doi.org/10.1039/C8BM01664J.

[89] C.N. Cheaburu-Yilmaz, C.E. Lupuşoru, C. Vasile, New Alginate/PNIPAAm Matrices for Drug Delivery, Polymers 2019, Vol. 11, Page 366. 11 (2019) 366. https://doi.org/10.3390/POLYM11020366.

[90] Y. Wei, Q. Zeng, Q. Hu, M. Wang, J. Tao, L. Wang, Self-cleaned electrochemical protein imprinting biosensor basing on a thermo-responsive memory hydrogel, Biosens Bioelectron. 99 (2018) 136–141. https://doi.org/10.1016/J.BIOS.2017.07.049.

[91] M. Theses Dissertations, P.K. Nayak, Thermo-Responsive Poly(N-Isopropylacrylamide) and its Critical Solution Temperature Type Behavior in Presence of Hydrophilic Ionic Liquids, (2015). https://doi.org/10.7275/6401325.

[92] H. Ren, X.P. Qiu, Y. Shi, P. Yang, F.M. Winnik, F.M. Winnik, The Two Phase Transitions of Hydrophobically End-Capped Poly(N-isopropylacrylamide)s in Water, Macromolecules. 53 (2020) 5105–5115. https://doi.org/10.1021/acs.macromol.0c00487.

[93] P. Werner, M. Münzberg, R. Hass, O. Reich, Process analytical approaches for the coil-to-globule transition of poly(N-isopropylacrylamide) in a concentrated aqueous suspension, Anal Bioanal Chem. 409 (2017) 807–819. https://doi.org/10.1007/s00216-016-0050-7.

[94] J.R. Morones-Ramirez, Environmentally responsive polymeric "intelligent" materials: The ideal components of non-mechanical valves that control flow in microfluidic systems, Brazilian Journal of Chemical Engineering. 27 (2010) 1–14. https://doi.org/10.1590/S0104-66322010000100001.

Chapter 3

Fabrication and characterization

3.1 Introduction

Various methodologies and techniques were practiced in the fabrication and characterization of micro-resonators. The fabrication process of suspended microchannel cantilevers is discussed in detail by Faheem et al [1]. We will discuss the detailed fabrication process for microchannel cantilever in the forthcoming chapters. Fabrication process was done at Nano-fab at University of Alberta involving all clean room processes for device fabrication. Laser Doppler Vibrometer (LDV) was used to probe the mechanical response of these devices at their respective resonance frequencies in first modes. SEM and PFIB were used to characterise the fabricated device morphology. We will discuss major techniques and processes involved in device design, fabrication, and characterization in this chapter.

3.2 Fabrication process for microchannel cantilever

MC-500 is a 500 µm long microchannel cantilever with a rectangular base. The cantilever has a rectangular base while the micro-channel has been designed in a U-tube shape. This shape is quite useful in microfluidics applications as it yielded a clogging free flow to particles and cells flowing through the channel [2]. The microchannel of MC-500 is designed with the internal dimensions of width, height and length to be 16 µm, 3 µm and ~1000 µm respectively. The cantilever has relatively low resonance frequency and a spring constant.

For the fabrication of the hollow cantilevers based on two- layer design, standard micromachining techniques are used to keep the whole process economical and easily compatible with micro/nano fabrication facilities at University of Alberta. The design consists of two structural layers which need sandwiched sacrificial layer to form microchannels.

Silicon nitride (Si_3N_4) is the most common material used in semiconductor industry for masking and passivation purposes but due to high residual stress it is not considered suitable as a structural material for micromechanical devices [3]. Therefore, to fabricate microchannel cantilever, silicon rich silicon nitride (SRN) is selected. Transparency of the microchannel is also a requirement which could also be achieved by using a polymer such as, SU-8, as a structural material. Also, high stiffness of the structures is required. SRN is chosen since it is transparent (refractive index: 2.2) and has 45 times higher Young's modulus than SU-8 (E=4 GPa) [3–5]. The high stiffness to density ratio of SRN resulted in high resonant frequencies of the cantilevers, which increased their sensitivity. Differences in thermal expansion coefficients are avoided by using the same material (SRN) for the cantilever and fluidic channel. This helps in achieving temperature stability. In our case SRN acted as a structural as well as a masking material.

Two-layer design needs a support material (sacrificial/molding layer) sandwiched between two layers of a structural material. To fabricate microchannels of the cantilevers, polycrystalline silicon (poly-Si) is chosen as a sacrificial material. Poly-Si can be deposited by low pressure chemical vapour deposition (LPCVD) technique without any significant pinholes.

The microchannel cantilever is supported on a silicon substrate (Si). Thin wafers of Si are easily available and have been extensively used for micromechanical devices. A schematic of the process is shown in Figure 3.1.

The starting material is a 500 µm thick, 4inch Si wafer on top of which a 500 nm thick SRN layer is deposited by low pressure chemical vapor deposition (LPCVD), as shown in Figure 3.1 a. First square holes are defined in the SRN using UV lithography and reactive ion etching (RIE). The SRN deposition was followed by a deposition of a 4 µm thick polycrystalline Si (Poly Si) sacrificial material using LPCVD, as shown in Figure 3.1 b. The thickness of poly-Si layer defines the height of the microchannel. The next step is to pattern the sacrificial layer (Poly Si) to form the shape of a microfluidic channel, as shown in Figure 3.1 c. To make the particles flow without any blockage, the internal walls of the channel are required to be vertical. Therefore, dry anisotropic etching of the Poly Si is preferred over wet etching.

Using a 1.5 µm thick photoresist (AZ 5214) as a masking material, the Poly Si is patterned by an Inductively Coupled Plasma– Deep Reactive Ion Etcher (ICP-DRIE) which uses the Bosch process. In Figure 3.1c, the vertical walls of an already released channel can be seen. Next, a 500 nm top-structural layer of SRN is deposited, as shown in Figure 3.1 d. Here, conformal step coverage and a uniform deposition of the thin film (SRN) are very critical and achieved using LPCVD. Afterwards, both structural layers (base and top) are patterned by dry etching (Reactive Ion Etcher).

Finally, the cantilevers are released from the substrate, dicing lines (v-grooves) are etched into the substrates and the sacrificial Poly Si layer is removed in a single wet etching step. For this purpose, KOH (28%) is used at 80 ^{0}C, because of its high Si-100/111 etch rate ratio and high selectivity to SRN. The average etch rate 500 µm Fluidic Inlet/Outlet 10 µm of KOH is recorded to be 1.3l m/min. The etching time required to fully release the cantilevers and to etch dicing lines is almost three hours while the etch time needed to remove the Poly Si in the fluidic channels is approximately 12 h. The schematic of a released cantilever is shown in Figure 3.1 e.

Figure 3.2 a shows the sem image of the microfluidic cantilever. Figure 3.2 b shows channel height of the microfluidic cantilever and Figure 3.2 c shows the top view of a released cantilever with the fluidic openings. The fabricated cantilevers are 500 µm long, 1 µm thick and the channel width/height is 4 µm/ 4µm. The released devices were diced and then tested by flowing liquids through a microfluidic set up with LDV and by observing their fundamental frequencies. The devices were heated in a vacuum oven at 300^0 C in order to release the residual stress.

a) Depositing base structural layer and sacrificial layer

b) Patterning sacrificial layer

c) Depositing top structural layer

d) Patterning top and base structural layers

e) Etching fluidic channel and releasing cantilever

Silicon-rich silicon nitride
Poly Silicon
Silicon
Air
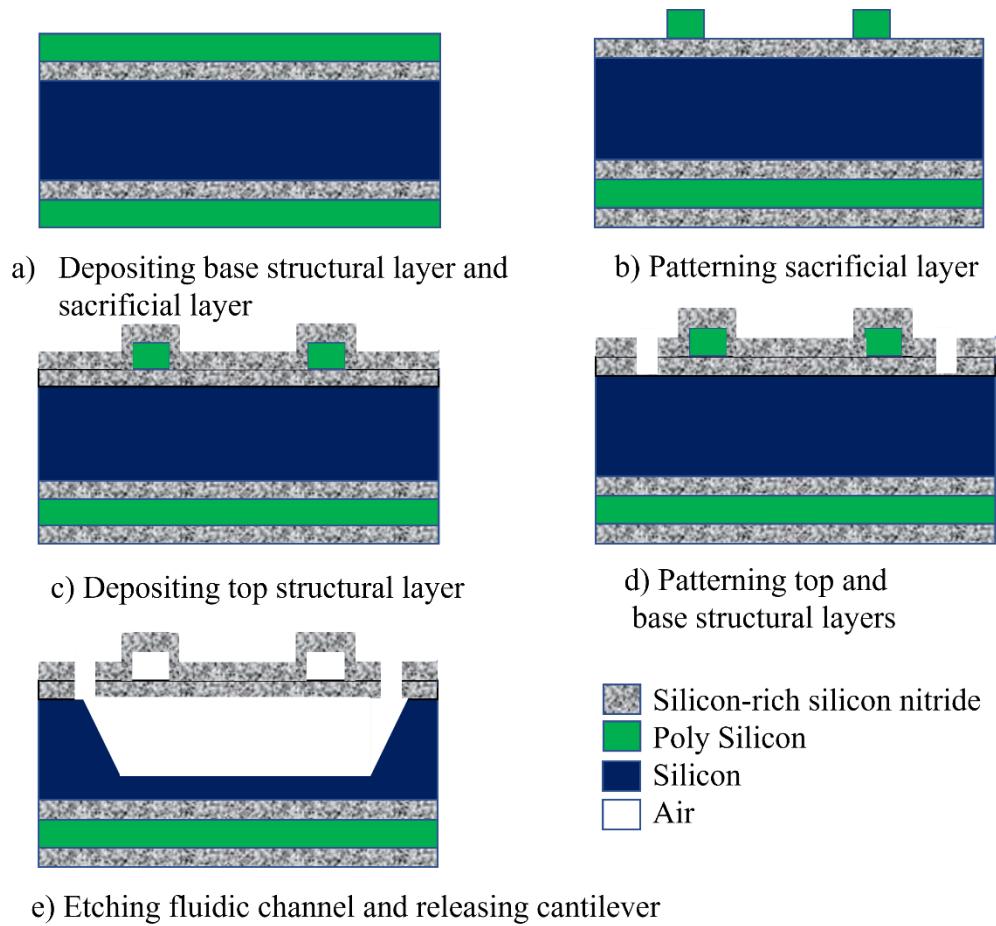
Figure 3.1: Schematic of the fabrication process of microchannel cantilever.
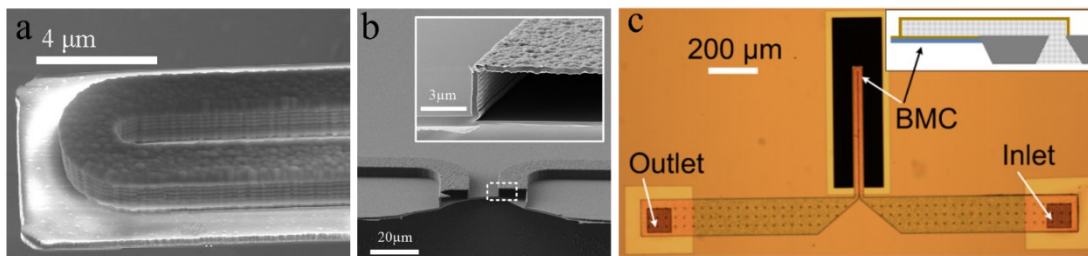
Figure 3.2: a) SEM image of top view of the microfluidic cantilever b) SEM image of the channel height of the microfluidic cantilever c) schematic of the microfluidic cantilever with outlets (Reproduced with permission from [6]

3.3 Laser Doppler vibrometer

Laser Doppler Vibrometers (LDV) allow remote, non-intrusive, high spatial resolution measurements with reduced testing time and increased performances (high-frequency bandwidth up to 20 MHz, velocity range of ±30 m/s, resolution of about 8 nm in displacement and 0.5 μm/s in velocity) [7]. It is a non-contact vibration measurement technique which allows to measure vibrations in pico meter resolution. The laser beam from the LDV is directed at the surface of moving sensor/micro-cantilever and by analysing the vibration amplitude and frequency, the mechanical parameters are obtained. The amplitude and resonance frequency are extracted from the Doppler shift of the reflected laser beam frequency due to the motion of the surface. The output is in the form of voltage generated by movement of reflected light onto the position sensitive diode which is proportional to the intensity of the light and the motion of the target object. This technique is made with two laser beam interferometers which measure the frequency or the phase difference between a reference beam and a test beam. The laser we used was helium-neon with a wavelength of 635 nm and maximum output power of < 1 mW.

Doppler effect states that the movement of the source changes the wavelength and the received frequency of wave even though the source frequency and the wave velocity are unchanged. The observed frequency of the wave depends on whether the source is moving away from the observer or moving towards an observer. In case of LDV, light with a known frequency and wavelength is reflected back from a moving object. The rate of change of frequency of the test beam is proportional to the rate of change of position which is the velocity v(t) of the vibrating surface. When a wave is reflected by a moving object and detected by the LDV, the wave's measured frequency shift can be expressed as follows

$$f_D = 2 \times \frac{v}{\lambda} \tag{3.1}$$

where, v is the velocity of the object and λ is the wavelength of the emitted wave.

In order to find out the velocity of the object, the shift in frequency f_o has to be measured at a known value of wavelength. This is measured in LDV by using laser interferometer. Working mechanism of LDV is explained in Figure 3.3.
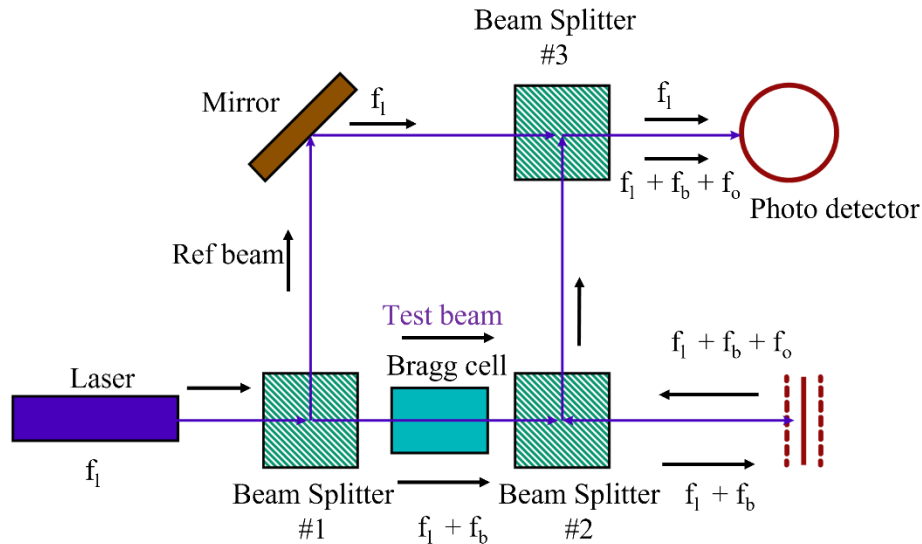
Figure 3.3: A reference beam of laser with frequency f_l interferes with a Bragg modulated beam $f_l + f_b + f_o$ on a position sensitive detector (PSD). The motion of the target object adds a Doppler shift to the beam which then combines with the reference beam to produce interference pattern on the photo detector. The output is a frequency modulated signal which then can be demodulated to extract the velocity versus time of the vibrating object. Reproduced with permission from [6]

The beam of laser with frequency f_l is split by a beam splitter 1 into a reference and a test beam. The test beam passes through a Bragg cell which typically shifts the frequency by 40 MHz. After adding this modulation in the frequency, a second beam splitter allows the part of the light to fall on the moving object and the reflected beam from the object has an additional component in the light frequency which is because of Doppler shift (motion of the object causes a change in frequency). Since the optical path length of the reference beam is constant, a movement of the object causes a change in optical path length which will generate bright/dark pattern on the photo detector. This beam combines with reference beam with frequency f_l at a third beam splitter and creates an interference on to the photodetector. The signal on photodetector is in the form of voltage which is de-convoluted to get the frequency and amplitude of vibration of the moving body. One complete light / dark cycle on the detector corresponds to an object displacement of exactly half of the wavelength of the light used.

The change in optical path length per unit time because of the motion of the object under investigation correlates with the Doppler's shift of the beam. This leads to modulation frequency of interference pattern on photo diode being related to the velocity of the object. Since the object moving away from the laser beam generates the same interference pattern as object moving towards the beam, the direction of motion of the object can be determined by using a Bragg cell which will add a constant frequency in the test beam which is around 40 MHz. The modulation frequency will increase if the object moves towards the interferometer and decreases if the object moves away from it. This makes it possible to not only measure the magnitude of the velocity but also the direction of motion of the vibrating object.

3.4 Packaging of microchannel cantilever and integrated instrumentation with LDV

The three main requirements to packaging the microchannel cantilever were safe handling the chip, operation in vacuum and microfluidic interconnections. Due to surface micromachining, the microchannels were lying 3 µm above the surface which made it quite tricky to implement all of the requirements. The micro cantilevers were packaged in such a way that the liquid sample can be provided from the bottom of the chip and vacuum on top side of the chip. Here the microfluidic interconnects were completely isolated from the vacuum which helped in reducing the risk of leakage at joints. This type of "plug and play" package made it easy to replace chips quickly and safely. A schematic of the packaging is shown in Figure 3.4.
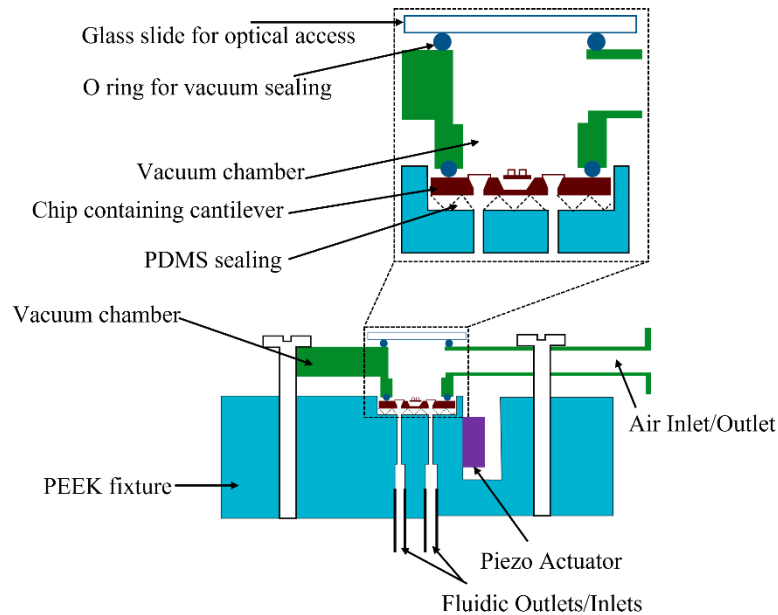
Figure 3.4: Schematic of the cross section of packaging of microchannel cantilever

The chip is packaged in polyetheretherketone (PEEK) base fixture which is inert to many organic and inorganic liquids including many solvents. The sealing between solid surface of silicon fixture and the chip was provided by a 300 μm thick poly dimethyl siloxane layer (PDMS). The top side of the chip was covered by the vacuum chamber. There is a glass slide on the top side of the vacuum chamber which allows the passage of laser. The sealing between the chip, vacuum chamber and the glass slide was provided by two o-rings (nitrile butadiene rubber). To load the samples, Teflon tubes were inserted on metallic tubes which were connected to the bottom side of the PEEK fixture. Figure 3.5 a show the photograph of the packaging of the microchannel cantilever and Figure 3.5 b shows the photograph of the PEEK fixture where microchannel cantilever is placed.
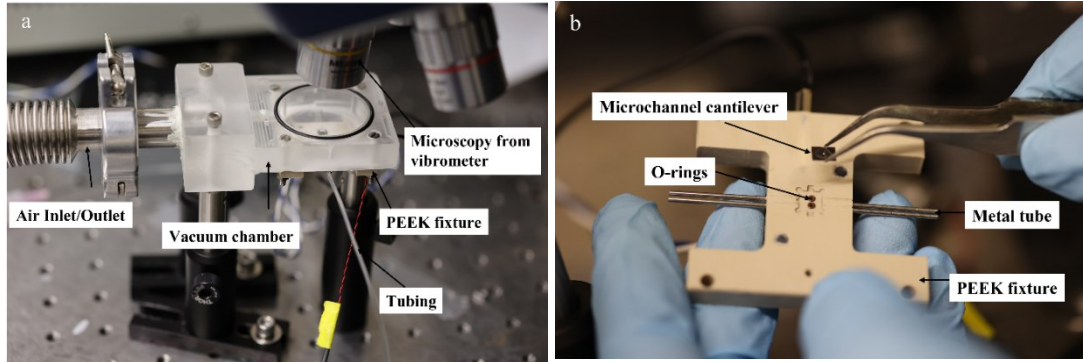
Figure 3.5: a) Photograph of the packaging of the microchannel cantilever. To operate the cantilever in vacuum, the packaging was connected to a vacuum chamber b) PEEK fixture with o-rings, metal tube and microchannel cantilever.

The methodology to investigate the thermomechanical properties of different liquids with various excitation methods such as temperature and optical power, we developed some auxiliary instrumentation which was integrated with LDV to carry out the excite-response measurements. To get high vibrational amplitude, the cantilever was externally excited acoustically by using a piezo actuator. It was fixed on the PEEK fixture right below the chip. It was driven by a periodic chirp over a specific bandwidth at a voltage of 200 mV. For the photothermal characterization of a liquid sample an external laser was used to heat the liquid sample. Figure 3.6 shows the conceptual schematic of the experiment where a U-shaped silicon nitride microfluidic channel (16 μm wide, 300 μm long and 3 μm high) fabricated on top of a plain cantilever (44 μm wide, 500 μm long and 500 nm thick) with a liquid sample is heated by a red laser (635 nm) with an optical power of 0.362 mW with a spot diameter of 20 μm.

In order to heat the liquid sample other than photothermal heating, a heater was attached to the bottom of the PEEK fixture on which the micro channel cantilever was placed. Also, to provide controlled heating to the resonators while accurately measuring temperature, a Pt 100 sensor was mounted on the bottom of the PEEK fixture. The temperature was measured using Keithley 197 micro-voltmeter.
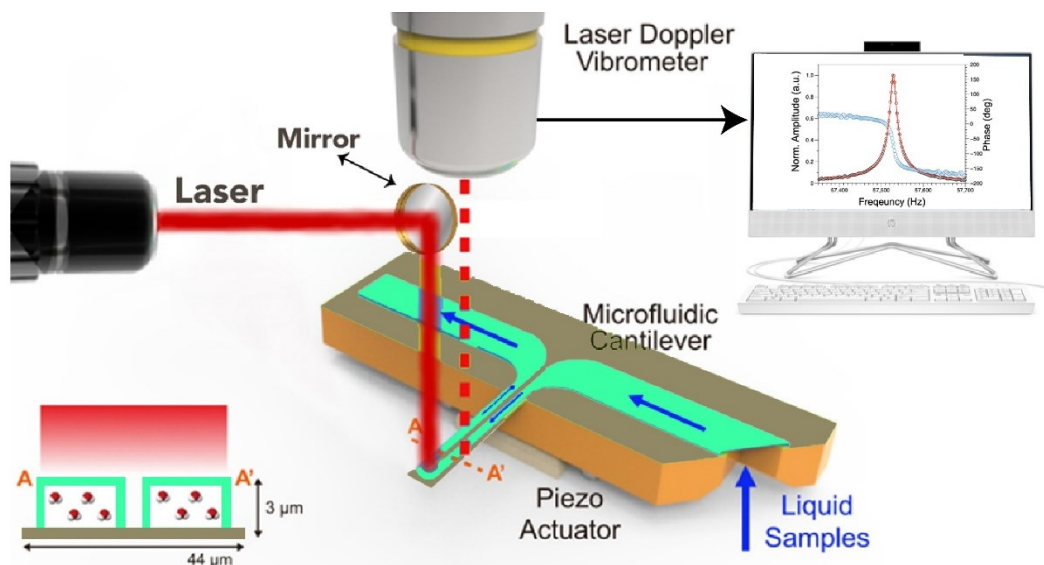
Figure 3.6: A conceptual schematic of the fluidic resonator filled with liquid samples subjected to photothermal modulation. (Subset) Top view of the resonator when the heating laser aligned and powered off/on. Scale bars are 100 μm.

3.5 Plasma focused Ion Beam (PFIB)

Plasma focused ion beam (PFIB) was used to analyse the clay samples inside the microchannel cantilever. The operation of PFIB is plasma-FIB is mainly used to perform micro cross sections on samples by using an ion source. The ion source is focused on the sample to obtain a small beam that can etch the surface with material removing. This small beam can be scanned on the surface of the sample reaching a precision smaller than 1 μm to produce local cross-section of the desired shape without the defects caused by standard mechanical polishing. The plasma-FIB instead of having a liquid gallium ions source like standard FIB has a xenon plasma ions source. This new source type allows cutting rate 50X faster than regular liquid gallium FIB. The plasma-FIB is coupled with a scanning electron microscope (SEM) and with an x-rays energy dispersive spectrometer (EDS) to observe and analyze the section obtained. A Gas Injection System (GIS) is also available, offering the possibility to locally coat the sample with platinum or tungsten (to protect the surface or to create pads), to deposit an electric insulating material or to use water or XeF_2 to accelerate milling of some materials.

In order to see the inside of the microchannel cantilever without dicing the micro-cantilever, Helios 5 Hydra Dual Beam PFIB from Thermo fisher available in Nanaofab at University of Alberta was used for the milling and scanning. 5 nm of Tungsten was coated on the desired milling surface and using xenon plasma ions, the surface was milled.
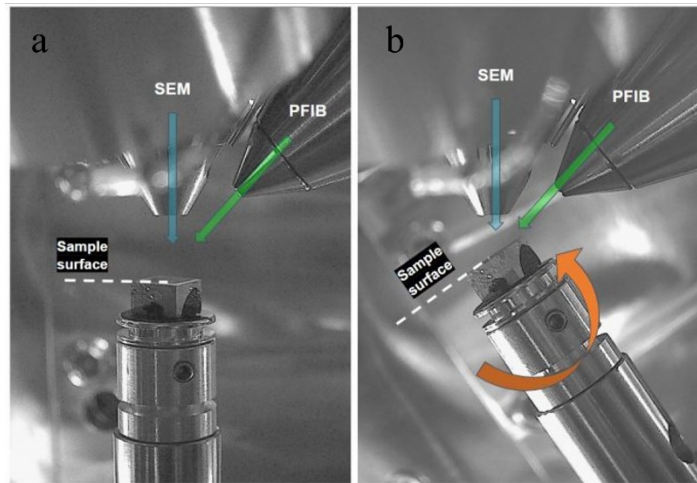
Figure 3.7: Photographs of PFIB-SEM set up. a) The sample is mounted horizontally on the stage. b) The stage is tilted negatively, so that the PFIB beam mills the sample surface at a nearly glancing angle. Reproduced with permission from [8]

3.6 References

[1]   M.F. Khan, S. Schmid, Z.J. Davis, S. Dohn, A. Boisen, Fabrication of resonant micro cantilevers with integrated transparent fluidic channel, Microelectron Eng. 88 (2011) 2300–2303. https://doi.org/10.1016/J.MEE.2011.02.096.

[2]   M.F. Khan, Microchannel resonators to characterize liquid samples : Ph. D. thesis, (2012). https://books.google.com/books/about/Microchannel_Resonators_to_Characterize.html?id=l4nfn gEACAAJ (accessed October 19, 2022).

[3]   J.G.E. Gardeniers, H.A.C. Tilmans, C.C.G. Visser, LPCVD silicon-rich silicon nitride films for applications in micromechanics, studied with statistical experimental design*, Journal of Vacuum Science & Technology A: Vacuum, Surfaces, and Films. 14 (1998) 2879. https://doi.org/10.1116/1.580239.

[4]   P.J. French, P.M. Sarro, R. Mallée, E.J.M. Fakkeldij Elke, R.F. Wolffenbuttel, Optimization of a low-stress silicon nitride process for surface-micromachining applications, Sens Actuators A Phys. 58 (1997) 149–157. https://doi.org/10.1016/S0924-4247(96)01397-0.

[5]   J. Yang, O. Paul, Fracture properties of LPCVD silicon nitride thin films from the load–deflection of long membranes, Sens Actuators A Phys. 97–98 (2002) 520–526. https://doi.org/10.1016/S0924-4247(02)00049-3.

[6]   S.A. Manzoor Bukhari, M.F. Khan, A. Goswami, R. McGee, T. Thundat, Thermomechanical analysis of picograms of polymers using a suspended microchannel cantilever, RSC Adv. 7 (2017) 8415–8420. https://doi.org/10.1039/c6ra25455a.

[7]   P. Castellini, M. Martarelli, E.P. Tomasini, Laser Doppler Vibrometry: Development of advanced solutions answering to technology's needs, Mech Syst Signal Process. 20 (2006) 1265–1285. https://doi.org/10.1016/J.YMSSP.2005.11.015.

[8]   Spin Mill with Plasma FIB | nanoFAB, (n.d.). https://www.nanofab.ualberta.ca/2022/news/spin-mill-with-plasma-fib/ (accessed October 19, 2022).

Chapter 4

Effect of surface and interfacial tension on the resonance frequency of microfluidic channel cantilever

4.1 Abstract

The bending resonance of micro-sized resonators has been utilized to study adsorption of analyte molecules in complex fluids of picogram quantity. Traditionally, the analysis to characterize the resonance frequency has been focusing solely on the mass change, while the effect of interfacial tension of the fluid has been largely neglected. By observing forced vibrations of a microfluidic cantilever filled with a series of alkanes using Laser Doppler Vibrometer (LDV), we studied the effect of surface and interfacial tension on the resonance frequency. Here, we incorporated the Young–Laplace equation into the Euler–Bernoulli beam theory to consider extra stress that surface and interface tension exerts to the vibration of the cantilever. Based on the hypothesis that the near-surface region of a continuum is subject to the extra stress, thin surface and interface layers are introduced to our model. The thin layer is subject to an axial force exerted by the extra stress, which in turn affects the transverse vibration of the cantilever. We tested the analytical model by varying the interfacial tension between the silicon nitride microchannel cantilever and the filled alkanes, whose interfacial tension varies with chain length. Compared to the conventional Euler–Bernoulli model, our enhanced model provides a better agreement to the experimental results, shedding light to precision measurements using micro-sized cantilever resonators.

4.2 Introduction

A microcantilever-based sensor driven in dynamic operation mode measures resonance frequencies in various vibrational modes, allowing chemical and biological sensing at extreme precision [1-5]. The resonance frequency can shift by any factors that cause subtle changes in the spring constant or the mass of the microcantilever [4-6]. For example, mass and stiffness of an adsorbate can alter those of the resonating microcantilever, resulting in the shift of the resonance

frequency with a precisely quantifiable manner [7]; its unprecedented precision level has been crucial in detecting trace number of biological analytes, such as toxin, hybridized DNAs, and pathogens [8].

Surface stress can be considered as a measurable macroscopic quantity that arises from the microscopic interactions of adsorbate on surface, surface/environment interaction or surface reconstruction [9]. As the surface/interface area to volume ratio increases considerably with the reduction of sizes of the sensors to micron scale, the effects from surface stress become increasingly important [10]. It has been well understood that the surface stress causes a static bending of thin microcantilevers [11]. The effect of surface stress in the natural resonance frequency has been hypothesized since 1975 when Lagowski et al. discovered a strong surface condition dependence on the natural frequency of GaAs crystals with thickness less than 15µm [12].

Chen et al. [13] and Cherian et al.[14] described the shift in resonance frequency of a cantilever as the combination of increased mass and changed spring constant when a chemical species adsorbs on the surface of the cantilever [10]. Wang et al. emphasized the effect of surface stress on nanomechanical properties of ultra-thin SCS resonators when explaining the effects of thermal treatments and gas adsorption [15]. Hwang et al. performed an experimental study on the correlation between the surface stress exerted by biomolecular interactions and the dynamical response of microcantilevers [16]. A nanomechanical spectrometry study of 100 nm-sized gold nanoparticles (GNPs) and Escherichia coli DH5α cells using microcantilever resonators conducted by Malvar et al. revealed that the ignorance of the effect of stiffness can lead to an underestimation of mass by 10% in microcantilevers [17]. A recent project by Stachiv et al. presented an interesting but alternate method to quantify the adsorbate mass by analyzing the changes in Q factor without even knowing the position of attachment, stiffness and surface stress effects [18].

On theoretical modelling side, McFarland et al. derived an axial beam model with a constant axial force acting on the cantilever based on Lagowski's hypothesis for explaining the influence of the surface stress on a deformed cantilever [19]. An alternative model was implemented by Ren et al using a variable axial force in the Euler–Bernoulli governing equation to determine surface stress

effect on the frequency of the microcantilever [20]. Another theoretical explanation for adsorption-induced change in resonance frequency was put forward by Huang et al. by considering the interaction between adsorbates and the cantilever [21]. Along with the experimental evidence, Hwang et al. presented a mechanical beam model for the surface stress driven dynamical response of nanomechanical microcantilevers [16]. In the same year, Dorignac et al. used the fluctuation-dissipation theorem to derive an exact expression for the frequency shift of the nanoscale cantilever placed in a viscous fluid. It was found that the frequency shift was generated by the surface stress due to biomolecular interaction rather than the mass loading [22].

Aforementioned theories based on the hypothesis of surface pressure effect, however, faced numerous criticisms. Gurtin et al. contradicted Lagowski's hypothesis by stating that within the framework of classical beam theory, strain independent surface stress has no effect on the natural resonance frequency of cantilever beams, but the surface elasticity can change the frequency [10]. In beam with axial force model, the effective external forces were considerably misinterpreted since the cantilever has a free end to allow deformation or bending to relieve the stress [23]. Wang et al. and Lu et al. analyzed the influence of surface elasticity, pure surface stress and adsorption induced surface stress on the vibration frequency on the cantilever while stating that only strain dependent surface stress affects the dynamics [23,24]. Strain dependent surface stress explains the external forces that affect the modulus of the cantilever system whereas strain independent stress is not associated with any generation of strain upon the influence of stress such as surface tension, interfacial tension etc.

To address the shortcomings of the previous models, Lachut et al. proposed an alternative approach based on the linear beam elastic theory about unreleased in-plane stress in the vicinity of the supporting clamp [25]. The unreleased stress arises from the clamping restriction for in-plane displacements. The article mentions that the strain independent stress has no role in the resonance frequency of the cantilever [25]. An improved model was employed by Sader et al. in which a cantilever plate model was introduced and considered the effect of cantilever width which was ignored in Euler-Bernoulli beam theory [26]. Still, there was a discrepancy of two orders of magnitude in the frequency calculations. Later, Karabalin et al. demonstrated controlled measurements of stress-induced change in cantilever stiffness with theoretical quantification. He

concluded that net in-plane stress generated in the immediate vicinity of the supporting clamp in a cantilever by the application of surface stress can alter the resonance frequency to a small but nonnegligible extent. But axial force model can predict stress effects in much larger magnitudes because of unspecified and uncontrolled effects [27].

In 2008 He et al. approached the influence of surface stress on resonance bending nanowires by incorporating the generalized Young–Laplace equation into Euler–Bernoulli beam theory and studying the solution for different boundary condition [28]. He stated that, in small deformations, the distributed transverse force resulting from the surface stress along the nanowires longitudinal direction is considered as a function of the curvature, and hence he accommodated the strain independent stress and the surface elasticity in the Euler–Bernoulli equation and validated the results [28]. A new model using classical lamination theory was developed by Sohi et al. using the Rayleigh–Ritz method [29]. They accounted for the biaxial curvature variation of the cantilever due to differential surface stress loading which is the main mechanism responsible for flexural resonance frequency shift. Similarly, Ruz et al. developed a model establishing the size- and vibration mode-dependent nonlinear relationship of change in microcantilever curvature due to surface stress loading and the variation of its resonance frequencies and vibration mode shapes [9]. A similar model by Sohi et al. investigated the modal response of microcantilevers where it relates the bending-extensional mode coupling associated with the flexural vibration modes of microcantilevers with a coupling strength that depends on the microcantilever curvature [30]. An interesting theoretical analysis which enabled the disentangling of the impact delivered by axial force and attached mass on resonant frequency shift of suspended nanomechanical based mass sensors under arbitrary applied axial load was put forth by Stachiv et al. in 2014 [31]. Followed by that, he introduced a similar theoretical investigation of the cantilever beams under an arbitrary value of the axial force vibrating in a specific environment such as vacuum, air or viscous fluid [32].

Apart from surface stress effect, higher order strain gradient theories such as generalized Cosserat theory of elasticity were considered for more accurate descriptions of micro-mechanical systems, including mathematically tractable formulations and associated analyses of microstructures. The introduction of couple-stress tensor into the models of continuum deformation and analysis of

Euler-Bernoulli equation revealed the size dependent nature of resonant frequencies of the microbeams [33-39]. The inclusion of a characteristic length parameter, l, shear modulus, μ, and width of the beam, A, in the calculation of Young's modulus, introduced the new effective modulus as $EI^* = EI + \mu A l^2$, and was used to estimate the resonant frequency according to the aforementioned couple stress model [33,34]. The Spencer and Soldatos type approach [40] is one of most widely adopted second gradient model for problems regarding planar beams and plates with meshed microstructures [41,42]. At the same time, the implementation of the non-classical continuum theories, as in their original forms, has faced formidable challenges especially in characterizing admissible higher forces (e.g., double and triple forces) and their energy couples (Piola-type double and triple stresses) sustained by the higher-order continua [35-39]. One author of this paper, Kim, has contributed to the developments of higher-order gradient models for the mechanics of micro-structured elastic solids subjected to finite plane deformations [43-49].

When the surface effects are not negligible, the bending and vibration analyses of beams can be modelled with the framework of the higher-order gradient-based continuum models with proper dimensional reductions. The dimensional reduction of higher-gradient models leads to the constitutive equations, which share close similarity to those obtained directly from the surface elasticity theory. This is because both approaches essentially result in the same orders of gradient fields once formulated in the form of Euler equilibrium equations.

Though the existing surface elasticity beam models provides comprehensive descriptions in the constitutive modeling level, implementation in an actual problem often results in unpractically heavy expressions or even analytically unsolvable expressions [51]. Therefore, it is necessary to devise a prediction model that is simple to implement. A practical target for such analytical model may be within the allowed error limit of 5%, when the use of heavy computational resources is not preferred.

Although the hypothesis of the surface stress effect on the resonance frequency has been supported by many studies, its practical effect on molecular sensing has been questioned because resonant vibration of cantilever dampens in liquid medium, which results in compromised quality factor of such resonance peaks. In order to address the challenge, microchannel cantilever vibrating in high

vacuum environment have been suggested [52-54]. The microchannel cantilever, a unique tool to characterize the properties of fluids in picograms of quantity with high sensitivity and selectivity, can operate in two modes [55]. In static mode, the displacement of the beam is converted to the surface stress associated with the adsorption on the cantilever. In dynamic mode, the frequency shift is associated with the surface stress resulting from the adsorption on the beam [56]. Since static mode involves a significant drift in the signal over a large period of time, dynamic mode is preferred for stable long-term operation.

In the present study, we hypothesized that the surface/interface tension of the microchannel cantilever exerts transverse force acting along the longitudinal direction of the deformed beam that modulates the effective modulus of the cantilever system. The presented model is based on the first gradient surface elasticity theory with an assumption of perfect adherence between the fluid substances and the surfaces of cantilever beam. The microchannel cantilever containing the fluid is considered as a single cantilever system, whose equilibrium shape is in the deformed state; the balance between the internal forces and the surface elasticity is considered [57,58]. Based on the hypothesis, we developed an improved Euler-Bernoulli model. Our main goal is to study the influence of the transverse force along the longitudinal direction, $q(x)$ in the Euler-Bernoulli equation, on the resonance frequency of the cantilever. This parameter is associated with the second derivative of displacement with respect to position [23,33]. Within these prescriptions, the influences of fluid substances are transmitted through the surfaces of beams, leading to the idealization of surface-influenced beam systems. Our model may be classified as a simplified surface elasticity-based continuum model. When formulating the effective moduli of the beam, EI^*, the size effects that lead to the frequency shift of the beam are already implied. Then, we tested the hypothesis by monitoring the resonance frequencies of a microchannel cantilever when empty, as well as when filled with a series of alkanes with a number of carbon atoms between 5 and 9. Our improved Euler-Bernoulli model showed a better agreement with experimental results when compared to the prediction from the conventional model.

4.3 Analytical Model Incorporating Surface Pressure

The classical Euler–Bernoulli beam differential equation for a freely vibrating cantilever with deflection $w(x,t)$ is

$$(\rho A)^* \frac{\partial^2 w(x,t)}{\partial t^2} + EI \frac{\partial^4 w(x,t)}{\partial x^4} = 0 \qquad (4.1)$$

and its associated natural resonance frequency in the fundamental flexural mode is given by

$$\omega = \left(\frac{\alpha}{L}\right)^2 \sqrt{\frac{EI}{\rho A}} \qquad (4.2)$$

where L denotes the cantilever length, $A = b \times h$ is cross section with b and h being width and thickness, respectively. I = bh³/12, E, ρ and α=1.876 are geometric moment of inertia, Young's modulus, mass density, and mode shape factor for the fundamental mode respectively.

We refine the classical beam model based on the following assumptions

1) The length to width ratio of the channel is greater than the order of 100.
2) The amplitude of the beam vibration is smaller than the any beam dimension.
3) The fluid inside the channel is considered as a homogeneous media and incompressible and the beam is a linearly elastic solid.
4) The deformed beam is in equilibrium considering that all the internal forces are balanced within.
5) The cross section of the beam is uniform over its entire length.

In order to study the surface effects on the natural resonance frequency of microfluidic cantilever, we consider the combined effects of residual surface tension and interfacial tension. The problem is addressed on the basis of a surface layer-based theory taking into account of the origin of interfacial tension and residual surface stress.

In our study, we use a hollow cannel cantilever filled with fluid. Figure 4.1a shows an overview of experimental setup, and Figures 1b and 1c show the top and the cross-sectional view of a microchannel cantilever, respectively.
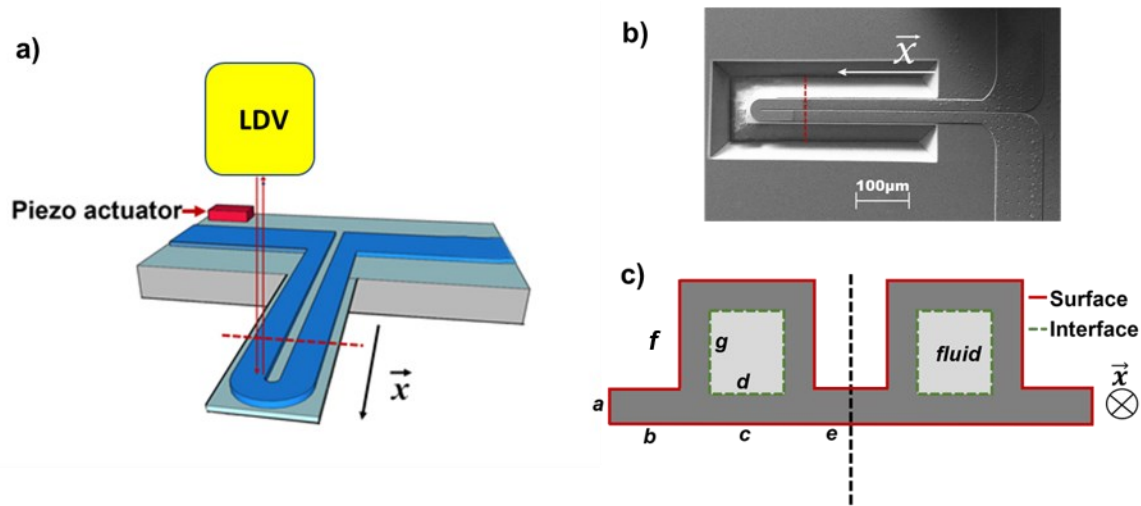
Figure 4.1: a) Schematic of the experimental system. The microchannel cantilever vibrates in vacuum environment with a pressure below than 1×10^{-3} mbar in order to ensure high quality factor resonance peaks. b) SEM image from the top of the sensor chip. c) A cross-sectional illustration of the cantilever (dotted red lines in a) and b)) denoting our definition of interface and surface, as well as the geometric description of the lengths used in our calculation ('a' to 'g').

The surface effects on the natural resonance frequency of the cantilever were studied based on the approach of surface layer model by Wang et al. [23]. Among surface effects, in order to consider both surface elasticity and residual tension on the resonance frequency, the surface elasticity theory of Gurtin *et al.* [10] was included along with Young Laplace equation in the governing differential equation [23]. The microbeam was considered as a sandwich model with thin upper and lower surface layers having near-surface material properties and the bulk material in between. They divided a microbeam into three laminated layers, including two surface layers and a bulk layer with Young's modulus E_1 and E and thickness h_1 and 2h respectively. The tensile stiffness of the surface layer was denoted as $Es=E_1h_1$. Letting h_1 approach zero while keeping Es as a constant, the surface layer model reduces to the theory of surface elasticity of Gurtin *et al.* [10] in which the surface has a zero thickness and a surface elastic modulus Es.

The effective bending moment of the sandwich beam is expressed as

$$(EI)^* = EI + 2E_s a h^2 \tag{4.3}$$

where I=2ah³ /3 and E are the inertia moment of the bulk layer and Young's modulus of bulk layer respectively. Here a is the beam width and $E_s = E_1 h_1$ is the tensile stiffness of the surface layer in which E_1, h_1 are the Young's modulus and thickness of surface layer, respectively [23].

Our model starts from the similar approach. Since the inner surface of the channel is in contact with the fluid, the system may be modelled as two homogeneous media, i.e., a bulk layer of silicon nitride in contact with a bulk layer of fluid. The Young's modulus of the channel and the fluid are denoted as E_H and E_f, and are 180×10^9 Pa and $0.7\text{-}0.9 \times 10^9$ Pa respectively [55,59,60].

The effective modulus (EI)* is then given by

$$(EI)^* = E_H I_H + E_f I_f \qquad (4.4)$$

where I_H is the inertia moment of the hollow channel, and the I_f is the inertia moment of bulk fluid and are calculated as $5.514 * 10^{-23} m^4$ and $1.8 * 10^{-23}$ m^4 respectively. In fact, the effective bending moduli of multilayered beams may be calculated in different ways, for example, those suggested in Zapomel el al. [61] which may result in more accurate predictions. In this a novel procedure for measurement of modulus of suspended micro/nano resonator with a deposited thin film was developed by utilizing the Monte Carlo probabilistic method combined with the finite-element method (FEM). In the present study, we adopt the model proposed by Wang et al. [23] based on the theory of surface elasticity for the sake of analytical simplicity and mathematically tractable models.

The peripheral regions of a continuum materials (i.e., atoms or molecules at and near the surface or the interface) have different local environment compared to the bulk region. Thus, the physical properties of these atoms are different; this is the origin of residual surface tension [28]. Here, we denote the residual surface tensions at the surface layer of the silicon nitride channel as σ, and the interfacial tension between the fluid surface and channel surface as σ_{if}.

In the present study we adapt the generalized Young–Laplace equation to account the out of plane stresses that are induced from in-plane stresses of the curved interface surfaces. Since the curvature of the beam ($\frac{\partial^2 w}{\partial x^2}$=0) vanishes prior to deformation, the residual surface stress has no effect on the bulk [22]. But for a deformed single beam, the curvature is not zero and the residual surface tension will generate a distributed transverse loading, $q(x)$, along the longitudinal direction on the surface as

$$q(x) = -pq \frac{\partial^2 w}{\partial x^2} \tag{4.5}$$

where $\frac{\partial^2 w}{\partial x^2}$ is the curvature of the beam, p is the surface stress and q are the beam width [28].

Considering the effects of, σ and σ_{if} on all four walls of the channel respectively, the Laplace-Young equation on the surfaces yields

$$q_{channel}(x) = -(2\sigma \left(a + 2(b + c + g + e)\right) \frac{\partial^2 w}{\partial x^2}) \tag{4.6}$$

and,

$$q_{fluid}(x) = -(4\sigma_{if}(d + g) \frac{\partial^2 w}{\partial x^2}) \tag{4.7}$$

where a, b, c, g and e are the characteristic dimension of the hollow channel. When channel is empty, σ_{if} becomes the same as σ. Here, positive $2\sigma \left(a + 2(b + c + g + e)\right)$ and $4\sigma_{if}(d + g)$ are considered as tensile stress and negative are compressive stress. In this case, since all surfaces are exposed to surface stresses, the situation is complex and compressive stress is taken into consideration as it improves the model value towards the experimental value.

Thus, effective distributed loading can be formulated as,

$$q\,(x) = q_{channel}(x) + q_{fluid}(x) = -(2\sigma\,(a + 2(b + c + g +$$
$$e))\frac{\partial^2 w}{\partial x^2} + 4\sigma_{if}(d +\ g)\frac{\partial^2 w}{\partial x^2} \qquad (4.8)$$

The equation of motion describing the motion of bending microfluidic channel incorporating the distributed transverse force in the Euler–Bernoulli beam theory is obtained as

$$(\rho A)^*\,\frac{\partial^2 w(x,t)}{\partial t^2} + EI^*\,\frac{\partial^4 w(x,t)}{\partial x^4} - q\,(x) = 0 \qquad (4.9)$$

and $(\rho A)^*$ is the effective density given as

$$(\rho A)^* =\ \rho A + \rho_f A_f \qquad (4.10)$$

in which ρ and ρ_f are the densities and A and A_f are the cross-sectional areas of the channel and fluids respectively. It is seen that both the surface elasticity and residual surface tension affect the dynamic behavior of the beam. The third term in the equation indicates that the influence of residual surface tensions is equivalent to a stretching axial loading $(2\sigma\,(a + 2(b + c + g + e))\frac{\partial^2 w}{\partial x^2} + 4\sigma_{if}(d +\ g)\frac{\partial^2 w}{\partial x^2}$ at the free end of the beam.
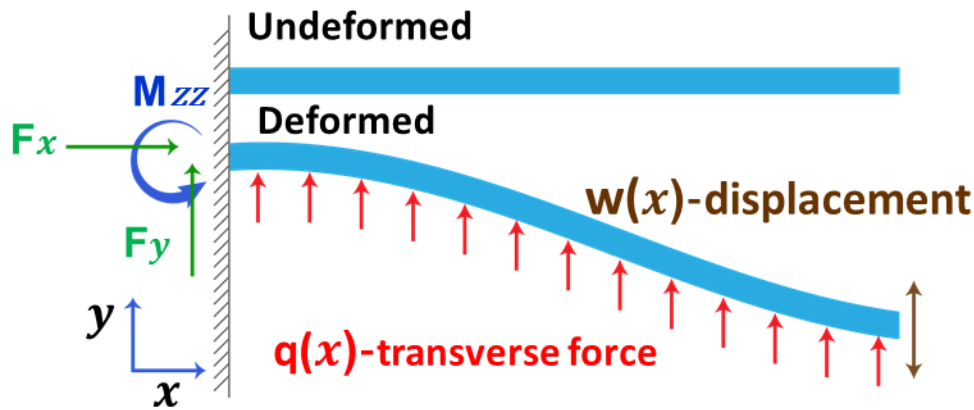
Figure 4.2: Schematic illustration of the distribution of surface stress on a cantilever under deformation.

For the small harmonic motion, the natural vibration mode of the channel can be decomposed as

$$w(x,t) = W(x)T(t) \tag{4.11}$$

where, $W(x)$ and T(t) are normal functions that define the displacement and time respectively. Plugging Eq (10) into the Euler -Bernoulli equation (Eq (9)) we obtain,

$$A\,W(x)\ddot{T}(t) + B\,W_{xxxx}T(t) - C\,W_{xx}T(t) = 0 \tag{4.12}$$

where, A= $(\rho A)^*$, B= EI^* and C = $-\left(-\left(2\sigma\left(a + 2(b + c + g + e)\right) + 4\sigma_{if}(d + g)\right)\right)$,

$W(x)\ddot{T}(t) = \frac{\partial^2 w(x,t)}{\partial t^2}$, $W_{xxxx}T(t) = \frac{\partial^4 w(x,t)}{\partial x^4}$ and $W_{xx}T(t) = \frac{\partial^2 w(x,t)}{\partial x^2}$

We consider a cantilever with clamped end at x=0 and free end at x=L. The boundary conditions for Eq (12) are expressed as

$$w(o) = 0,\; w'(0) = 0,\;\; w''(L) = 0,\; w'''(L) = 0 \tag{4.13}$$

By substituting Eq (12) into 11, Eq (11) becomes

$$r_1^5 + r_1 r_2^4 + 2\,r_1^3\,r_2^2\,\cos h r_1 L \cos r_2 L + r_1^2\,r_2^3\,\sin h r_1 L \sin r_2 L - $$
$$r_2 r_1^4 \sin h r_1 L \sin r_2 L = 0 \tag{4.14}$$

where,

$$r_1 = \frac{1}{\sqrt{2}L}\sqrt{\left[-s + \sqrt{s^2 + 4\varpi^2}\right]}, \tag{4.15}$$

$$r_2 = \frac{1}{\sqrt{2}L}\sqrt{\left[s + \sqrt{s^2 + 4\varpi^2}\right]} \tag{4.16}$$

and $S = \frac{C}{B}L^2$; $\varpi^2 = \frac{A}{B}\omega^2 L^4$, in which S is the surface effect factor. When S approaches zero, the surface effect vanishes, and the above equation yields the same resonance frequency as the classical Euler- Bernoulli equation.

4.4 Estimating Interfacial Tension

The parameter of interfacial tension can be obtained for individual alkanes from the geometric mean equation based on Owens-Wendt-Rabel-Kaelble method,

$$\gamma_{sl} = \gamma_s + \gamma_l - 2\left(\sqrt{\gamma_s^D \gamma_l^D} + \sqrt{\gamma_s^P \gamma_l^P}\right) \tag{4.17}$$

where superscripts D and P represent the dispersive and polar components, γ_s, γ_l are the surface free energies of solid and liquid respectively [62]. Since alkanes are considered to be nonpolar, their polar component is zero. The surface energy of silicon nitride is given by 74mN/m of which the dispersive component is 29 mN/m and the polar component is 45 mN/m [62]. The γ_l, γ_l^D, and γ_{sl} values are summarized in Table 4.1.

Table 4.1. Surface energy of alkanes and their respective interfacial energy to microchannel cantilever walls made of silicon nitride (estimated) [63]. Note, alkanes can be considered as purely nonpolar (i.e., $\gamma_l \approx \gamma_l^D$).

Alkane	γ_l (mN/m)	γ_l^D (mN/m)	γ_{sl} (mN/m)
Pentane	15.82	15.82	46.9817
Hexane	18.4	18.4	46.2004
Heptane	19.9	19.9	45.8542
Octane	21.3	21.3	45.5929
Nonane	23	23	45.3473

Interfacial tension can contribute as either a positive or a negative stress factor depending on the interaction of fluid with silicon nitride channel. Theoretical model modified with the interfacial

stress is represented in Figure 4.a as green line. When the beam height reduces to nanometers or microns, surface effects can be taken into consideration. To further improve the model, the residual surface tension value of silicon nitride is added to the model which is then obtained as

$$(\rho A)^* \frac{\partial^2 w(x,t)}{\partial t^2} + EI \frac{\partial^4 w(x,t)}{\partial x^4} - q\,(x) = 0 \qquad (4.18)$$

and,

$$q\,(x) = -(2\sigma\,(a + 2(b + c + g + e)\frac{\partial^2 w}{\partial x^2} + 4\sigma_{if}(d + \quad g)\frac{\partial^2 w}{\partial x^2}) \qquad (4.19)$$

is the transverse loading term arising from the resultant residual surface tension of silicon nitride and interfacial tension between the fluid and silicon nitride.

4.5 Experimental Details

Alkane series such as pentane, hexane, heptane, octane, nonane were the test materials due to their absence of polar nature in surface tension, which lessens uncertainty in estimating the interfacial tension. A U-shaped microfluidic channel of 600 μm in length is fabricated on top of the plain cantilever by conventional top-down microfabrication techniques (Figure 4.1a). The dimensions of the microfluidic channel in Figure 4.1c are given as a, b, c, d, e, f and g where they are 0.90 μm, 10 μm, 32.9 μm, 32 μm, 2.5 μm, 3.9 μm and 3 μm respectively.

Prior to loading the alkane samples, the cantilever was cleaned with piranha (in order to remove organic contaminants) and heated on a hot plate at 200° C for two hours to drive out any residual moisture. Before loading alkanes, the resonance frequency of the empty channel was noted as a part of calibration procedure. The cantilever was filled with alkane samples using syringes by applying pressure difference where the liquid is pushed through one inlet and the air is pulled out of the other outlet. As a result, in pressure difference, the liquid gets filled inside the channel.

In order to enhance the signal to noise ratio (SNR), the cantilever was mechanically excited by an external piezo actuator in the linear regime. The resonance frequency was measured optically using a laser Doppler Vibrometer (MSA 500, Polytec, USA) with 10 times averaging and was monitored continuously during the experiments. The resonance frequency and quality factor were extracted from the resonance peak. Because the viscosities of alkanes are low and the alkanes are miscible between each other, it was easy to flush and refill the channel to exchange alkane. The alkane inside the channel was completely removed using vacuum and put again on the hotplate in order to remove the residues. Prior to loading each sample, the empty cantilever was characterized to determine their resonance frequency and phase. All of the experiments were carried out at a vacuum level of 10^{-3} mbar in order to enhance the quality factor of the system.

4.6 Results and discussion

The filled microchannel cantilevers follow the same dynamics of a plain cantilever because the fluid inside the channel behaves as a homogeneous media. Figure 4.3 shows the cantilever fundamental frequency as a result of filling of alkanes in the channel. Since the fundamental frequency is dependent on the stiffness and mass, there will be frequency shift as the cantilever is filled with the alkanes.

The frequency of the empty channel cantilever was obtained as 21.19 kHz and the introduction of alkanes caused the resonance frequency of cantilever to shift varying from 4.20 kHz to 4.59 kHz from the empty channel cantilever frequency. The resonance frequencies of the channel filled with pentane, hexane, heptane, octane, nonane were obtained as 16.9875 kHz, 16.8672 kHz, 16.7437 kHz, 16.6672 kHz, 16.5969 kHz respectively. Once the channel was emptied prior to the filling of next alkane, it was observed that the frequency increased to 21. 19 kHz which is similar to empty channel frequency. As the density of alkanes varies from 626 kg/m3 to 718 kg/m3, it is evident from the shift in frequency is dependent on the mass-density addition in the channel. Here, we show that the variation of frequency shift depends not only on the mass density of the filled liquids, but also on the transverse force that the liquids cause as the result of exerted interfacial tension.

In order to explain how our enhanced model improves the fitting to the experimental results, we defined nomenclature for the three components in the model as follows: (A) the theoretical prediction of the natural resonance frequency by the conventional model, (B) our new term that includes the effect of the surface and interfacial tension and (C) The correction factor that takes account for the uncertainty in geometry.
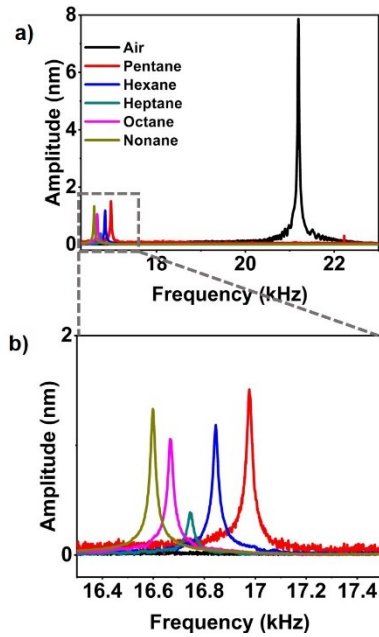
Figure 4.3: Characterisation of resonance frequency of the microchannel cantilever filled with a series of alkanes a) with and b) without the resonance peak of empty channel cantilever.

For empty channels, the conventional Euler–Bernoulli model (A) shows 5.10% discrepancy when compared to the experimental values (Experimental) as shown in Figure 4.4 a. This value (A) is obtained when we substitute s=0 in the Eq 15 and 16. When we incorporated the effect of surface tension (A+B), the discrepancy decreases to 3.24%. Here, we introduced the correction factor (A+B+C) to reconcile the discrepancy between (A+B) and (Experimental). For the microchannel cantilever that we used in the current study, we obtained the value of correction factor to be 1.03 and is the ratio of the experimental value to the conventional model value for empty channel cantilever. Accurate prediction of the resonance frequency of the microfluidic channel can be obtained with the help of finite element analysis of the structure [64,65].

When channels are filled with alkane liquids with carbon numbers between 5 to 9 (Figure 4.4 b), there is a discrepancy of 5.87 % between the conventional model (A) and the experimental values (Experimental). Using the surface tension value and the interfacial tension values from Table 1, our modified model (A+B) decreased the discrepancy to 4.19%. Using the correction factor obtained from the empty channel to the filled channel cases, we could achieve good agreement with the experimental results with an accuracy of 99.03%.

Incorporating the effect of the surface and the interfacial tension into Euler–Bernoulli beam theory in predicting the natural resonance frequency led to a partial reconciliation between the conventional model and the experimental value. In order to further the reconciliation, we introduced the correction factor. Whereas we attribute the physical origin of the correction factor to be an uncertainty in the geometry of fabricated microchannel cantilevers, there is a possibility that the correction factor includes some physics that we overlooked. One observation is that the required correction factor values for empty channel cantilever is clearly different from that for filled cantilevers. This may imply viscoelastic energy dissipation from the enclosed fluid, whereas testing the hypothesis will require a series of dedicated theoretical and experimental studies. In addition, it may be of particular mechanical interest to consider slip frictions between the cantilever and liquid medium through an interacting interface. The effects of slip friction may appear in the form of dissipative energy which was intrinsically limited in the present study where only conservative loads in the sense of virtual work statement are considered.
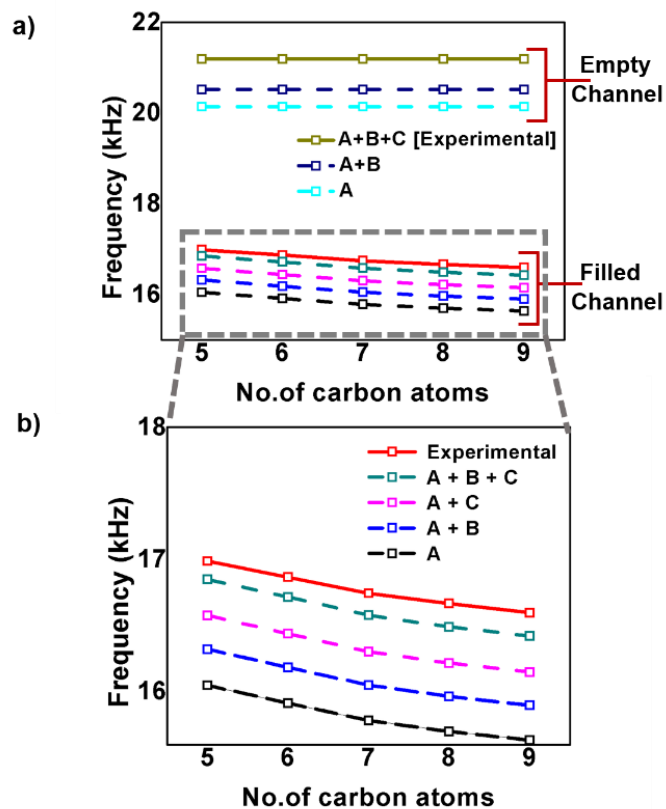
Figure 4.4: a) Experimentally observed (solid lines) and theoretically predicted (dashed lines) resonance frequencies of the microchannel cantilever. b) Enlarged view of the values from the channel filled with alkane liquids with varying carbon atoms in the chain.

4.7 Conclusion

In this study, we developed an enhanced Euler–Bernoulli beam model by incorporating Young–Laplace equation to consider transverse force along the longitudinal direction that surface, and

interface tension exerts to the vibration of the cantilever. Our model, which hypothesizes the importance of transverse force on modulating the effective modulus of the microchannel cantilever, emphasizes the importance of surface and interface tension on the natural resonance frequency of the cantilever. We tested the adequacy of our model in a cantilever in its empty channel and alkane-filled channel states, respectively. While the conventional Euler–Bernoulli beam model expects the resonance frequency value to be 5.10% and 5.87% lower than the experimental value for empty and filled channel states, the discrepancy value decreases to 3.24% and 4.19% respectively. It should be noted that our microchannel cantilevers have wall thickness values of less than a micron, and thus the interfacial tension plays a significant role in the resonance frequency of the cantilever. While our model contributes a partial reconciliation, more studies are needed to elucidate the origin of the remaining discrepancies.

4.8 References

[1] Goeders, K.M.; Colton, J.S.; Bottomley, L.A. Microcantilevers: Sensing Chemical Interactions via Mechanical Motion. Chemical Reviews 2008, 108, 522-542.

[2] Lavrik, N. v.; Sepaniak, M.J.; Datskos, P.G. Cantilever transducers as a platform for chemical and biological sensors. Review of Scientific Instruments 2004, 75, 2229.

[3] Alvarez, M.; Lechuga, L.M. Microcantilever-based platforms as biosensing tools. Analyst 2010, 135, 827.

[4] Burg, Thomas P. ; Godin, Michel.; Knudsen, Scott M.; Shen, Wenjiang.; Carlson, Greg.; Foster, John S.; Babcock, Ken.; Manalis, Scott R. Weighing of biomolecules, single cells and single nanoparticles in fluid. Nature 2007,446,1066-1069.

[5] Olcum, Selim.; Cermak, Nathan.; Wasserman, Steven C.; Christine, Kathleen S.; Atsumi, Hiroshi.; Payer, Kris R.; Shen, Wenjiang.; Lee, Jungchul.; Belcher, Angela M. .; Bhatia, Sangeeta N.; Manalis, Scott R. Weighing nanoparticles in solution at the attogram scale. Proceedings of the National Acacdemy of sciences 2014, 4, 1310-1315.

[6] Wachter, E.A.; Thundat, T. Micromechanical sensors for chemical and physical measurements. Review of Scientific Instruments 1995, 66, 3662.

[7] Tamayo, J.; Ramos, D.; Mertens, J.; Calleja, M. Effect of the adsorbate stiffness on the resonance response of microcantilever sensors. Applied Physics Letters 2006, 89, 224104.

[8] Datar, R.; Kim, S.; Jeon, S.; Hesketh, P.; Manalis, S.; Boisen, A.; Thundat, T. Cantilever Sensors: Nanomechanical Tools for Diagnostics. MRS Bulletin 2009, 34, 449.

[9] Ruz, J.J.; Pini, V.; Malvar, O.; Kosaka, P.M.; Calleja, M.; Tamayo, J. Effect of surface stress induced curvature on the eigenfrequencies of microcantilever plates. AIP Advances 2018, 8, 105213.

[10] Gurtin, M.E.; Markenscoff, X.; Thurston, R.N. Effect of surface stress on the natural frequency of thin crystals. Applied Physics Letters 1976, 29, 529.

[11] Butt, H.-J. A Sensitive Method to Measure Changes in the Surface Stress of Solids. Journal of Colloid and Interface Science 1996, 180, 251.

[12] Lagowski, J.; Gatos, H.C.; Sproles, E.S. Surface stress and the normal mode of vibration of thin crystals: GaAs. Applied Physics Letters 1975, 26, 493.

[13] Chen, G.Y.; Thundat, T.; Wachter, E.A.; Warmack. R.J. Adsorption-induced surface stress and its effects on resonance frequency of microcantilevers. Journal of Applied Physics 1995, 77, 3618.

[14] Cherian, S.; Thundat, T. Determination of adsorption-induced variation in the spring constant of a microcantilever. Applied Physics Letters 2002, 80, 2219.

[15] Wang, D.F.; Ono, T.; Esashi, M. Thermal treatments and gas adsorption influences on nano mechanics of ultra-thin silicon resonators for ultimate sensing. Nanotechnology 2004, 15, 1851.

[16] Hwang, K.S; Eom, K.; Lee, J.H.; Chun, D.W.; Cha, B.H.; Yoon, D.S.; Kim, T.S.; Park, J.H. Dominant surface stress driven by biomolecular interactions in the dynamical response of nanomechanical microcantilevers. Applied Physics Letters 2006, 89, 173905.

[17] Malvar, O.; Ruz, J. J.; Kosaka, P. M.; Domínguez, C. M.; Gil-Santos, E.; Calleja, M.; Tamayo, J. Mass and stiffness spectrometry of nanoparticles and whole intact bacteria by multimode nanomechanical resonators. Nat. Commun. 2016; 7: 13452.

[18] Stachiv, I.; Gan, L.; Kuo, C.-Y.; Šittner P., Ševeček, O. Mass Spectrometry of Heavy Analytes and Large Biological Aggregates by Monitoring Changes in the Quality Factor of Nanomechanical Resonators in Air. ACS Sens. 2020, 5, 7, 2128–2135

[19] McFarland, A.W.; Poggi, M.A.; Doyle, M.J.; Bottomley, L.A.; Colton, J.S. Influence of surface stress on the resonance behavior of microcantilevers. Applied Physics Letters 2005, 87, 053505.

[20] Ren, Q.; Zhao, Y.; Influence of surface stress on frequency of microcantilever-based biosensors. Microsystem Technologies 2004, 10, 307-314.

[21] Huang, G.Y.; Gao, W.; Yu, S.W.; Model for the adsorption-induced change in resonance frequency of a cantilever. Applied Physics Letters 2006, 89, 043506.

[22] Dorignac, J.; Kalinowski, A.; Erramilli, S.; Mohanty, P. Dynamical Response of Nanomechanical Oscillators in Immiscible Viscous Fluid for In Vitro Biomolecular Recognition. Physical Review Letters 2006, 96, 186105.

[23] Wang, G.F.; Feng, X.Q. Effects of surface elasticity and residual surface tension on the natural frequency of microbeams. Applied Physics Letters 2007, 90, 231904.

[24] Lu, P.; Lee, H.P.; Lu, C.; O'Shea, S.J. Surface stress effects on the resonance properties of cantilever sensors, Physical Review B 2005, 72, 085405.

[25] Lachut, M.J.; Sader, J.E. Effect of Surface Stress on the Stiffness of Cantilever Plates. Physical Review Letters 2007, 99, 206102.

[26] Sader, J.E. Surface stress induced deflections of cantilever plates with applications to the atomic force microscope: Rectangular plates. Journal of Applied Physics 2001, 89, 2911.

[27] R. B. Karabalin, L. G. Villanueva, M. H. Matheny, J. E. Sader, and M. L. Roukes. Stress-Induced Variations in the Stiffness of Micro- and Nanocantilever Beams. Phys. Rev. Lett. 108, 236101

[28] He, J.; Lilley, C.M. Surface stress effect on bending resonance of nanowires with different boundary conditions. Applied Physics Letters 2008, 93, 263108.

[29] Sohi, A.N.; Nieva, P.M. Frequency response of curved bilayer microcantilevers with applications to surface stress measurement. Journal of Applied Physics 2016, 119, 044503.

[30] Najafi Sohi, A.; Nieva, P.M. Size-dependent effects of surface stress on resonance behavior of microcantilever-based sensor. Sensors and Actuators, A: Physical 2018, 269, 505.

[31] Stachiva, I. Impact of surface and residual stresses and electro-/magnetostatic axial loading on the suspended nanomechanical based mass sensors: A theoretical study, Journal of Applied Physics, 2014, 115, 214310

[32] Stachiv, I.; Fang, T.-H..; Chen, T.-H. Micro-/nanosized cantilever beams and mass sensors under applied axial tensile/compressive force vibrating in vacuum and viscous fluid. AIP Advances 2015,5, 117140

[33] Kong, S.; Zhou, S.; Nie, Z.; Wang, K. The size-dependent natural frequency of Bernoulli–Euler micro-beams. International Journal of Engineering Science 2008, 46, 427-437.

[34] Zhao, J.; Zhou, S.; Wang, B.; Wang, X. Nonlinear microbeam model based on strain gradient theory. Applied Mathematical Modelling 2012, 36,2674-2686.

[35] Javili, A.; dell'Isola, F.; Steinmann, P. Geometrically nonlinear higher-gradient elasticity with energetic boundaries. J. Mech.Phys. Solids 2013, 61, 2381–2401.

[36] dell'Isola, F.; Seppecher, P.; Madeo, A. How contact interactions may depend on the shape of Cauchy cuts in Nth gradient continua: approach "à la D'Alembert". Z. Angew. Math. Phys 2012, 63, 1119–1141.

[37] dell'Isola, F.; Corte, A.D; Giorgio, I. Higher-gradient continua: The legacy of Piola, Mindlin, Sedov and Toupin and some future research perspectives. Math. Mech. Solids 2016, 22, 852–872.

[38] Mindlin, R.D; Tiersten, H.F. Effects of couple-stresses in linear elasticity. Arch Ration Mech Anal 1962, 11, 415–448.

[39] Germain, P.; The Method of Virtual Power in Continuum Mechanics. Part 2: Microstructure. SIAM J Appl Math, 1973, 25, 556–575

[40] Spencer, A.J.M.; Soldatos, K.P. Finite deformations of fibre-reinforced elastic solids with fibre bending stiffness. Int J Nonlin Mech. 2007, 42, 355–368.

[41] Alibert, J.J.; Seppecher, P.; Dell'Isola, F. Truss Modular Beams with Deformation Energy Depending on Higher Displacement Gradients. Math Mech Solids 2003, 8, 51–73.

[42] Dell'Isola, F.; Giorgio, I.; Pawlikowski, M.; N.L. Rizzi. Large deformations of planar extensible beams and pantographic lattices: heuristic homogenization, experimental and numerical examples of equilibrium. Proc R Soc A 2016, 472, 0790.

[43] Seyed Bolouri, SE; Kim, C.I; Yang, S. Linear theory for the mechanics of third-gradient continua reinforced with fibers resistance to flexure. Mathematics and Mechanics of Solids 2019, 25, 937-960.

[44] Kim, C.I; Islam, S. Mechanics of third-gradient continua reinforced with fibers resistant to flexure in finite plane elastostatics. Continuum Mechanics and Thermodynamics 2020, 32, 1-23

[45] Kim, C.I. Strain-Gradient Elasticity Theory for the Mechanics of Fiber Composites Subjected to Finite Plane Deformations: Comprehensive Analysis. Multiscale Science and Engineering 2019, 1, 150-160

[46] Zeidi, M.; Kim, C.I. Mechanics of fiber composites with fibers resistant to extension and flexure. Mathematics and Mechanics of Solids 2017, 24, 3-17.

[47] Kim, C.I; Zeidi. M. Gradient elasticity theory for fiber composites with fibers resistant to extension and flexure. International Journal of Engineering Science 2018, 131, 80-99.

[48] Zeidi, M.; Kim, C.I. Finite plane deformations of elastic solids reinforced with fibers resistant to flexure: complete solution. Archive of Applied Mechanics 2018, 88, 819-835.

[49] Zeidi, M.; Kim, C.I. Mechanics of an elastic solid reinforced with bidirectional fiber in finite plane elastostatics: complete analysis, Continuum Mechanics and Thermodynamics 2018, 30, 573-592.

[50] Kim, C.I. Superposed Incremental Deformations of an Elastic Solid Reinforced with Fibers Resistant to Extension and Flexure. Advances in Materials Science and Engineering 2018, 2018.

[51] Liu, C.; Rajapakse, N. Continuum Models Incorporating Surface Energy for Static and Dynamic Response of Nanoscale Beams. IEEE Transactions on Nanotechnology 2010, 9, 422 - 431.

[52] Manzoor Bukhari, S.A.; Khan, M.F.; Goswami, A.; McGee, R.; Thundat, T. Thermomechanical analysis of picograms of polymers using a suspended microchannel cantilever. RSC Advances 2017, 7, 8415.

[53] Gimzewski, J.K.; Gerber, C.; Meyer, E.; Schlittler, R.R. Observation of a chemical reaction using a micromechanical sensor, Chemical Physics Letters 1994, 217, 589-594.

[54] Jiang, K.; Khan, F.; Thomas, J.; Desai, P.R.; Phani, A.; Das, S.; Thundat, T. Thermomechanical responses of microfluidic cantilever capture DNA melting and properties of DNA premelting states using picoliters of DNA solution, Applied Physics Letters 2019, 114, 173703.

[55] Khan, M.F.; Schmid, S.; Larsen, P.E.; Davis, Z.J.; Yan, W.; Stenby, E.H.; Boisen, A. Online measurement of mass density and viscosity of pL fluid samples with suspended microchannel resonator, Sensors and Actuators, B: Chemical 2013, 185, 456-461.

[56] Etayash, H.; Khan, M.F.; Kaur, K.; Thundat, T. Microfluidic cantilever detects bacteria and measures their susceptibility to antibiotics in small confined volumes, Nature Communications 2016, 7, 1-9.

[57] Gurtin, M.E.; Murdoch, A.I. A continuum theory of elastic material surfaces, Arch. Rational Mech. Anal. 1975, 57,291–323.

[58] Gurtin, M.E; Weissmuller, J.; Larche, F. A general theory of curved deformable interface in solids at equilibrium, Philos. Mag. A 1998, 78, 1093–1109.

[50] Prak ,Dianne J. Luning.; Cowart ,Jim S.; Trulove ,Paul C. Density, Viscosity, Speed of Sound, Bulk Modulus, and Surface Tension of Binary Mixtures of n-Heptane + 2,2,4-Trimethylpentane at (293.15 to 338.15) K and 0.1 MPa, J. Chem. Eng. Data 2014, 59, 11, 3842–3851

[60] Mougin, Pascal.; Rasaolofosaon, Patrick.; Zinszer, Bernard. Petroacoustics of poorly consolidated reservoir rocks saturated with co2/methane/brine mixtures, SACS2 european research project 2002.

[61] Zapomel, J.; Stachiv, I.; Ferfecki, P. A novel method combining Monte Carlo–FEM simulations and experiments for simultaneous evaluation of the ultrathin film mass density and Young′s modulus. Mech Syst Signal Process 2016, 66-67, 223

[62] Park, S.J.; Seo, M.K. Solid-Liquid Interface in Interface Science and Technology 2011, 18, 147-252.

[63] Grigoryev, B.A.; Nemzer, B.V.; Kurumov, D.S. Surface tension of normal pentane, hexane, heptane, and octane, Int J Thermophys 1992,13,453-464.

[64] Cheri M. S.; Latifi H.; Sadeghi J.; Moghaddam M.S.; Shahraki H.; Hajghassem H. Real-time measurement of flow rate in microfluidic devices using a cantilever-based optofluidic sensor. Analyst 2014, 139, 431-438.

[65] Hajesfandiari, A.; Sukhotskiy, V.; Alodhayb, A.; Khan, F.; Thundat, T. Furlani, E.P. Microfluidic microcantilever as a sensitive platform to measure evaporation rate of picoliters of ethanol, Measurement 2020, in press. doi:10.1016/j.measurement.2020.108617

Chapter 5

Measurement of Thermal Properties of Liquid Analytes using Microfluidic Resonators via Photothermal Modulation

5.1 Abstract

Understanding the thermal properties of fluids at the nanoscale with high spatial, temporal, and thermal resolution are on great demand in the fields of MEMS, drug development, biomedical devices, and analytical systems. Microfluidic channel-integrated cantilevers are considered as an established benchtop sensor platform for physical and thermal characterization of materials at the picogram amount of analytes. This chapter reports analysis of the thermal characteristics of liquid analytes using photothermal heating effect of the microfluidic cantilever. While the liquid analyte in the cantilever is locally heated by laser-induced irradiation, real-time tracking of resonance frequency shift of the microfluidic resonator allows the estimation of thermal properties of liquid samples. The heating results in the expansion of the liquid inside the channel which induces thermal stress on the walls of the channel. This thermal stress contributes to a rise of the resonance frequency of the microfluidic resonator and, therefore, the frequency shift is linearly dependent of the volumetric coefficient expansion of the liquid. A threefold improved sensitivity is observed when the second order flexural vibration mode is analyzed compared to that of the fundamental resonance. This approach, which combines photothermal heating and the dynamic mode of operation, can serve as a platform for the development of a portable, lab on a chip device for the use of real time detection of thermomechanical properties of fluids at low cost.

5.2 Introduction

When studying thermal properties of precious analytes, for example DNA[1], protein [2], precision polymers [3], colloidal nanofluids in microelectronic industry [4,5] and antigen-antibody pairs [6], the ability to analyze nanogram-scale amount of fluids is a key eligibility requirement for a sensing

technology [1,2,3,4,5,6,7]. The nanoscale sensing ability can also enable the miniaturization of the analytical platforms, which have significant advantages such as portability, quick throughput, and facilitated control of local reaction environment [7,8]. The matured micro and nanofabrication technology over the past two decades allows single miniaturized sensing platform to provide orthogonality between multiple sensing with enhanced sensitivity and selectivity [8,9]. Among the miniaturized tools, microcantilever-based sensors have unique advantages including high sensitivity, low power consumption, label-free detection, and array-based sensing of multiple analytes in real-time [9]. The large ratio of surface area to mass renders the microcantilevers to have extreme sensitivity at the surface, allowing them to detect small changes in mass, density, stress, temperature even in fluid environment [10]. The sensing concept relies on the transduction of surface interactions into mechanical signals as either cantilever deflection (static mode) or a shift in resonance frequency (dynamic mode), whereas the surface interactions may include adsorption of analytes from environment [9].

The bi material microcantilever beam (BMC) with a metal layer on top of silicon or silicon nitride cantilever provides highly sensitive thermomechanical characterization tool for various applications including calorimetry [7], spectroscopy [11], chemical or biological analyte detector [12] , IR detectors [13], scanning thermal imaging probes [14]. A bi-material cantilever is fabricated from two different materials with dissimilar coefficients of thermal expansion. It experiences a thermal stress generated by the mismatch of the thermal expansion coefficients of the constituent materials for a temperature rise and results in bending [15]. Deflection of a bi-material microcantilever is calculated by considering the heat transfer to and within the cantilever, whereas the heating changes the mechanical behavior of the cantilever [15].They have demonstrated their ability as excellent thermomechanical sensors detecting as small as 40 pW for power, 10 fJ for energy and a temperature resolution of 10^{-5} K [16]. Consequently, it is possible to detect local heat generation produced by a chemical reaction at the end of the cantilever beam [17].

Various studies have attempted to analyze the liquid properties using a microcantilever in the dynamic mode. In the dynamic mode, the cantilever is mechanical driven at its fundamental or higher-mode resonance frequency, whereas an increase of the cantilever mass due to analyte

absorption causes a decrease of the cantilever resonance frequency. The resonant characteristics of a micro cantilever immersed in fluid had been studied experimentally [18] and theoretically [19,20] for measuring viscosity [19], density [19], liquid damping force [10], and biomolecular recognition [20]. An important parameter in the resonant mode of operation is the mechanical quality factor which determines the frequency stability and, consequently, the limit of detection (LOD) [10]. The quality factor of the resonant microcantilever immersed in a liquid is low due to energy dissipation in the surrounding dense medium and directly affects the sensitivity and detection limit of this type of sensor. When studying the chemical and biological analytes in a liquid media, the viscosity of the media often causes damping of the oscillation so that the resonance peaks become broadened and undefined (i.e., poor quality factor) [10]. One may argue that static-mode cantilevers operation based on surface stress is free from damping concerns and thus is preferable, but they are often prone to noise and drift [21]. Another constrain that limits the application of the microcantilever sensor is the change in signal to noise ratio by the presence of liquid flow [22].

Microfluidic channel-integrated cantilevers (*i.e.*, microchannel cantilevers) introduced by Manalis group overcome the limitations of liquid damping in the dynamic mode operation, and thus achieves unprecedented precision in thermomechanical characterization with enhanced signal stability [15,23,24]. The resonance frequency shift of the resonators can detect minuscule fluctuation of physical [3], chemical [24], and biological stimulus [9] within medium of fluidic channel. These microchannel cantilevers produce resonance peaks with quality factors up to three orders of magnitude higher than the beam resonator immersed in liquid [25]. Since the liquid is inside the cantilever, the microchannel cantilever can operate in a vacuum for increased mass resolution and higher reproducibility [25,23]. The resonance frequency and the quality factor of a microfluidic cantilever imply various physical parameters, such as density and viscosity of the confined liquid [26]. Measuring the Q-factor, determined by the full-width at half-maximum (FWHM) of the resonance peak, reveals viscosity information of the liquid sample [27]. The fluid-filled microchannel cantilevers enabled weighing of surface-adhered biomolecules and single cells in fluid with extremely high sensitivity [28]. The unmatched sensitivity and signal reliability of the microchannel cantilever enabled the precise real-time measurement of mass accumulation rate

of a single cell during the events of gene expression and cancer cell development by monitoring resonance frequency and cantilever deflection [9,29,30].

A BMC concept that incorporates an embedded microchannel enabled thermal analysis of liquids at sub-nanolitre level while the detection is performed in the static mode [7]. In the study, the capacity of liquid sample of 150 pL was measured with a resolution of 23 mJ/g·K when the sample is irradiated by a Quantum cascade laser (QCL) that generate infrared light with well-defined wavelengths [7]. The localized light-induced heating of the liquid resulted in a static deflection of the BMC due to thermal expansion mismatch between the constituent materials. The BMC deflection is proportional to multiple factors, including the thermomechanical sensitivity of the device, the optical intensity, the irradiation time, the light absorption coefficient of a sample inside the microchannel, the thermal properties of the sample, and the difference between the thermal expansion coefficients of the constituting materials. Therefore, the selection of the proper bi-material elements and optimization of thickness of the layers are limiting factors while considering BMC cantilevers for thermal sensitivity experiments. Also, the bending response of resonators based on static mode where the results are prone to be affected by mechanical drift and higher noise level of the photodetector have brought need of the simpler experimental model and dynamic response.

In dynamic mode, the thermal properties of the confined liquid analytes are characterized by the resonation frequency shift, whereas the shift is driven by the stress due to thermal expansion/contraction of the analyte [31]. In explaining the thermally induced bending of BMCs with an analytical model, Tamayo et al. introduced the concept of differential surface stress [31]. In addition, He and Lilley approached the influence of surface stress on resonance bending nanowires by incorporating the generalized Young-Laplace equation into Euler-Bernoulli beam theory and studying the solution for different boundary conditions [32]. They considered that the distributed transverse force resulting from the surface stress along the nanowires longitudinal direction is considered as a function of the curvature in small deformations. Hence, the strain independent stress and the surface elasticity in the Euler-Bernoulli equation is accommodated by the concept of surface stress [36]. The effect of interfacial tension on the resonance frequency of the micro-fluidic channel has been discussed with the inclusion of Young-Laplace equation in the

Euler-Bernoulli equation in a recent study [33]. In the present work, we hypothesized that the thermal stress generated by the liquid inside the microchannel cantilever exerts transverse force acting along the longitudinal direction of the deformed beam that modulates the effective modulus of the cantilever system.

In this paper, a silicon nitride microchannel cantilever operating in dynamic mode is proposed to be a measurement platform for comparing thermal properties of liquids. By the application of the pressure, the liquids are loaded inside the microchannel cantilever and are optically heated at vacuum to obtain their thermal properties. The liquid filled resonator is modulated by a continuous wave laser diode to provide the necessary optical heating. The use of microchannel cantilever enabled the detection of thermal properties of liquid analytes, such as volumetric expansion and heat capacity, by monitoring the resonance frequency shift and the transition time of this shift. The purpose of this study is to develop a miniature, robust, and sensitive platform to obtain real time information about the thermomechanical characterization of liquids.

5.3 Experimental Details

In photothermal characterization of a volume of fluid sample with a picolitre amount is heated by laser light with desired wavelengths while the sample is contained in the microchannel cantilever. The resonance frequency shift of the cantilever provides real time information regarding the thermal properties of the fluid such as volumetric expansion, heat capacity and thermal diffusivity. Figure 5.1 shows the conceptual schematic of the experiment where a U-shaped silicon nitride microfluidic channel (16 µm wide, 300 µm long and 3 µm high) fabricated on top of a plain cantilever (44 µm wide, 500 µm long and 500 nm thick) with a liquid sample is heated by a red laser (635 nm) with an optical power of 0.362 mW with a spot diameter of 20 µm. This microchannel cantilever is supported on a 350 µm thick silicon chip, which provides fluidic inlets and outlets for delivering sample fluids to the microchannel on the cantilever.
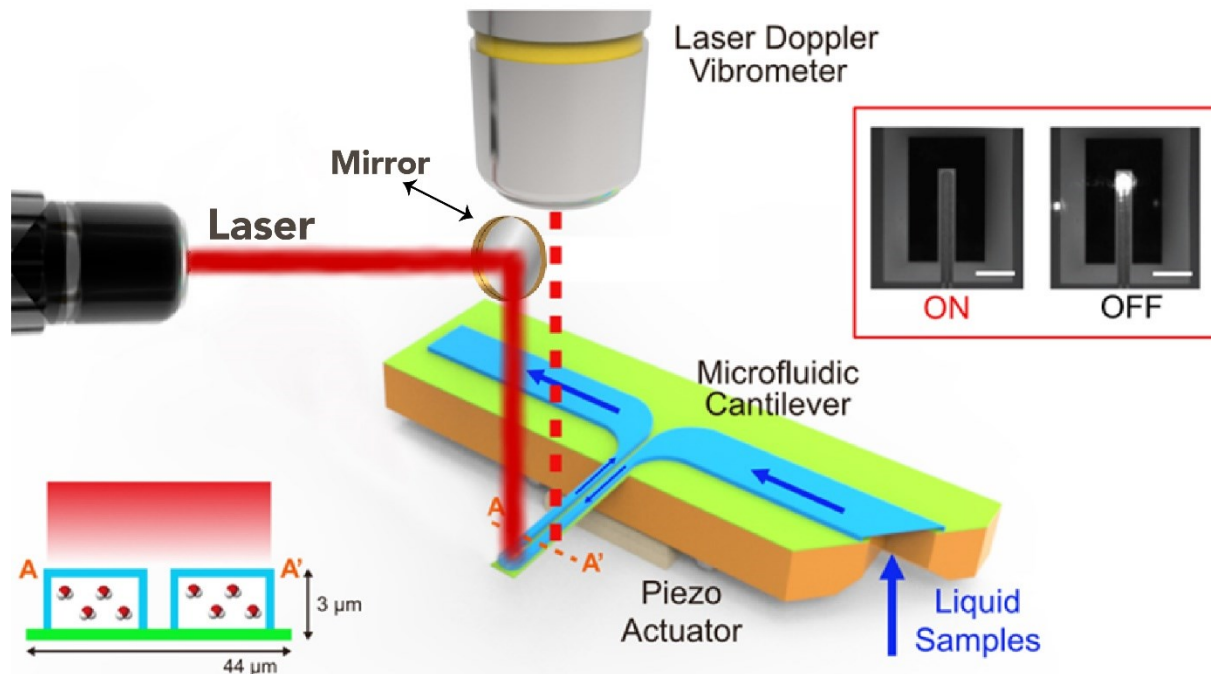
Figure 5.1: A conceptual schematic of the fluidic resonator filled with liquid samples subjected to photothermal modulation. (Subset) Top view of the resonator when the heating laser aligned and powered off/on. Scale bars are 100 μm.

Two openings at the bottom of the chip provide a fluidic interface between the chip and connecting Teflon tubes. The fluid sample is loaded inside the channel by applying pressure and then unloaded by applying the negative pressure to outlet. Upon completion of measurement, the channel is thoroughly washed with deionized water then completely dried before another loading of liquid sample. In the vacuum environment (3×10^{-5} mbar), the resonator is externally excited by a piezo actuator as shown in Figure 5.2. This method offers a high quality factor thus high frequency stability while the integrated channel is at atmospheric pressure or filled with a stationary liquid. The resonance frequency of the resonator is simultaneously measured with a laser Doppler vibrometer (LDV) (MSA-500, Polytec). While open loop sweep is run by the LDV system, the closed loop modulation of the resonator is controlled by custom-made circuit, which enables real time tracking of frequency variation. All of the measurements are conducted at room temperature.
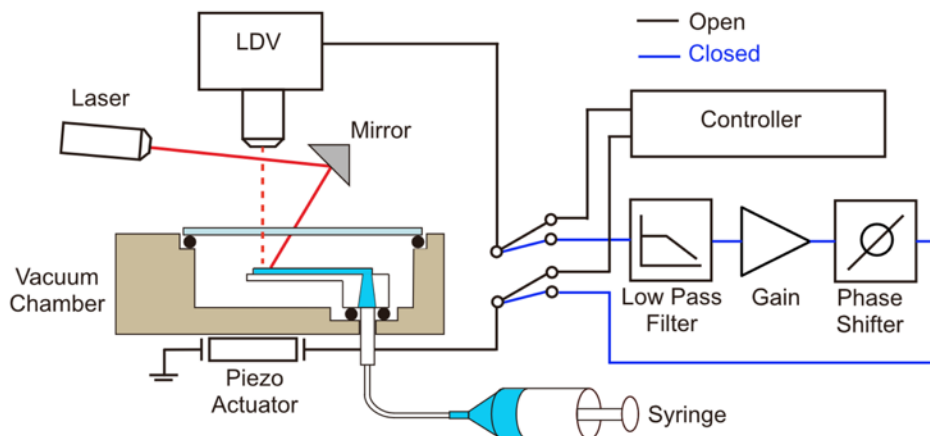
Figure 5.2: Schematic and of the measurement setup composed of a commercial laser Doppler vibrometer, vacuum chamber, closed loop circuit and custom modification for photothermal modulation

5.4 Characterization

Figure 5.3 a and 5.3 b shows the frequency response of the microchannel cantilever filled with air, water and Ethanol, respectively, without laser heating. The resonance frequencies of the different liquids filled in the channel cantilever such as ethanol, methanol, butanol, ethylene glycol, toluene, n- heptane, chloroform and water are shown as a function of their densities in Figure 5.3 c. As a reference, resonance frequency of the air-filled cantilever is characterized upon different the heating position on the cantilever (Supplementary Figure S1). The modulation frequency of the laser is maintained at 25 mHz with 50% duty cycle which is controlled by an optical chopper (MC2000B, Thorlabs). The cantilever is therefore exposed to an optical pulse every 20 seconds which is enough to provide the thermal relaxation or establish thermal equilibrium in the cantilever liquid system.
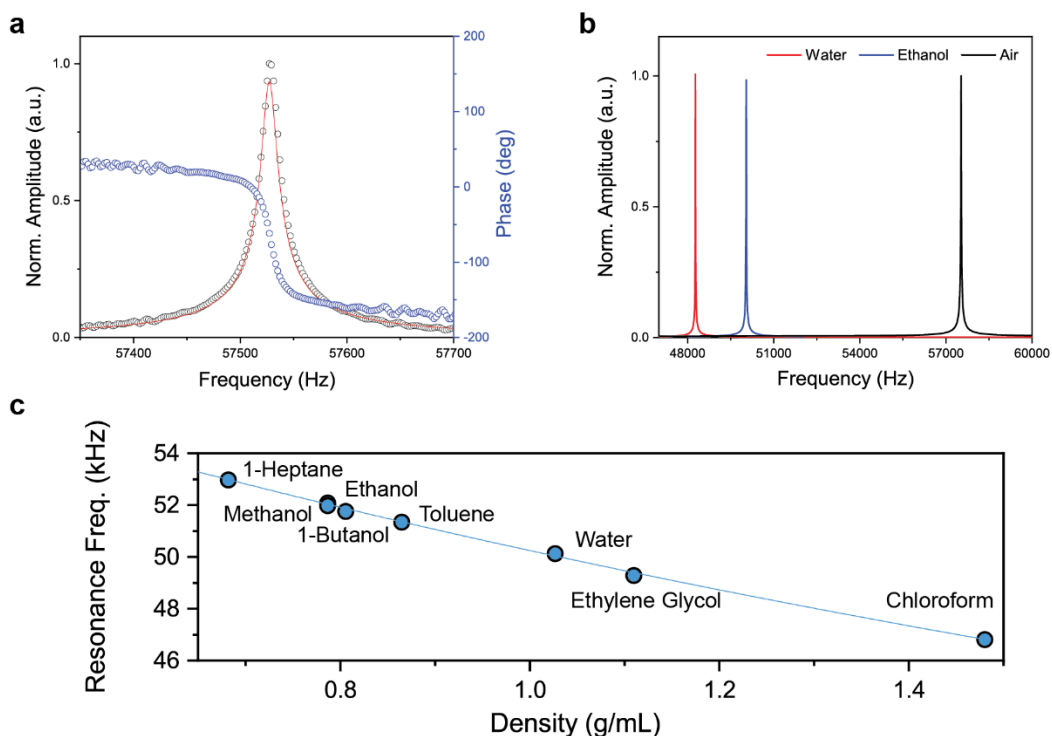
Figure 5.3: (a) 1st flexural mode resonance spectra of the air-filled microfluidic resonator in vacuum, and (b) frequency response of the microfluidic resonator when filled with air and other liquid loadings c) frequency response of cantilever filled with liquid samples as a function of liquid density.

The air-filled cantilever at atmospheric pressure shows an immediate drop of the resonance frequency when the photothermal heating is applied, followed by a slow surge towards saturation (Figure 5.4 a). When the heating is turned off, the resonance frequency instantly surges, followed by a gradual recovery towards the initial frequency level. The water-filled cantilever, however, shows an instant increase of the resonance frequency of the 1st (2nd) flexural mode from 48.28 (290.38) kHz to 48.32 (290.52) kHz within a few seconds upon the laser heating (Figure 5.4 b). The behavior of frequency shift of the water filled cantilever for different laser heating time is shown in Figure S2 and it is evident from the figure that the frequency reached towards a saturation level when the laser has kept on for 40 seconds. Throughout the heating time, the resonance frequency is nearly constant, implying that the cantilever is at a steady-state condition. When the laser is off, the frequency recovery is immediate and to the initial value.
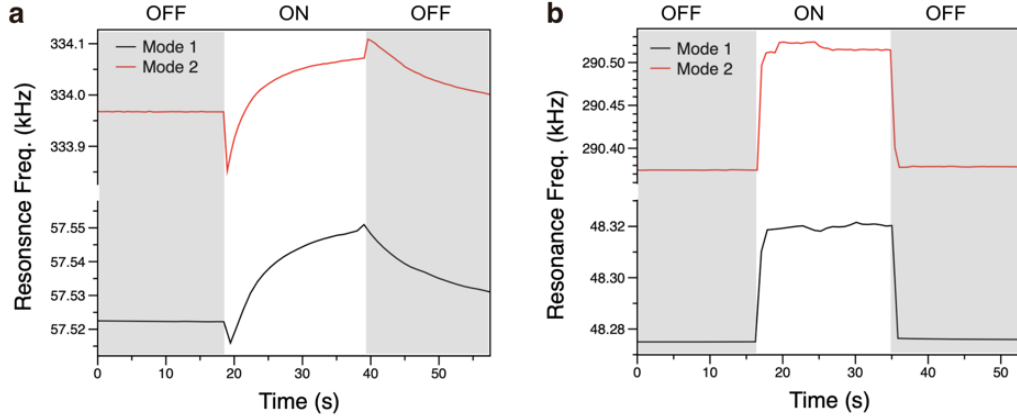
Figure 5.4: 1st and 2nd flexural mode resonance frequency shifts of the resonator filled with (a) air and (b) water as a result of the photothermal modulation. In both cases of air and water filled cantilevers, the frequency increases as the laser is turned on and decreases as the laser is turned off.

5.5 Discussion

In order to study the photothermal effects on the natural resonance frequency of microfluidic cantilever, the following factors were considered: (i) stiffness change of the cantilever, (ii) surface stress induced by the volumetric expansion of the fluid upon heating, and (iii) density change of the system. When the laser illuminates on the fluid filled cantilever, two processes are occurring simultaneously. One is the softening of the cantilever because of the reduction in the Young's modulus of the cantilever due to the light-induced heating, which decreases the resonance frequency of the cantilever[34]. Another is the thermal expansion of the fluid inside the channel that builds up an internal pressure, which increases the resonance frequency of the cantilever. The reduction in the frequency of the cantilever due to the heating-induced change in Young's modulus is expressed as

$$\frac{\delta f_n}{f_n^o} = \frac{1}{2}\frac{\delta E}{E} \approx \frac{1}{2}\alpha_E\frac{dT}{dI}I \tag{5.1}$$

where δf_n and f_n^o are the shift in the frequency and initial frequency, respectively, and $\delta E, E, \alpha_E$ are the change in the modulus, initial modulus and temperature coefficient of modulus, respectively[34]. Also, dT and dI are the change in temperature and moment of inertia,

respectively. Since α_E of Si₃N₄ is -64×10^{-6} [°K⁻¹], the reduction in the frequency can be explained with the increase in temperature upon the irradiation of laser light.

The internal pressure buildup stems from the fact that the fluids in the microchannel have higher expansion coefficient than solid cantilever made of silicon nitride; the order of thermal expansion coefficient of liquids is ~10^{-3} K⁻¹ and of solids is ~10^{-5} K⁻¹ [35]. Therefore, we can consider the contribution of liquid expansion is more than the channel expansion to shift in the frequency.

The thermal expansion of the liquid with the increase in temperature inside the channel is calculated as follows,

$$\Delta V_f = \gamma_f V_f \Delta T \qquad (5.2)$$

where ΔV_f is the change in volume, V_f is the initial volume, γ_f is the volumetric expansion coefficient and ΔT is the change in temperature[36].

The temperature rise in the cantilever can be obtained based on the following assumptions.
1) The temperature is assumed to vary only along the length of the cantilever.
2) The fluid inside the channel is considered as a homogeneous and incompressible media, and the beam is a linearly elastic solid.
3) The temperature at the base of the cantilever is assumed to be same as the ambient, T_∞ [37].

The temperature rise in the system because of the absorption of photons of red laser light depends on the power of the light absorbed and is inversely proportional to heat loss mechanisms available. The heat transfer analysis of the microfluidic channel beam could be explained using a fin conduction model. The governing equation for the cantilever beam operating in air, according to fin conduction model, is given as

$$\frac{d^2T}{dx^2} - m^2(T - T_\infty) = 0 \qquad (5.3)$$

and

$$m^2 = \frac{2h}{2(\lambda_1 t_1) + \lambda_2 t_2}$$

(5.4)

where T_∞ is the ambient temperature and x is the distance along the axis of the cantilever[37]. In this equation, h is the natural convection coefficient of the fluid, $\lambda_1 = 29\,\frac{W}{mK}$, $\lambda_2 = 0.119$ to 0.607 $\frac{W}{mK}$, are the thermal conductivities and $t_1 = 0.4 \times 10^{-6}m$, $t_2 = 3 \times 10^{-6}m$,are the thickness of the silicon nitride channel and fluid respectively. In this case, the temperature distribution along the cross sections of a cantilever beam could be neglected, and only the temperature distribution along the beam axis (one dimensional) is considered. In this way the heat transfer analysis of the cantilever beam could be approximate as a fin conduction model. Assuming $T_o = T_\infty$, the temperature distribution along the length of the cantilever placed in a uniform ambient temperature bath and heated at one end is calculated as

$$T(x) - T_\infty = \frac{P}{m\,(2(\lambda_1 t_1) + \lambda_2 t_2)\,w} \frac{\sinh\,(m(L-x))}{\cosh\,(mL)}$$

(5.5)

given P as the absorbed power and x as the distance from the free end of the cantilever. [37,38].
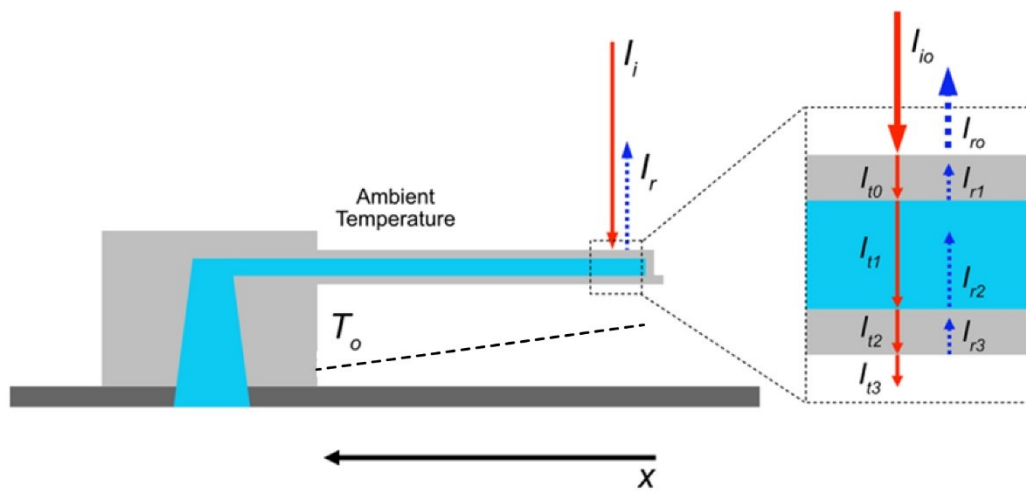
Figure 5.5: Schematic of the incident laser, reflected laser and transmitted laser light on the microfluidic channel in a uniform temperature bath. Only the free end of the cantilever is optically heated, and the base of the cantilever has a temperature of T_o.

 The absorbed power for each fluid is calculated using Fresnel's equation and Beer-Lambert law. When light strikes the interface between a medium with refractive index n_1 (air) and a second medium with refractive index n_2 (silicon nitride), both reflection and refraction of the light may occur as shown in Figure 5.5. The incident light intensity on a surface can be represented as the summation of the transmitted intensity and reflected intensity, provided the scattering losses are negligible [39]. Using Fresnel's equation, at normal incidence the reflectance and transmittance of the laser light entering from air to channel, a medium of refractive index n_1 to a medium of refractive index n_2, are obtained using the given equation.

$$\text{Reflectance, } R = \left(\frac{n_0 - n_1}{n_0 + n_1}\right)^2 \tag{5.6}$$

$$\text{Transmittance, } T = 1 - \left(\frac{n_0 - n_1}{n_0 + n_1}\right)^2 \tag{5.7}$$

A fraction of the refracted light is absorbed by the channel depending upon the absorption coefficient of the silicon nitride. The net transmitted power through the silicon nitride layer is the incident power on the liquid interface. It again undergoes reflection and transmission. The transmittance through liquid is calculated using Eq (8) with the refractive indices of silicon nitride and liquid.

$$T = 1 - \left(\frac{n_1 - n_2}{n_1 + n_2}\right)^2 \tag{5.8}$$

where T is the transmittance, n_1 and n_2 are the refractive indices of the silicon nitride and fluid respectively and is listed in Table 5.1. And transmitted intensity I_t is given as

$$I_t = T \times I_{in} \tag{5.9}$$

The absorbed intensity by each liquid is calculated as

$$I_{abs} = I_t - I_t e^{-\alpha t} \tag{5.10}$$

where α is the absorption coefficient and t is the thickness of the layer through which laser passes.

Table 5.1. Refractive indices and transmittance of liquids and channel material at 635 nm[42].

Sample or channel material	Refractive index (n)	Transmittance (T)
Water	1.33	0.97
Ethylene Glycol	1.46	0.95
Butanol	1.39	0.94
Methanol	1.31	0.92
Ethanol	1.36	0.93
Toluene	1.48	0.95
n-Heptane	1.38	0.94
Chloroform	1.44	0.94
Silicon nitride	2.28	0.84

Now, considering T_∞ as 293 K, ΔT calculated for water is calculated as 2.35×10^{-4}. The value of natural convective heat transfer coefficient h was approximated from literature[38,40,41]. In thermal modelling, the values were chosen based on the literature as they provide a good fit for the experimental results. The h values are approximated as 0.75 W/m²K, 0.5 W/m²K, 0.8 W/m²K, 0.88 W/m²K, 0.89 W/m²K, 1.3 W/m²K, 0.9 W/m²K, 1.3 W/m²K for water, ethylene glycol, butanol, methanol, ethanol, toluene. n-heptane, chloroform respectively. Thermal stress is generated by the thermal expansion of liquid and is calculated as

$$\sigma = \frac{\Delta V_f}{V_f} B \tag{5.11}$$

where σ is the thermal stress, B is the bulk modulus of the fluid [35]. The thermal stress appears as a surface stress on the walls of the channel of the cantilever. Surface stress generated by different fluids is different depending on their volumetric coefficient of expansion and bulk modulus as

$$\sigma \propto \Delta V_f , B , \gamma_f \tag{5.12}$$

For a bending beam, the curvature is not zero and the surface stress will generate a distributed transverse loading, $q(x,t)$, along the longitudinal direction on the surface as

$$q(x) = \sigma dL \frac{\partial^2 w}{\partial x^2} \tag{5.13}$$

where σ is the surface stress, d is the width and L is the length of the beam[33]. The enhanced Euler Bernoulli beam equation is given then given as

$$(\rho A)^* \frac{\partial^2 w(x,t)}{\partial t^2} + (EI)^* \frac{\partial^4 w(x,t)}{\partial x^4} + q(x) = 0 \tag{5.14}$$

Here $(\rho A)^*$ is the is the effective density given as

$$(\rho A)^* = \rho A + \rho_f A_f \tag{5.15}$$

in which ρ and ρ_f are the densities and A and A_f are the cross-sectional areas of the channel and fluids respectively. The change in density for both channel and fluid upon heating is calculated as

$$\rho_1 = \frac{\rho_0}{1 + \gamma \Delta T} \tag{5.16}$$

in which ρ_1 is the modified density due to change in temperature, ρ_0 is the initial density at room temperature, γ is the thermal expansion coefficient and ΔT is the rise in temperature. The effective modulus *(EI)** is then given by

$$(EI)^* = E_H I_H + E_f I_f \qquad\qquad (5.17)$$

where E_H *and* E_f are the Young's modulus of the channel and fluid and are given as 180×10^9 Pa and $0.7\text{-} 3.2 \times 10^9$ Pa respectively. Here I_H is the inertia moment of the hollow channel, and the I_f is the inertia moment of bulk fluid and are calculated as $5.514 * 10^{-23}$m^4 and $1.8 * 10^{-23}$ m^4 respectively.

The thermal stress calculated above appears as surface stress and tend to increase the resonance frequency of the beam.
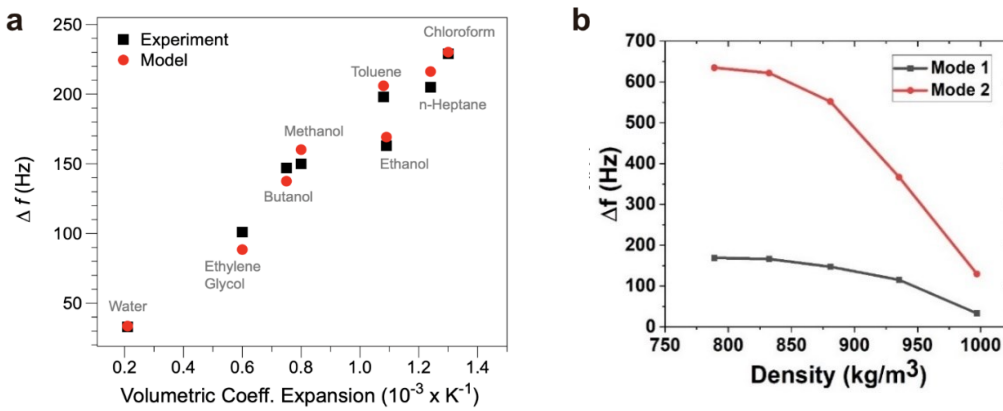
Figure 5.6: (a) 1st mode resonance frequency shifts of the resonator filled with different liquids upon the photothermal modulation as a function of volumetric thermal expansion, and (b) Saturated 1st and 2nd flexural mode resonance frequency shift of the water-ethanol mixture filled resonator as a function of the mass -density of ethanol-water mixture.

To demonstrate the capability of the microfluidic channel-based photo thermal characterization, we obtained the frequency shift of different fluids such as ethanol, ethylene glycol, methanol, heptane, butanol, toluene, chloroform and water. The frequency shift corresponding to the four concentrations of the ethanol (1, 0.75, 0.5, and 0.25) in deionized water is also measured. The resonance shifts of the resonator filled with various liquids are plotted as a function of the volumetric thermal expansion coefficient of liquids (Figure 5.6 a). As the volumetric thermal expansion coefficient increases, the resonance shift increases proportionally. The trend of

measured and calculated frequency shifts for different liquids are shown in Table 5.2. The shift in frequency for the air-filled cantilever as shown in Figure 5.4 a, is also determined by the combined effects of thermal stress, sample density reduction, and elastic modulus reduction, canceling out individual effects upon photothermal heating. The elastic modulus change might be the dominant parameter in the first few seconds (~10 seconds) of laser heating leading to a sudden decrease in the frequency for air filled cantilever. The further increase in frequency is attributed to the dominating effect of thermal stress and density reduction upon laser heating. A calibration experiment of application of known pressure inside the microfluidic cantilever could be an interesting study in the future. Also, an experiment with liquids at different flow rates in microchannel cantilever could be an interesting study to analyze the effect of different flow rates on the frequency of the resonator. The effect of composition in the two completely miscible liquids of water and ethanol on the cantilever's resonance frequency is shown in Figure 5.6 b. The resonance frequency shift decreases with respect to the increase in the density of the total solution. The value of $\frac{\Delta f}{\Delta t}$, where Δf is the frequency shift and Δt is the change in time, has an increase of 3.8 to 4.4 times in the 2nd flexural mode which explains the higher sensitivity in the higher modes.
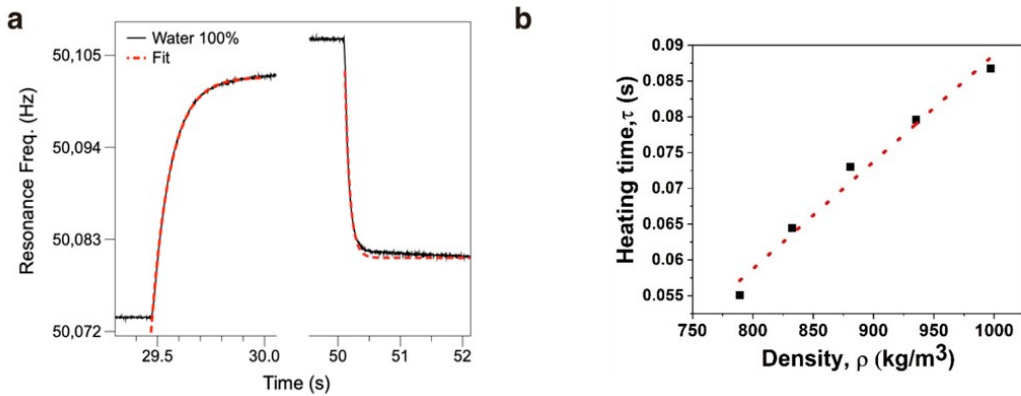
Figure 5.7: (a) 1st flexural mode resonance frequency change of the water-filled resonator and its exponential fits for heating and cooling events. (b) Extracted heating time constants of the water-ethanol mixture filled resonator as a function of mass-density for water-ethanol mixtures.

Table 5.2. Trend of rise in temperature in liquids due to laser irradiation and the corresponding volume expansion. These values are estimated from the fin conduction model.

Sample	Rise in temperature ΔT (x10^{-4} K)	ΔV (x10^{-21} m³)	σ (Pa)	Δf (Hz) (model)	Δf (Hz) (experimental)
Water	2.35	0.72	103	33	33.568
Ethylene Glycol	2.51	2.16	450	101	88.475
Butanol	3.65	4.02	307	147	137.55
Methanol	2.7	3.11	177	150	160.18
Ethanol	3.54	5.71	414	163	169.20
Toluene	3.8	5.9	417	198	206
n-Heptane	3.69	6.58	539	205	216.23
Chloroform	4.20	7.8	544	229	230.15

To estimate the time period for which the resonator is being heated and cooled down, transition times are derived from exponential fits (Figure 5.7 a). The equation used for the fitting is as below,

$$f = a + b \cdot \exp\left(-\frac{t - c}{\tau}\right) \qquad (5.18)$$

where f is resonance frequency, a, b, and c are adjustment constants, t is time, and τ is time constant. For water-filled resonator, transition time for heating and cooling are 85.6 ms and 64.0 ms. The derived heating transition times and the mole fraction ratio of water-ethanol mixtures is compared (Figure 5.7 b) where time constant is linearly increased with the mixing ratio. The time taken for the frequency shift during volumetric expansion of fluids depends on how fast the heat is being transferred through the fluid.

To calculate the complete time required for the frequency shift during which the thermal expansion happens

$$S = t_2 - t_1 = \frac{L^2}{\alpha} \qquad (5.19)$$

where S is the total duration of the frequency shift, t_1 and t_2 are the time when laser is on and off respectively.

While plugging the numbers, $L = 300 \times 10^{-6}$ m, $\alpha = 0.14 \times 10^{-6}$ /K for water, we get S = 0.642 s. This is in good agreement with the experimental value. Further, the time constant and heat capacity can be related by

$$\tau = (\frac{L}{KA})\rho C_p V \tag{5.20}$$

The relation of thermal conductivity and the temperature rise of the system can be expressed as follows.

$$k \propto \frac{1}{T - T_\infty} \propto \frac{1}{\Delta T} \tag{5.21}$$

From Eqs 5.20 and 5.21, it is evident that,

$$\rho C_p \propto \tau k \propto \frac{\tau}{\Delta T} \tag{5.22}$$

The variation of thermal conductivity and temperature rise for each liquid is shown in Figure 5.8 a. Figure 5.8 b provides the change of $\frac{\tau}{\Delta T}$ with respect to volumetric heat capacity ρC_p.
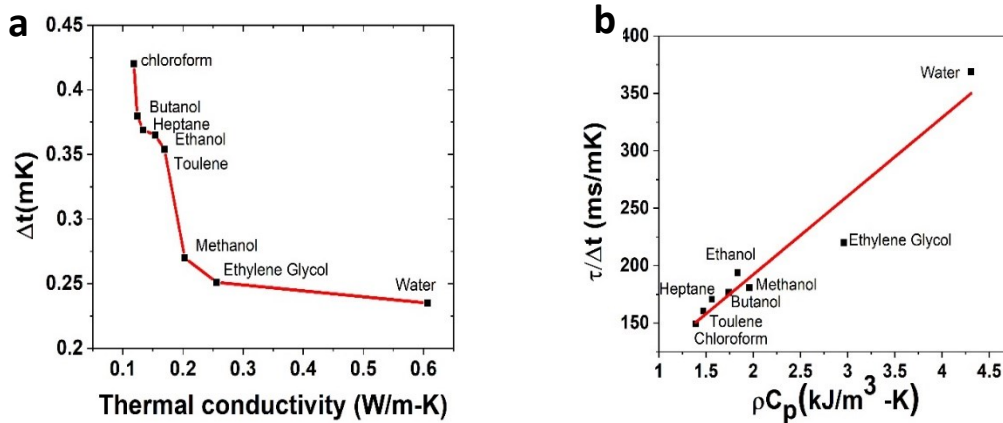
Figure 5.8: (a) Thermal conductivity of liquids plotted against temperature rise of each liquid. (b) Volumetric heat capacity of liquids plotted against $\frac{\tau}{\Delta t}$ for each liquid.

5.6 Conclusion

To conclude, a simple way of measuring and estimating thermal properties of pico litre scale liquid samples by analyzing at frequency fluctuations with microfluidic resonator is demonstrated in this paper. Simultaneous measurements of thermal expansion and volumetric heat capacities of sub nanolitre volumes of 8 liquids are obtained. It is shown that frequency shift of the resonator is affected from surface stress change due to expansion of the liquid inside the microfluidic channel, and frequency shifts of the samples are determined by their thermal expansion coefficient. Also, by looking at frequency transition time, a relationship between volumetric heat capacity and transition time is studied upon. This procedure can be further applicable to estimate thermal properties of various liquid analytes where extremely small volume of liquid is required. An optical heating mechanism and the structural material of the microfluidic channel cantilever allow it to be used for a wide range of liquids, including those which may be corrosive towards metallic heaters in resistive heating-based calorimeters. Instead of using an expensive QCL, the introduction of low-cost LED as light source made this technique quite inexpensive to perform thermal measurements of chemicals.

5.7 References

[1]   K. Jiang, F. Khan, J. Thomas, P.R. Desai, A. Phani, S. Das, T. Thundat, Thermomechanical responses of microfluidic cantilever capture DNA melting and properties of DNA premelting states using picoliters of DNA solution, Applied Physics Letters. 114 (2019). https://doi.org/10.1063/1.5092333.

[2]   A. Cooper, Heat capacity effects in protein folding and ligand binding: A re-evaluation of the role of water in biomolecular thermodynamics, in: Biophysical Chemistry, Elsevier, 2005: pp. 89–97. https://doi.org/10.1016/j.bpc.2004.12.011.

[3]   S.A. Manzoor Bukhari, M.F. Khan, A. Goswami, R. McGee, T. Thundat, Thermomechanical analysis of picograms of polymers using a suspended microchannel cantilever, RSC Advances. 7 (2017) 8415–8420. https://doi.org/10.1039/c6ra25455a.

[4]   L. Qiu, N. Zhu, Y. Feng, E.E. Michaelides, G. Żyła, D. Jing, X. Zhang, P.M. Norris, C.N. Markides, O. Mahian, A review of recent advances in thermophysical properties at the nanoscale: From solid state to colloids, Physics Reports. 843 (2020) 1–81. https://doi.org/10.1016/j.physrep.2019.12.001.

[5]   S.T. Huxtable, D.G. Cahill, S. Shenogin, L. Xue, R. Ozisik, P. Barone, M. Usrey, M.S. Strano, G. Siddons, M. Shim, P. Keblinski, Interfacial heat flow in carbon nanotube suspensions., Nat Mater. 2 (2003) 731–4. https://doi.org/10.1038/nmat996.

[6]   M.J. Simmonds, H.J. Meiselman, O.K. Baskurt, Blood rheology and aging., J Geriatr Cardiol. 10 (2013) 291–301. https://doi.org/10.3969/j.issn.1671-5411.2013.03.010.

[7]   M.F. Khan, N. Miriyala, J. Lee, M. Hassanpourfard, A. Kumar, T. Thundat, Heat capacity measurements of sub-nanoliter volumes of liquids using bimaterial microchannel cantilevers, Applied Physics Letters. 108 (2016). https://doi.org/10.1063/1.4952614.

[8]   M. Mirasoli, M. Guardigli, E. Michelini, A. Roda, Recent advancements in chemical luminescence-based lab-on-chip and microfluidic platforms for bioanalysis, Journal of Pharmaceutical and Biomedical Analysis. 87 (2014) 36–52. https://doi.org/10.1016/j.jpba.2013.07.008.

[9]   H. Etayash, M.F. Khan, K. Kaur, T. Thundat, Microfluidic cantilever detects bacteria and measures their susceptibility to antibiotics in small confined volumes, Nature Communications. 7 (2016). https://doi.org/10.1038/ncomms12947.

[10]   C. Vančura, I. Dufour, S.M. Heinrich, F. Josse, A. Hierlemann, Analysis of Resonating Microcantilevers Operating in a Viscous Analysis of Resonating Microcantilevers Operating in a Viscous Liquid Environment Liquid Environment Recommended Citation Recommended Citation Analysis of Resonating Microcantilevers Operating in A Viscous Liquid Environment, 2007. https://epublications.marquette.edu/civengin_fac/75.

[11]   M. Faheem Khan, S. Kim, D. Lee, S. Schmid, A. Boisen, T. Thundat, Nanomechanical identification of liquid reagents in a microfluidic channel, Lab on a Chip. 14 (2014) 1302–1307. https://doi.org/10.1039/c3lc51273h.

[12]   A. Wig, E.T. Arakawa, A. Passian, T.L. Ferrell, T. Thundat, Photothermal spectroscopy of Bacillus anthracis and Bacillus cereus with microcantilevers, Sensors and Actuators, B: Chemical. 114 (2006) 206–211. https://doi.org/10.1016/j.snb.2005.04.029.

[13]   E.T. Arakawa, N. v Lavrik, S. Rajic, P.G. Datskos, Detection and differentiation of biological species using microcalorimetric spectroscopy., Ultramicroscopy. 97 (n.d.) 459–65. https://doi.org/10.1016/S0304-3991(03)00074-3.

[14]   P. Ian Oden, E. A. Wachter, P. G. Datskos, T. Thundat, R. J. Warmack, "Optical and infrared detection using microcantilevers," Proc. SPIE 2744, Infrared Technology and Applications XXII, (27 June 1996) https://doi.org/10.1117/12.243523

[15]   A. Alodhayb, F. Khan, H. Etayash, T. Thundat, Review—Nanomechanical Calorimetric Infrared Spectroscopy using Bi-Material Microfluidic Cantilevers, Journal of The Electrochemical Society. 167 (2020) 037504. https://doi.org/10.1149/2.0042003jes.

[16]   N. Miriyala, Photothermal effects in micro/nano electromechanical systems, University of Alberta, Edmonton, Canada.2016

[17]   J.K. Gimzewski, C. Gerber, E. Meyer, R.R. Schlittler, Observation of a chemical reaction using a micromechanical sensor, 1994.

[18]   J. Mouro, R. Pinto, P. Paoletti, B. Tiribilli, Microcantilever: Dynamical response for mass sensing and fluid characterization, Sensors (Switzerland). 21 (2021) 1–35. https://doi.org/10.3390/s21010115.

[19]   A.F. Payam, W. Trewby, K. Voïtchovsky, Simultaneous viscosity and density measurement of small volumes of liquids using a vibrating microcantilever, Analyst. 142 (2017) 1492–1498. https://doi.org/10.1039/c6an02674e.

[20]   J. Dorignac, A. Kalinowski, S. Erramilli, P. Mohanty, Dynamical response of nanomechanical oscillators in immiscible viscous fluid for in Vitro biomolecular Recognition, Physical Review Letters. 96 (2006). https://doi.org/10.1103/PhysRevLett.96.186105.

[21]   G. Longo, L. Alonso-Sarduy, L.M. Rio, A. Bizzini, A. Trampuz, J. Notz, G. Dietler, S. Kasas, Rapid detection of bacterial resistance to antibiotics using AFM cantilevers as nanomechanical sensors., Nat Nanotechnol. 8 (2013) 522–6. https://doi.org/10.1038/nnano.2013.120.

[22]   Q. Zhang, W. Ruan, H. Wang, Y. Zhou, Z. Wang, L. Liu, A self-bended piezoresistive microcantilever flow sensor for low flow rate measurement, Sensors and Actuators, A: Physical. 158 (2010) 273–279. https://doi.org/10.1016/j.sna.2010.02.002.

[23] M. Faheem Khan, S. Kim, D. Lee, S. Schmid, A. Boisen, T. Thundat, Nanomechanical identification of liquid reagents in a microfluidic channel, Lab on a Chip. 14 (2014) 1302–1307. https://doi.org/10.1039/c3lc51273h.

[24] T. Gavoille, N. Pannacci, G. Bergeot, C. Marliere, S. Marre, Microfluidic approaches for accessing thermophysical properties of fluid systems, Reaction Chemistry and Engineering. 4 (2019) 1721–1739. https://doi.org/10.1039/c9re00130a.

[25] T.P. Burg, S.R. Manalis, Suspended microchannel resonators for biomolecular detection, Applied Physics Letters. 83 (2003) 2698–2700. https://doi.org/10.1063/1.1611625.

[26] I. Lee, K. Park, J. Lee, Precision density and volume contraction measurements of ethanol-water binary mixtures using suspended microchannel resonators, Sensors and Actuators, A: Physical. 194 (2013) 62–66. https://doi.org/10.1016/j.sna.2013.01.046.

[27] N. Belmiloud, F. Lochon, I. Dufour, P. Guillot, M. Guirardel, A. Colin, L. Nicu, Determination of fluid viscoelastic properties using resonant microcantilever, 2006. https://hal.archives-ouvertes.fr/hal-00181953.

[28] T.P. Burg, M. Godin, S.M. Knudsen, W. Shen, G. Carlson, J.S. Foster, K. Babcock, S.R. Manalis, Weighing of biomolecules, single cells and single nanoparticles in fluid, Nature. 446 (2007) 1066–1069. https://doi.org/10.1038/nature05741.

[29] R.J. Kimmerling, S.M. Prakadan, A.J. Gupta, N.L. Calistri, M.M. Stevens, S. Olcum, N. Cermak, R.S. Drake, K. Pelton, F. de Smet, K.L. Ligon, A.K. Shalek, S.R. Manalis, Linking single-cell measurements of mass, growth rate, and gene expression 06 Biological Sciences 0604 Genetics, Genome Biology. 19 (2018). https://doi.org/10.1186/s13059-018-1576-0.

[30] A.E. Cetin, M.M. Stevens, N.L. Calistri, M. Fulciniti, S. Olcum, R.J. Kimmerling, N.C. Munshi, S.R. Manalis, Determining therapeutic susceptibility in multiple myeloma by single-cell mass accumulation, Nature Communications. 8 (2017). https://doi.org/10.1038/s41467-017-01593-2.

[31] Y. Yoon, F. Khan, T. Thundat and J. Lee, "Thermal Characterization of Liquid Analytes via Photothermal Modulation of Microfluidic Resonators," 2019 IEEE 32nd International Conference on Micro Electro Mechanical Systems (MEMS), 2019, pp. 712-715, doi: 10.1109/MEMSYS.2019.8870825.

[32]   D. Ramos, J. Mertens, M. Calleja, J. Tamayo, Study of the Origin of Bending Induced by Bimetallic Effect on Microcantilever, Sensors. 7 (2007) 1757–1765. www.mdpi.org/sensors.

[33]   J. He, C.M. Lilley, Surface stress effect on bending resonance of nanowires with different boundary conditions, Applied Physics Letters. 93 (2008). https://doi.org/10.1063/1.3050108.

[34]   R. Abraham, F. Khan, S.A. Bukhari, Q. Liu, T. Thundat, H.J. Chung, C. il Kim, Effect of surface and interfacial tension on the resonance frequency of microfluidic channel cantilever, Sensors (Switzerland). 20 (2020) 1–14. https://doi.org/10.3390/s20226459.

[35]   F. Aguilar Sandoval, M. Geitner, É. Bertin, L. Bellon, Resonance frequency shift of strongly heated micro-cantilevers, Journal of Applied Physics. 117 (2015). https://doi.org/10.1063/1.4922785.

[36]   https://courses.lumenlearning.com/physics/chapter/13-2-thermal-expansion-of-solids-and-liquids/, (n.d.).

[37]   https://pressbooks.bccampus.ca/practicalphysicsphys1104/chapter/13-2-thermal-expansion-of-solids-and-liquids/, (n.d.).

[38]   M. Toda, T. Ono, F. Liu, I. Voiculescu, Evaluation of bimaterial cantilever beam for heat sensing at atmospheric pressure, Review of Scientific Instruments. 81 (2010). https://doi.org/10.1063/1.3397320.

[39]   A. Narayanaswamy, N. Gu, Heat transfer from freely suspended bimaterial microcantilevers, Journal of Heat Transfer. 133 (2011). https://doi.org/10.1115/1.4001126.

[40]   http://orca.phys.uvic.ca/~tatum/physopt/physopt2.pdf, (n.d.).

[41]   S. Shen, A. Narayanaswamy, S. Goh, G. Chen, Thermal conductance of bimaterial microcantilevers, Applied Physics Letters. 92 (2008). https://doi.org/10.1063/1.2829999.

[42]   J.R. Serrano, L.M. Phinney, J.W. Rogers, Temperature amplification during laser heating of polycrystalline silicon microcantilevers due to temperature-dependent optical properties, International Journal of Heat and Mass Transfer. 52 (2009) 2255–2264. https://doi.org/10.1016/j.ijheatmasstransfer.2008.12.003.

[43]   https://refractiveindex.info/?shelf=main&book=H2O&page=Hale, (n.d.).

5.6 Supplementary Figures
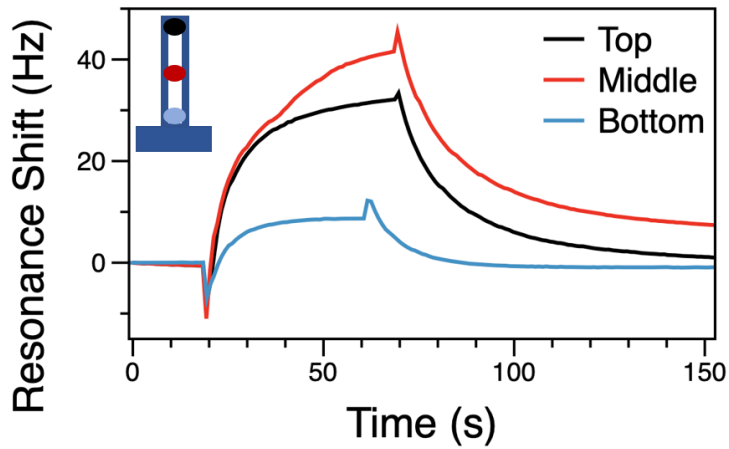
Figure S1: Resonance frequency shifts of air-filled resonator when the laser is positioned at three different positions on the cantilever, the top position which is the free end of the cantilever, the middle position and the bottom, near the base of the cantilever. The temperature rise in the cantilever is the highest when the laser is shined at the middle of the cantilever and hence a higher frequency shift is observed in the case.
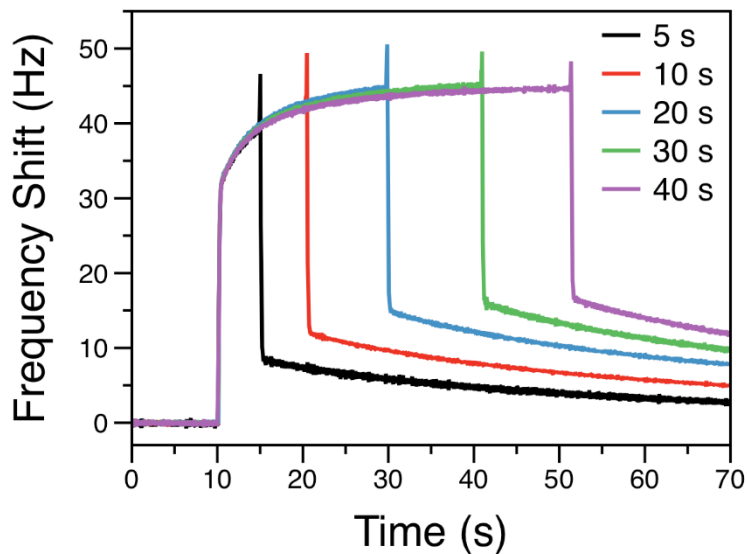
Figure S2: The frequency shift of the water filled cantilever when exposed to different laser durations of 5s,10s,20s,30s and 40 s.

Chapter 6

Thermomechanical characterization of phase change of PNIPAM and flocculation of Kaolinite and PNIPAM using microfluidic cantilever

6.1 Abstract

Materials which adjust their properties reversibly in response to environmental factors such as temperature, pH and ionic strength are rapidly evolving and known as smart materials. Poly(N-isopropylacrylamide) (PNIPAM), a thermo-responsive polymer, is considered as a promising smart polymer, due to its well-defined structure and tunable thermomechanical properties. PNIPAM exists in an expanded coil like conformation in water below its lower critical solution temperature (LCST) which gives a transparent homogenous solution but at temperature, T > LCST it undergoes hydrophobic collapse and conformational change from coil to globule state resulting in a shrunken state. Along with changes in size, significant changes are also expected for the mechanical response of the polymer. A microchannel cantilever resonating at its resonance frequency can be used as a tool of non-destructive technique to measure the thermomechanical property changes of PNIPAM with change in temperature. The mechanical signals obtained from the microfluidic cantilever, filled with a picogram solution PNIPAM, are used to analyze the stiffness change of the solution at LCST. When the mixture of Kaolinite and PNIPAM is taken through the thermal cycle, the coil to globule transition of PNIPAM adsorbed on Kaolinite at LCST, results in the sedimentation of Kaolinite on the walls of the cantilever. This would increase the stiffness of the cantilever which increases the resonance frequency of the system. The flocculation performance of the PNIPAM and Kaolinite in the microfluidic channel is compared with the macro scale flocculation experiments. This approach which combines the mechanical response of the cantilever with the flocculation and phase change dynamics can serve as a platform for the development of a portable, high thorough put the device for the in situ real-time detections of effective flocculation using various flocculants.

6.2 Introduction

Oil sands are naturally occurring mixtures of sand, clay, water, and a thick, heavy type of petroleum called bitumen. Unlike conventional crude oil, oil sand does not flow, and it must be mined or heated underground before any further processing. Alberta, Canada is fourth largest oil reserve in the world with oil sands deposits estimated at 28.3 billion cubic meters [1].One method of bitumen extraction is mining and about 20% of Canada's oil sands is close enough to the surface to be mined [1,2]. In Clark hot water bitumen extraction process, the oil sand ores are mined, crushed, and mixed with warm alkaline water, followed by the separation of bitumen using a flotation process [3]. The large volumes of slurry waste produced from the extraction of bitumen is hydraulically transported and stored within surface tailings ponds [4]. The tailings stored in the tailing ponds are separated into three layers by gravity after settling over several months [3]. The heaviest coarse sands settle to the bottom, and water released from tailings form the top layer. The middle layer is known as mature fine tailings (MFT) which contains fine clays (~30wt%), water (~65wt%), and residual bitumen (~5wt%) [1,3,4]. MFT appears as a "gel-like" suspension with dispersed particles of sizes smaller than 44 μm and consolidates extremely slowly because of trapped water and the negatively charged nature of fine clay particles [1]. MFT suspensions take several years to settle and release the entrapped water due to the small particle size and high-water retention capacity.

There are numerous approaches developed to accelerate the settling rates of the fine particles in MFT and enhance the water recovery rates for reuse in the industry [3]. The use of synthetic polymers is one among the chemical treatment for achieving effective flocculation of particles in MFT. The polymers allow the bridging of the fine particles and subsequently flocculate them into big flocs. Temperature-responsive poly(N-isopropylacrylamide) (PNIPAM) is one among the well-known novel flocculant to accelerate settling rate and enhance consolidation [5].

PNIPAM has a lower critical solution temperature (LCST) at 32˚C. At temperatures below its lower critical solution temperature (LCST) (≈32 °C), PNIPAM exists in the form of fully extended water-soluble molecules. When these molecules are adsorbed on the surface of clay particles at room temperature, they act as a dispersant though steric repulsion. However, at temperatures above the LCST, the hydrogen bonds between water molecules and polymer chains begin to break and

instead, intramolecular and intermolecular hydrogen bonds begin to form. The formation of such bonds causes the molecule to coil up, exposing its hydrophobic core. This renders the polymer hydrophobic and insoluble in water, which causes it to precipitate from solution in the form of hydrophobic colloidal particles onto the particle surfaces. The presence of these colloids on mineral surfaces renders them hydrophobic. For this reason, at temperature above the LSCT, PNIPAM can act as an effective flocculant, causing particle aggregation through hydrophobic attraction.

Many design concepts of the polymer flocculants have been suggested, and precision of their synthesis has been well studied in the disciplines of reaction engineering[3,5]. The performance of the flocculants has been studied in the context of nanoscopic flocculants-particle interaction measurements[6], macroscopic dewatering measurements[7], and aggregate characterization[8]. But an investigation of the mechanical property evolution of the solution as a function of external stimulant such as temperature has yet to be discovered.

Sensor technologies stemming from the micro and nano electromechanical systems (MEMS/NEMS) are capable of investigating the evolution of mechanical property in a non-destructive manner from extremely small amount of samples with exceptional resolution and sensitivity at a low power consumption [43–46]. A change in the bulk stiffness of the sample filled inside the microfluidic cantilever and the surface stress/interfacial stress provided by the fluid can significantly affect the dynamics of the microcantilever. Whenever there is adsorption on one side of the cantilever or occurrence of any kind of thermal/chemical/electromagnetic events on the surface, a differential stress is generated on the cantilever leading to cantilever bending in static response. An addition of mass or change in stiffness of cantilever changes the resonance frequency of the cantilever in dynamic response. For thermo-responsive polymers that undergo a phase transition with variation in temperature, the change in the elastic properties of the polymer will significantly affect the Young's modulus of the microfluidic cantilever- polymer system and will change the resonance frequency of the cantilever.

In this chapter, we are investigating the thermomechanical property changes of PNIPAM and PNIPAM-Kaolinite solution using the dynamics of the microchannel cantilever filled with

picograms of respective solutions. This study reveals the mechanical property evolution associated with the phase change of the PNIPAM solution at LCST using the stiffness change of the microchannel cantilever. Further, the effect of flocculation on the dynamics of the cantilever is used to analyse the aggregate formation and stiffness change of the PNIPAM-Kaolinite solutions at LCST.

6.3 Experimental Details

Preparation of PNIPAM: 992 mg N-Isopropylacrylamide (NIPAM) was dissolved into 19 mL deionized water (DI H2O), and the solution was degassed with nitrogen gas for 10 min. Subsequently, 2 mL DI H2O, that pre-dissolved 40 mg ammonium persulfate (APS) and 100 μL tetramethylethylenediamine (TEMED), was added into the solution. After the addition, the mixture was degassed with nitrogen gas for another 25 min, and then reacted at 23°C for 24 h. After the reaction, the reaction was terminated by air exposure. The sample was purified via dialysis (6-8 kDa) against DI H2O for five days. The white dried film of polymer was recovered by freeze-dryer.

Flocculation Performance at macroscale: Flocculation performance is screened at different doses using a 2.5 wt% solution of Kaolinite in DI water. A stock solution of polymer flocculant is prepared at a concentration of 1 mg/mL. Doses of polymer are calculated as a ratio of the mass of polymer added to the mass of solids present. To check the polymer for flocculation activity doses of 1000 mg polymer/kg solids, 4000 mg/kg, and 8000 mg/kg are used. Each screening test consisted of adding the appropriate dose of the polymer stock solution to a 10 mL Kaolinite suspension. One the polymer is added the vial is sealed an inverted 10 times to mix the solution. Any flocs formed are then allowed to settle. Flocculation, with larger flocs was formed in 0.8 wt% of PNIPAM and 2.3 wt% of Kaolinite solution and is shown in Figure 6.1.
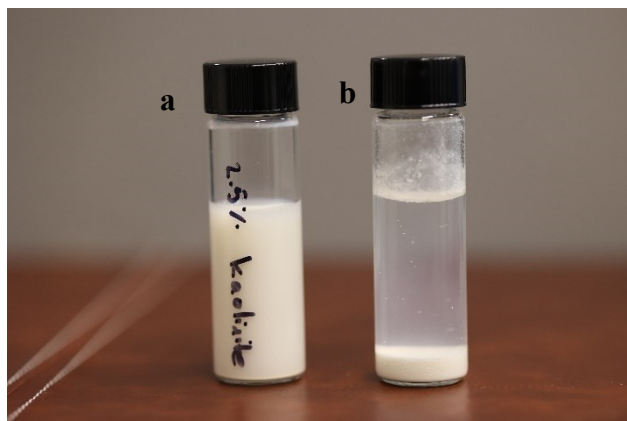
Figure 6.1: Images of a) 2.5 wt % of Kaolinite solution b) Visible flocs formed during flocculation of Kaolinite with 0.8 wt% of PNIPAM

Thermomechanical Characterization by Microfluidic Cantilever: For in-situ flocculation study of PNIPAM-Kaolinite sample using a microfluidic cantilever, a pico litre volume of the sample is filled inside the cantilever and the whole system is heated by a heater at a desired temperature. The resonance frequency shift of the cantilever provides real time information regarding the thermo-mechanical properties of the fluid such as volumetric expansion, density change and bulk modulus change. Figure 6. 2 a show the conceptual schematic of the experiment where a U-shaped silicon nitride microfluidic channel (16 μm wide, 300 μm long and 3 μm high) fabricated on top of a plain cantilever (44 μm wide, 500 μm long and 500 nm thick) with a liquid sample is heated by a heater attached to the sample holder and actuated by a piezo. This microchannel cantilever is supported on a 350 μm thick silicon chip, which provides fluidic inlets and outlets for delivering sample fluids to the microchannel on the cantilever. Two openings at the bottom of the chip provide a fluidic interface between the chip and connecting Teflon tubes. The fluid sample is loaded inside the channel by applying pressure and then unloaded by applying the negative pressure to outlet. Upon completion of measurement, the channel is thoroughly washed with deionized water then completely dried before another loading of liquid sample.

The empty channel cantilever, the cantilever filled with DI water, PNIPAM solution, Kaolinite solution and the mix of PNIPAM and Kaolinite solutions are subjected to the heating and cooling test. The cantilever is heated from room temperature to 45 °C at a heating rate of 1 °C per min. The resonance frequency of the resonator is simultaneously measured with a laser Doppler vibrometer

(LDV) (MSA-500, Polytec. All of the measurements are conducted at room temperature and at atmospheric pressure. Figure 6.10 b and c shows the PFIB image of Kaolinite inside the microfluidic cantilever.
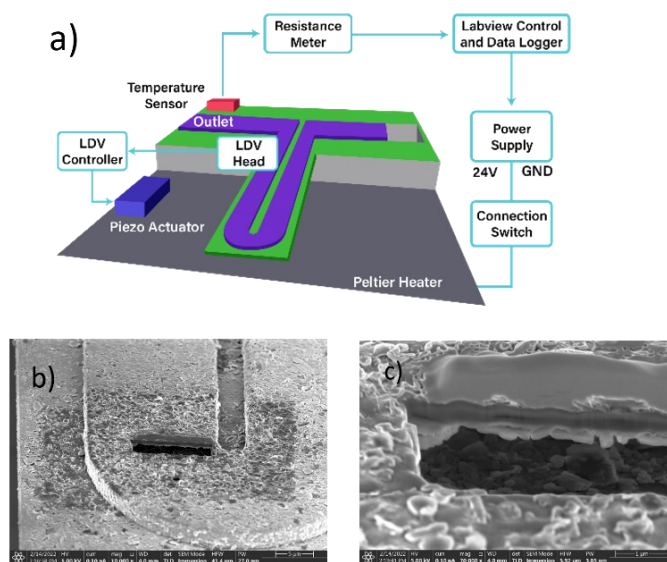
Figure 6.2: a) Conceptual schematic of the experiment where a U-shaped silicon nitride microfluidic channel is placed on heater and b & c) PFIB images of filled channel with Kaolinite

6.4 Results

Figure 6.3 shows the frequency response of microchannel cantilever filled with air, DI water and Kaolinite respectively. Phase change of PNIPAM and flocculation performance of Kaolinite solution with PNIPAM in macro scale are observed for validating the microfluidic channel experimental results.   Table 6.1 shows the images of PNIPAM, and PNIPAM-Kaolinite suspensions heated at different temperatures and for different durations. The optimum concentration of PNIPAM (0.8 wt%) and Kaolinite (2.3 wt%) mixture were heated on a hotplate and observed the aggregation at different temperatures as shown in Table 6.1. When reached to a target temperature, the sample displayed a seemingly stable phase behavior within 2 minutes.
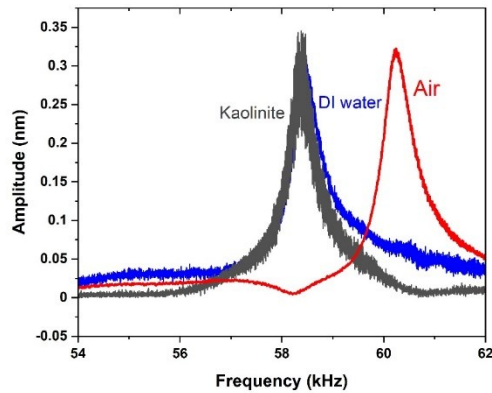
Figure 6.3: FFT spectrum of air filled, and liquid filled channel

Table 6.1: Images of the PNIPAM solution and PNIPAM and Kaolinite mixture heated at different temperatures in vials of 5cm height and 5 cm in diameter. The images are taken once the solution remains at desired temperature for 5 minutes.

Temperature	0.8 wt % of PNIAPM	0.8 wt % of PNIPAM and 2.3 wt% Kaolinite
25^0C		

30 ^{0}C		
35^{0}C		
40^{0}C		
45^{0}C		

The temperature of the liquid-filled microchannel cantilever is controlled by an attached heater on the sample holder. When the cantilever is filled with air at atmospheric pressure, the resonance frequency drops immediately once the heating is applied and slowly surges until saturation which is similar to the behaviour in photothermal heating of empty channel cantilever in Chapter 5 (Figure 6.4 a). Since the photo thermal experiments in Chapter 5 were done at high vacuum and a laser was used to heat the cantilever locally, the heating and curves were following a clear trend of rise and fall. The experiments in this study are done in atmospheric pressure using an external heater and hence, the conduction and convection heat losses are subjected to change with environment parameters. When the heating is turned off, the resonance frequency of the air-filled channel cantilever slowly recovers and would get rid of any residual stresses in the cantilever thus lowering the frequency than the initial level.

The resonance frequency response of the cantilever filled with liquid is different depending on the type of solution because of thermal effects upon the heating. Frequency of the DI water filled channel rises upon heating and then decreases once the heater is turned of and is shown in Figure 6.4 b. The frequency shift of Kaolinite is quite similar to that of DI water filled channel (Figure 6.4 c). But in case of PNIPAM, the frequency increases slowly once the heater is turned on, but as it reaches the LCST at 35 °C the frequency drops down immediately and then it increases sharply. The quality factor also follows the same trend of the frequency response in case of PNIPAM (Figure 6.4 d). Once the heater is turned off, the frequency gradually decreases for the PNIPAM filled channel cantilever. The response of PNIPAM and Kaolinite mix solution, which is the flocculation sample, is slightly different than from the PNIPAM response. There is a gradual rise in the frequency from 20° C to 25 ° C and then the frequency shift enters a plateau and at 35 ° C there is an immediate increase in the frequency till 43^0 C. The quality factor for this sample decreases in the initial stage till 25 ° C and then rises till 32^0 C. But as the system approaches the LCST temperature, the quality factor drops down with temperature and then returns to the initial higher value as shown in Figure 6.4 e.
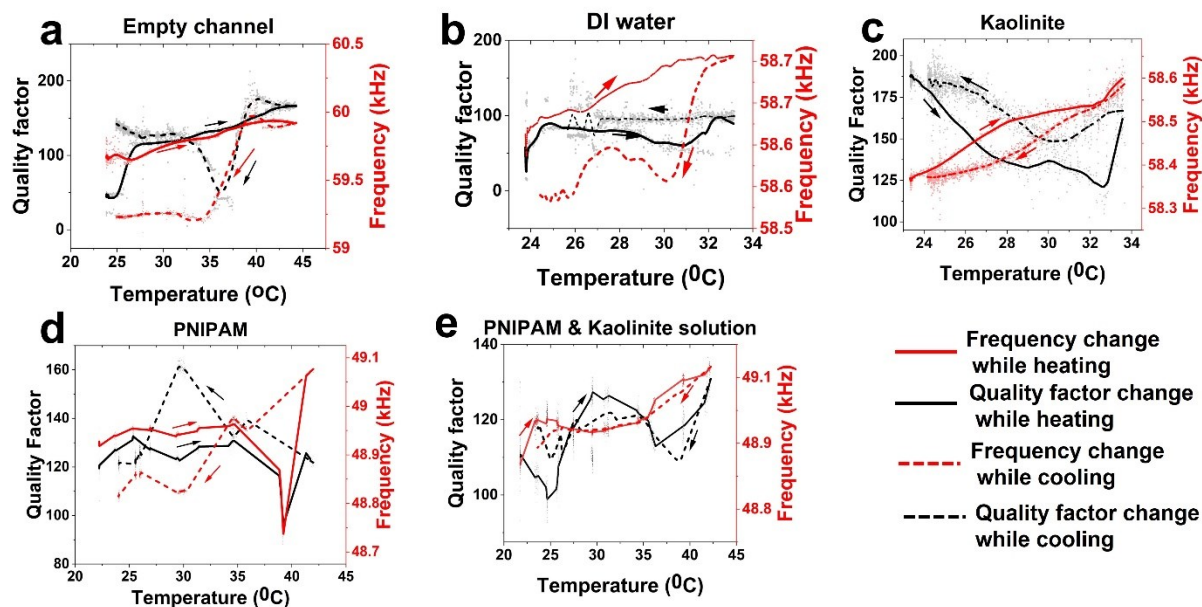
Figure 6.4: 1st flexural mode resonance frequency shifts of the resonator filled with (a) air, (b) DI water, (c) Kaolinite, (d) PNIPAM and (e) PNIPAM and Kaolinite solution because of the heating and cooling. The tiny dots are the measured raw data points and the lines in the plots are the smoothened average of the raw data points.

6.5 Discussion

Several properties of PNIPAM changes significantly during the collapse such as volume, stiffness, optical transmittance, contact angle, and the internal solvent diffusion. The LCST can be obtained by various analytical methods like optical techniques (e.g., UV-Vis spectroscopy [28], dynamic and static light scattering [29], infrared spectroscopy [30,31], Raman spectroscopy [32], fluorescence spectroscopy [33], differential scanning calorimetry [34], or viscometry [35].

The volume phase transition of PNIPAM solution is explored vastly but the mechanical properties induced by phase transition are still being investigated. Zhang et al carried out a quantitative experimental study on the phase transition effects on the mechanical properties of NIPA hydrogel with LCST around 35^{0}C [36]. They observed a dramatic increase of Young's modulus values of

NIPA hydrogel from 13 kPa to 28 kPa under tensile test as the temperature increases through the phase transition. The elastic properties of PNIPAM particles as a function of both temperature and cross-linking concentration using Capillary Micromechanics was presented by Voudouris et al [37]. It was found that the compressive elastic modulus K of the microgel exhibits a dip close to the LCST while the shear modulus G increased monotonously upon increasing temperature as shown in Figure 6.8 [37]. It is explained that in the absence of a large increase of the heat capacity of the material in this minute change in temperature at LCST, the dramatic deswelling of the particles indicates that the energy required to change particle volume should be significantly lowered [37]. Hence, a drop in the compressive elastic modulus around the LCST of the material can be expected[37].
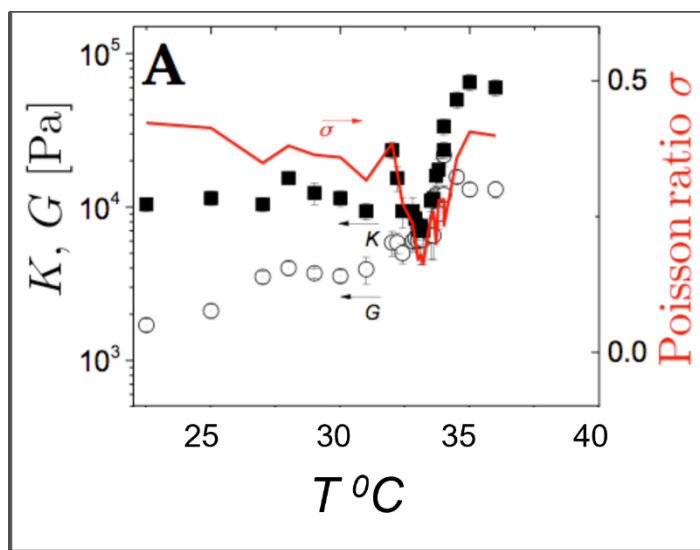
Figure 6.5: Elastic properties as a function of temperature for particles prepared with initial cross-linker-to-monomer ratios of 1/36. The compressive modulus K (solid squares, left axis) exhibited a pronounced decrease close to the LCST, while the shear modulus G (open circles, left axis) increased continuously. Reproduced with permission from [37]

An intriguing property of PNIPAM microgel suspensions is that the viscoelasticity is thermally controllable without changing the mass concentration of particles, because the temperature variations change the volume fraction of the microgel particles in the suspensions [38]. Several research had been done to understand the thermal effects on the rheological properties of PNIPAM microgel suspensions [39–41]. It is reported that in the swollen state below LCST, dense

suspensions exhibited an elastic response and liquified while heating because of decrease in effective volume fraction of microgels [40]. Richtering et al. found that the suspensions exhibited an elastic response again when heated above LCST, despite a considerable reduction in effective volume fraction of microgels. The origin of the elastic behavior at temperature above LCST is found as the formation of solid gel by attractive interactions between collapsed microgels [39].

Due to the reversible solubility of PNIPAM, it has been used as a flocculant in several studies [42] When PNIPAM is applied as a flocculant, PNIPAM adsorbs on the surface of the soil particles below 32^0C. Above 32˚C, PNIPAM aggregates with soil particles and dewaters due to dehydrating and subsequent shrinking nature of PNIPAM. An aggregation study of mixture of silica and alumina with PNIPAM is carried out by Franks et al. Flocculation and dewatering of mature fine tailings using mixture of PNIPAM and cationic polymers are as a function of initial settling rates (ISR), supernatant turbidity, sediment solid content, and water recovery are conducted by Dan et al and established that particles in tailing suspensions are rapidly flocculated above LCST [5].

The behaviour of aqueous PNIPAM solutions and PNIPAM flocculant systems at LCST is well investigated, however, the analysis of mechanical property changes of PNIPAM solution and PNIPAM flocculant systems at LCST still need to be addressed. In this work, we are aiming to qualitatively analyse the mechanical property change of the PNIPAM solution and the PNIPAM flocculant system by characterising the dynamics of a microfluidic cantilever filled with respective samples.

In case of air, DI water and Kaolinites samples, the frequency shift is majorly dominated by the thermal expansion of air, water and Kaolinite samples inside the channel respectively as shown in Chapter 5. As the increased thermal stress resulting the expansion of air and fluid samples inside the channel, appears as surface stress that increases the stiffness of the whole system, the frequency tends to rise according. For PNIPAM filled channel, the initial rise in frequency is associated with the thermal expansion. Below the LCST, p-NIPAM network is swollen and interacts repulsively. During heating, the swollen polymer network undergoes a process of changing hydrophilicity at the LCST, inducing a release of water and a shrinkage of the polymer particles in the network. As the temperature is raised, the bonds between polymer chains and water molecules starts to break

around 28 º C. During shrinkage of volume at LCST, the elastic modulus might decrease correspondingly at this temperature range [27,37]. As a result of the decrease in modulus of the PNIPAM solution at LCST, the overall stiffness of the microfluidic cantilever system filled with PNIPAM solution tend to decrease at LCST leading to a major downward shift in the frequency. The formation of two distinct phases in PNIPAM aqueous solution at LCST would contribute to the damping of the system and hence results in low quality factor. Above this transition temperature, the entire PNIPAM layer is collapsed. As temperature increases, de-swelling is accompanied by a second effect- solid-like behavior. The increased forces between the chains and possible agglomerate formation might result in the increase of the modulus of the PNIPAM phase in the aqueous solution above LCST [27,37]. When the newly formed PNIPAM phase becomes stiffer, it leads to an increase in the overall modulus of the cantilever system resulting in an increase in the frequency of the cantilever.

The flocculation sample, which is the mixture of Kaolinite and PNIPAM solution, experiences an increase in frequency in the initial stage until 25ºC and then after LCST temperature, which is at 35ºC, a further increase in frequency is observed. This might be due to the flocculation of clay particles inside the channel. The polymer adsorbs the clay particles and at LCST, the polymer becomes hydrophobic and expels water from the swollen body. The polymer and clay aggregates would settle down in the channel due to gravity as a separate layer as shown in Figure 6.6. The sedimentation of clay and polymer on the walls of the cantilever would create additional stiffness to the system and hence increases the frequency.
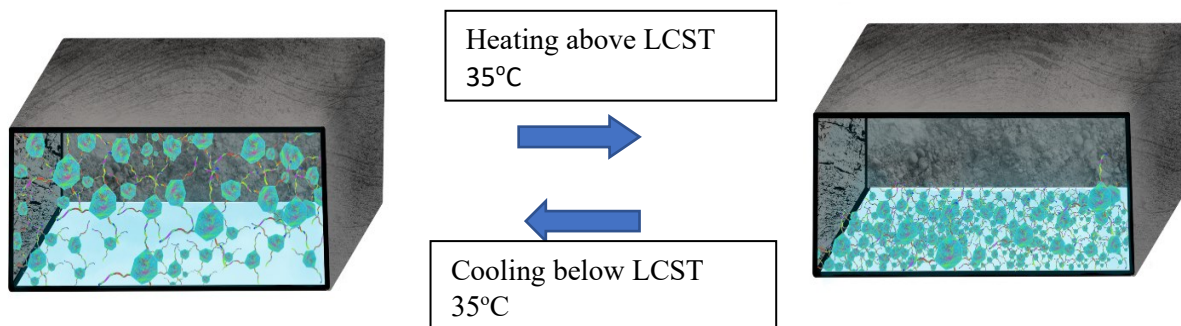
Figure 6.6: Schematic of reversible process of flocculation using PNIPAM. The PNIPAM polymer is adsorbed on the surface of clay particles and then undergoes a phase transition above LCST. As a result, the suspended water is expelled out of the polymer-clay particles and the polymer – clay aggregates eventually settle down inside the microchannel.

Thus, the thermomechanical change of the PNIPAM polymer as a function of temperature is observed using the frequency shift of the microchannel cantilever. Also, the in-situ flocculation of Kaolinite using the thermo-responsive polymer PNIPAM as a flocculant is observed using the microchannel cantilever as a function of temperature. The sedimentation of flocs on the walls of the cantilever alters the stiffness of the cantilever which results in the frequency shift of the cantilever.

6.6 Conclusion

To conclude, a simple way of investigating the thermo-mechanical property of PNIPAM as a function of temperature is demonstrated in this thesis. Along with that in situ flocculation and associated mechanical property change of the Kaolinite-PNIPAM system during flocculation is discussed with the help of frequency fluctuations with microfluidic resonator. The thermo-mechanical property changes such as the thermal expansion, phase change and modulus change of PNIPAM solution and PNIPAM and Kaolinite mixtures are obtained. It is shown that frequency shift of the resonator is affected from surface stress change due to expansion of the aqueous solution, bulk modulus changes of aqueous solution and the sedimentation of clay particles inside the microfluidic channel. This procedure can be further applicable to estimate real time flocculation of Kaolinite with different thermo-responsive polymers where extremely small volume of liquid is required.

6.7 References

[1]   V. Vajihinejad, J.B.P. Soares, Monitoring polymer flocculation in oil sands tailings: A population balance model approach, Chemical Engineering Journal. 346 (2018) 447–457. https://doi.org/10.1016/J.CEJ.2018.04.039.

[2]   H.L. Cossey, A.E. Batycky, H. Kaminsky, A.C. Ulrich, Geochemical Stability of Oil Sands Tailings in Mine Closure Landforms, Minerals 2021, Vol. 11, Page 830. 11 (2021) 830. https://doi.org/10.3390/MIN11080830.

[3]   S. Prakash Gumfekar, Multifunctional Water-Soluble Polymers for Dewatering of Oil Sands Tailings, n.d.

[4]   R.J. Chalaturnyk, J.D. Scott, B. Özüm, MANAGEMENT OF OIL SANDS TAILINGS, Http://Dx.Doi.Org/10.1081/LFT-120003695. 20 (2007) 1025–1046. https://doi.org/10.1081/LFT-120003695.

[5]   D. Zhang, T. Thundat, R. Narain, Flocculation and dewatering of mature fine tailings using temperature-responsive cationic polymers, Langmuir. 33 (2017) 5900–5909. https://doi.org/10.1021/ACS.LANGMUIR.7B01160/ASSET/IMAGES/LARGE/LA-2017-01160K_0010.JPEG.

[6]   M. Digital, M. Digital Scholar, S. Youn, Quantitative Understanding of Nanoparticle Flocculation in Water Quantitative Understanding of Nanoparticle Flocculation in Water Treatment Treatment, 2017. https://mds.marshall.edu/wde_faculty.

[7]   V. Vajihinejad, S.P. Gumfekar, B. Bazoubandi, Z.R. Najafabadi, J.B.P. Soares, V. Vajihinejad, S.P. Gumfekar, B. Bazoubandi, Z. Rostami, N.B.P. Soares, Water Soluble Polymer Flocculants: Synthesis, Characterization, and Performance Assessment, Macromol Mater Eng. 304 (2019) 1800526. https://doi.org/10.1002/MAME.201800526.

[8]   L. Besra, D.K. Sengupta, S.K. Roy, P. Ay, Flocculation and dewatering of kaolin suspensions in the presence of polyacrylamide and surfactants (0 2) 0 0 0 6 6-2, 2002. www.elsevier.com/locate/ijminpro.

[9]   O. Rivera, O. Pavez, J.L. Kao, A. Nazer, Metallurgical characterization of kaolin from Atacama, Chile, Revista Escola de Minas. 69 (2016) 473–478. https://doi.org/10.1590/0370-44672016690005.

[10]   X. Xu, N. Bizmark, K.S.S. Christie, S.S. Datta, Z.J. Ren, R.D. Priestley, Thermoresponsive Polymers for Water Treatment and Collection, Macromolecules. 55 (2022) 1894–1909. https://doi.org/10.1021/ACS.MACROMOL.1C01502/ASSET/IMAGES/MEDIUM/MA1C01502_0007.GIF.

[11]   Z. Ayar, M. Shafieian, N. Mahmoodi, O. Sabzevari, Z. Hassannejad, A rechargeable drug delivery system based on pNIPAM hydrogel for the local release of curcumin, J Appl Polym Sci. 138 (2021) 51167. https://doi.org/10.1002/APP.51167.

[12]   F. Doberenz, K. Zeng, C. Willems, K. Zhang, T. Groth, Thermoresponsive polymers and their biomedical application in tissue engineering-A review, J Mater Chem B. 8 (2020) 607–628. https://doi.org/10.1039/C9TB02052G.

[13]   A. Nakamura, K. Murakami, A. Nakamura, K. Murakami, The Aggregation of Bentonite Using Poly(N-isopropylacrylamide) as a Flocculant, Journal of Materials Science and Chemical Engineering. 6 (2018) 94–108. https://doi.org/10.4236/MSCE.2018.64011.

[14]   Q. Zhang, R. Hoogenboom, Polymers with upper critical solution temperature behavior in alcohol/water solvent mixtures, Prog Polym Sci. 48 (2015) 122–142. https://doi.org/10.1016/J.PROGPOLYMSCI.2015.02.003.

[15]   J. Lu, M. Xu, Y. Lei, L. Gong, C. Zhao, Aqueous Synthesis of Upper Critical Solution Temperature and Lower Critical Solution Temperature Copolymers through Combination of Hydrogen-Donors and Hydrogen-Acceptors, Macromol Rapid Commun. 42 (2021). https://doi.org/10.1002/MARC.202000661.

[16]   H.Y. Tian, J.J. Yan, D. Wang, C. Gu, Y.Z. You, X.S. Chen, Synthesis of thermo-responsive polymers with both tunable UCST and LCST, Macromol Rapid Commun. 32 (2011) 660–664. https://doi.org/10.1002/MARC.201000713.

[17]   J. Seuring, S. Agarwal, Polymers with Upper Critical Solution Temperature in Aqueous Solution, Macromol Rapid Commun. 33 (2012) 1898–1920. https://doi.org/10.1002/MARC.201200433.

[18]   H.G. Schild, Poly(N-isopropylacrylamide): experiment, theory and application, Prog Polym Sci. 17 (1992) 163–249. https://doi.org/10.1016/0079-6700(92)90023-R.

[19]   A. Choi, K.D. Seo, H. Yoon, S.J. Han, D.S. Kim, Bulk poly(N-isopropylacrylamide) (PNIPAAm) thermoresponsive cell culture platform: toward a new horizon in cell sheet engineering, Biomater Sci. 7 (2019) 2277–2287. https://doi.org/10.1039/C8BM01664J.

[20]   C.N. Cheaburu-Yilmaz, C.E. Lupuşoru, C. Vasile, New Alginate/PNIPAAm Matrices for Drug Delivery, Polymers 2019, Vol. 11, Page 366. 11 (2019) 366. https://doi.org/10.3390/POLYM11020366.

[21]   Y. Wei, Q. Zeng, Q. Hu, M. Wang, J. Tao, L. Wang, Self-cleaned electrochemical protein imprinting biosensor basing on a thermo-responsive memory hydrogel, Biosens Bioelectron. 99 (2018) 136–141. https://doi.org/10.1016/J.BIOS.2017.07.049.

[22]   M. Theses Dissertations, P.K. Nayak, Thermo-Responsive Poly(N-Isopropylacrylamide) and its Critical Solution Temperature Type Behavior in Presence of Hydrophilic Ionic Liquids, (2015). https://doi.org/10.7275/6401325.

[23]   J.R. Morones-Ramirez, Environmentally responsive polymeric "intelligent" materials: The ideal components of non-mechanical valves that control flow in microfluidic systems, Brazilian Journal of Chemical Engineering. 27 (2010) 1–14. https://doi.org/10.1590/S0104-66322010000100001.

[24]   H. Ren, X.P. Qiu, Y. Shi, P. Yang, F.M. Winnik, F.M. Winnik, The Two Phase Transitions of Hydrophobically End-Capped Poly(N-isopropylacrylamide)s in Water, Macromolecules. 53 (2020) 5105–5115. https://doi.org/10.1021/acs.macromol.0c00487.

[25]   C. Wu, X. Wang, Globule-to-Coil Transition of a Single Homopolymer Chain in Solution, (1998).

[26]   F. Doberenz, K. Zeng, C. Willems, K. Zhang, T. Groth, Thermoresponsive polymers and their biomedical application in tissue engineering-A review, J Mater Chem B. 8 (2020) 607–628. https://doi.org/10.1039/c9tb02052g.

[27]   P. Werner, M. Münzberg, R. Hass, O. Reich, Process analytical approaches for the coil-to-globule transition of poly(N-isopropylacrylamide) in a concentrated aqueous suspension, Anal Bioanal Chem. 409 (2017) 807–819. https://doi.org/10.1007/s00216-016-0050-7.

[28]   X. Gao, Y. Cao, X. Song, Z. Zhang, C. Xiao, C. He, X. Chen, pH- and thermo-responsive poly(N-isopropylacrylamide-co-acrylic acid derivative) copolymers and hydrogels with LCST dependent on pH and alkyl side groups, J Mater Chem B. 1 (2013) 5578–5587. https://doi.org/10.1039/C3TB20901F.

[29]   Effects of pH, salt, surfactant and composition on phase transition of poly(NIPAm/MAA) nanoparticles, (n.d.). https://onlinelibrary-wiley-com.login.ezproxy.library.ualberta.ca/doi/epdf/10.1002/%28SICI%291099-0518%2819990715%2937%3A14%3C2667%3A%3AAID-POLA42%3E3.0.CO%3B2-J (accessed September 20, 2022).

[30]   H. Cheng, L. Shen, C. Wu, LLS and FTIR Studies on the Hysteresis in Association and Dissociation of Poly(N-isopropylacrylamide) Chains in Water, Undefined. 39 (2006) 2325–2329. https://doi.org/10.1021/MA052561M.

[31]   B. Sun, Y. Lin, P. Wu, H.W. Siesler, A FTIR and 2D-IR Spectroscopic Study on the Microdynamics Phase Separation Mechanism of the Poly(N-isopropylacrylamide) Aqueous Solution, Undefined. 41 (2008) 1512–1520. https://doi.org/10.1021/MA702062H.

[32]   M.M. Coleman, D.J. Skrovanek, P.C. Painter, A Simple Method for Determining the Lower Critical Solution Temperature of Polymer Blends Using a Raman Spectrometer, Http://Dx.Doi.Org/10.1366/0003702844555647. 38 (2016) 448–450. https://doi.org/10.1366/0003702844555647.

[33]   F.M. Winnik, Fluorescence Studies of Aqueous Solutions of Poly(AT-isopropylacrylamide) below and above Their LCST, Macromolecules. 23 (1990) 233–242. https://doi.org/10.1021/MA00203A040/ASSET/MA00203A040.FP.PNG_V03.

[34]   E.C. Cho, J. Lee, K. Cho, Role of bound water and hydrophobic interaction in phase transition of poly(N-isopropylacrylamide) aqueous solution, Macromolecules. 36 (2003) 9929–9934. https://doi.org/10.1021/MA034851D.

[35]   K.C. Tam%, X.Y. Wu, R.H. Pelton, Viscometry-a useful tool for studying conformational changes of poly(N-isopropylacrylamide) in solutions, 1991.

[36]   N. Zhang, S. Zheng, Z. Pan, Z. Liu, Phase Transition Effects on Mechanical Properties of NIPA Hydrogel, Polymers 2018, Vol. 10, Page 358. 10 (2018) 358. https://doi.org/10.3390/POLYM10040358.

[37]   P. Voudouris, D. Florea, P. van der Schoot, H.M. Wyss, Micromechanics of temperature sensitive microgels: Dip in the Poisson ratio near the LCST, Soft Matter. 9 (2013) 7158–7166. https://doi.org/10.1039/c3sm50917f.

[38]   S. Minami, T. Watanabe, D. Suzuki, K. Urayama, Rheological properties of suspensions of thermo-responsive poly(N-isopropylacrylamide) microgels undergoing volume phase transition, Polymer Journal 2016 48:11. 48 (2016) 1079–1086. https://doi.org/10.1038/pj.2016.79.

[39]   H. Senff, W. Richtering, Influence of cross-link density on rheological properties of temperature-sensitive microgel suspensions, Colloid and Polymer Science 2000 278:9. 278 (2000) 830–840. https://doi.org/10.1007/S003960000329.

[40]   H. Senff, W. Richtering, H. Senff, W. Richtering, Temperature sensitive microgel suspensions: Colloidal phase behavior and rheology of soft spheres, JChPh. 111 (1999) 1705–1711. https://doi.org/10.1063/1.479430.

[41]   D.M. Öle Kiminta, P.F. Luckham, S. Lenon, The rheology of deformable and thermoresponsive microgel particles, Polymer (Guildf). 36 (1995) 4827–4831. https://doi.org/10.1016/0032-3861(95)99299-A.

[42]   A. Nakamura, K. Murakami, A. Nakamura, K. Murakami, The Aggregation of Bentonite Using Poly(N-isopropylacrylamide) as a Flocculant, Journal of Materials Science and Chemical Engineering. 6 (2018) 94–108. https://doi.org/10.4236/MSCE.2018.64011.

[43]   M. Alvarez, L.M. Lechuga, Microcantilever-based platforms as biosensing tools, Analyst. 135 (2010) 827–836. https://doi.org/10.1039/b908503n.

[44]   Q. Ren, Y.P. Zhao, Influence of surface stress on frequency of microcantilever-based biosensors, Microsystem Technologies. 10 (2004) 307–314. https://doi.org/10.1007/s00542-003-0329-4.

[45]   S. Vowell, Microfluidics: the effects of surface tension, 2009-03-19)[2010-09-21], Http://Www, Phys. …. (2009) 1–10. http://www.phys.washington.edu/users/sharpe/486/vowell_f.pdf.

[46]   N. Miriyala, Photothermal effects in micro/nano electromechanical systems, n.d.

[47]   J. Mouro, R. Pinto, P. Paoletti, B. Tiribilli, Microcantilever: Dynamical response for mass sensing and fluid characterization, Sensors (Switzerland). 21 (2021) 1–35. https://doi.org/10.3390/s21010115.

[48]   E.T. Arakawa, N. v Lavrik, S. Rajic, P.G. Datskos, Detection and differentiation of biological species using microcalorimetric spectroscopy., Ultramicroscopy. 97 (n.d.) 459–65. https://doi.org/10.1016/S0304-3991(03)00074-3.

[49]   K.M. Goeders, J.S. Colton, L.A. Bottomley, Microcantilevers: Sensing chemical interactions via mechanical motion, Chem Rev. 108 (2008) 522–542. https://doi.org/10.1021/cr0681041.

[50]   K.M. Goeders, J.S. Colton, L.A. Bottomley, Microcantilevers: Sensing chemical interactions via mechanical motion, Chem Rev. 108 (2008) 522–542. https://doi.org/10.1021/cr0681041.

[51]   A. Najafi Sohi, P.M. Nieva, Size-dependent effects of surface stress on resonance behavior of microcantilever-based sensors, Sens Actuators A Phys. 269 (2018) 505–514. https://doi.org/10.1016/j.sna.2017.12.001.

Chapter 7

Conclusions

7.1 Summary of completed work

This thesis was focused on the thermo-mechanical analysis of picograms of fluids using the dynamical mechanical response of the microfluidic cantilevers. We incorporated the interfacial effects of the fluids which appears as interfacial tension and thermal stress on the walls of the channel cantilever to understand about their effects on the frequency of the microfluidic cantilever. The major application of this project is to characterise rare fluids using microfluidic cantilever that requires only picograms of sample for physical, chemical, thermal and biological applications. The understanding of the influence of surface and interfacial effects of fluids on the dynamics of the microfluidic cantilever is crucial while analysing the notable macroscale observations. This would pave way to the in-depth analysis of interaction of physical, chemical and biological adsorbates inside the microfluidic cantilever for various sensing applications.

Three projects are covered in this thesis: effect of surface stress and interfacial effects on the resonance frequency of the microfluidic cantilever, measurement of thermal properties of liquids using photothermal modulation of microfluidic cantilever and thermo-mechanical analysis of PNIPAM and Kaolinite mixtures using microfluidic cantilever in dynamic mode. The first project explains the analytical model that can be used to incorporate the effects of surface stress and interfacial tension on the dynamics of the cantilever. The second project is the demonstration of the theory and the analytical model explained in the first chapter by analysing the thermal properties of liquids using a microfluidic cantilever irradiated by a laser. The last project is the application of the second project in which we investigated the mechanical property evolution of a thermos-sensitive polymer PNIPAA as a function of temperature and the flocculation of Kaolinite using the PNIPAM polymer inside the microfluidic cantilever. The mechanical property evaluation

of PNIPAM at LCST and the in-situ flocculation of Kaolinite were obtained by analysing the frequency shift of the cantilever.

The major findings of the first project may be summarized as follows.

1. The existing Euler Bernoulli beam equation used to calculate the frequency of microchannel cantilever doesn't incorporate the surface effects and interfacial effects of the liquid in the case of microfluidic cantilever filled with liquid. Hence there are discrepancies between the calculated values and experimental values.

2. When the cantilever has a curvature, the Young- Laplace equation can be incorporated to the Euler Bernoulli beam equation to consider the surface and interfacial effects of fluids on the resonance frequency of the cantilever. In this case, a transverse force, which has the surface stress and interfacial stress term, is acting along the axial direction of the cantilever which changes the frequency of the cantilever.

3. Alkanes were used to fill the microfluidic cantilever and the obtained resonance frequency from the experimental results were compared with the theoretical results obtained from the established Euler Bernoulli beam equation. A discrepancy of 5.53 % was found between the experimental values and the conventional model values.

4. The modified Euler Bernoulli beam equation incorporated with Young-Laplace equation considered the modified stiffness of the fluid-cantilever system, and the surface/interfacial effects of liquid and provided the theoretical results that matches the experimental values with an error of only 0.065%.

The major findings of the second project can be summarized as follows.

1. A microfluidic cantilever was used to measure the thermal properties of picograms of several liquids such as Ethanol, Methanol, Butanol and so on using the photothermal modulation by a laser.

2. The laser light locally heats the liquid along with the microfluidic cantilever and leads to a volumetric expansion of liquids inside the cantilever because of rise in temperature.

3. The thermal expansion of liquids inside the microfluidic cantilever creates a thermal stress on the walls of the cantilever. This appears as a surface stress and affects the resonance frequency of the system. There is a linear relation between the volumetric expansion coefficient of liquids and the shift in the resonance frequency of the cantilever.

4. The change in modulus, density and geometry were considered while calculating the frequency shift of the heated cantilever with liquids. It was found out that the thermal expansion of the liquids is the dominating factor in the shift in the frequency of the cantilever.

5. The modified Euler Bernoulli beam equation incorporated with Young- Laplace equation was used to calculate the modified frequency of the microfluidic cantilever with the thermal stress effects upon photothermal heating and the calculated values were validated with the experimental values.

The major findings of the third project can be summarized as follows.

1. The mechanical property change of the thermo-sensitive polymer PNIPAM was evaluated using the frequency shift of the microfluidic cantilever. PNIPAM polymer is hydrophilic and in single phase below LCST whereas it is hydrophobic, and phase separated above LCST. The phase change of PNIPAM at LCST is assisted with a change in confirmation of the polymer which results in the change of volume and stiffness of the polymer solution.

2. At LCST, the elastic modulus of the PNIPAM aqueous solution decreases and it reduces the stiffness of the cantilever which is reflected as a decrease in its frequency. Above LCST, when phase separation happens followed by agglomerate formation, the stiffness of the PNIPAM phase increases and it leads to the overall increase of the stiffness of the cantilever resulting in an increase in the frequency.

3. The in-situ flocculation of Kaolinite in the presence of PNIPAM at LCST inside the microfluidic cantilever leads to the sedimentation of Kaolinite and PNIPAM flocs on the walls of the cantilever. This increases the stiffness of the cantilever which in turn increases the stiffness of the cantilever.

7.2 Recommendation for future work

As a first step, the quantitative analysis of the mechanical property changes during the phase change of PNIPAM and in-situ flocculation of Kaolinite samples could be done for practical applications. The analytical model developed can be used to study the interfacial effects developed during phase transition of polymers and fluids. Furthermore, this can be used to study the chemical and biological interactions with specific adsorbates where the effects can be captured through the dynamics of the cantilever. The ability of suspended resonator system to analyze a pico-litre volume and its extraordinary sensitivity to study changes in density, viscosity and viscoelasticity in liquids, this technique has definitely huge potential studying biological systems where higher sensitivities are required and sample size is small.

Bibliography

Abraham, R., Khan, F., Bukhari, S. A., Liu, Q., Thundat, T., Chung, H. J., & Kim, C. il. (2020). Effect of surface and interfacial tension on the resonance frequency of microfluidic channel cantilever. *Sensors (Switzerland)*, *20*(22), 1–14.

Aguilar Sandoval, F., Geitner, M., Bertin, É., & Bellon, L. (2015). Resonance frequency shift of strongly heated micro-cantilevers. *Journal of Applied Physics*, *117*(23).

Alibert, J.J.; Seppecher, P.; Dell'Isola, F. Truss Modular Beams with Deformation Energy Depending on Higher Displacement Gradients. Math Mech Solids 2003, 8, 51–73.

Alodhayb, A., Khan, F., Etayash, H., & Thundat, T. (2020). Review—Nanomechanical Calorimetric Infrared Spectroscopy using Bi-Material Microfluidic Cantilevers. *Journal of The Electrochemical Society*, *167*(3), 037504.

Alvarez, M., & Lechuga, L. M. (2010). Microcantilever-based platforms as biosensing tools. *Analyst*, *135*(5), 827–836.

Ansari, M. Z., & Cho, C. (2009). Deflection, frequency, and stress characteristics of rectangular, triangular, and step profile microcantilevers for biosensors. *Sensors*, *9*(8), 6046–6057.

Arakawa, E. T., Lavrik, N. v, Rajic, S., & Datskos, P. G. (n.d.). Detection and differentiation of biological species using microcalorimetric spectroscopy. *Ultramicroscopy*, *97*(1–4), 459–465.

Aruna Mastani, D., & Anitha, D. (2014). *MEMS Microcantilevers Sensor Modes of Operation and Transduction Principles*.

Babaei Gavan, K., Westra, H. J. R., van der Drift, E. W. J. M., Venstra, W. J., & van der Zant, H. S. J. (2009). Size-dependent effective Young's modulus of silicon nitride cantilevers. *Applied Physics Letters*, *94*(23), 2007

Bahri, A., Martin, M., Gergely, C., Pugnière, M., Chevalier-Lucia, D., & Marchesseau, S. (2017). Atomic Force Microscopy Study of the Topography and Nanomechanics of Casein Micelles Captured by an Antibody. *Langmuir*, *33*(19), 4720–4728.

Barnes, J. R., Stephenson, R. J., Welland, M. E., Gerber, C., & Gimzewski, J. K. (1994). Photothermal spectroscopy with femtojoule sensitivity using a micromechanical device. *Nature*, *372*(6501), 79–81.

Beaulieu, L. Y., Godin, M., Laroche, O., Tabard-Cossa, V., & Grütter, P. (2007). A complete analysis of the laser beam deflection systems used in cantilever-based systems. *Ultramicroscopy*, *107*(4–5), 422–430.

Belmiloud, N., Lochon, F., Dufour, I., Guillot, P., Guirardel, M., Colin, A., & Nicu, L. (2006). Determination of fluid viscoelastic properties using resonant microcantilever. In *International Workshop on Nanomechanical Sensors*.

Besra, L., Sengupta, D. K., Roy, S. K., & Ay, P. (2002). Flocculation and dewatering of kaolin suspensions in the presence of polyacrylamide and surfactants (0 2) 0 0 0 6 6-2. In *Int. J. Miner. Process* (Vol. 66).

Beulah Sujan, K., & Shanmuganantham, T. (2018). Bio-MEMS cantilever sensor design and analysis for detecting multiple diseases. *IEEE International Conference on Circuits and Systems, ICCS 2017*, *2018-January*, 206–210.

Binnig, G., Quate, C. F., & Gerber, C. (1986). Atomic force microscope. *Physical Review Letters*, *56*(9), 930–933.

Binnig, G., Quate, C. F., & Gerber, C. (1986a). Atomic force microscope. *Physical Review Letters*, *56*(9), 930–933.

Bischofberger, I., & Trappe, V. (2015). New aspects in the phase behaviour of poly-N-isopropyl acrylamide: Systematic temperature dependent shrinking of PNiPAM assemblies well beyond the LCST. *Scientific Reports*, *5*.

Boisen, A., Thaysen, J., Jensenius, H., & Hansen, O. (2000). Environmental sensors based on micromachined cantilevers with integrated read-out. *Ultramicroscopy*, *82*(1–4), 11–16.

Burg, T. P., & Manalis, S. R. (2003). Suspended microchannel resonators for biomolecular detection. *Applied Physics Letters*, *83*(13), 2698.

Burg, Thomas P.; Godin, Michel.; Knudsen, Scott M.; Shen, Wenjiang.; Carlson, Greg.; Foster, John S.; Babcock, Ken.; Manalis, Scott R. Weighing of biomolecules, single cells and single nanoparticles in fluid. Nature 2007,446,1066-1069.

Butt, H.-J. A Sensitive Method to Measure Changes in the Surface Stress of Solids. Journal of Colloid and Interface Science 1996, 180, 251.

Castellini, P., Martarelli, M., & Tomasini, E. P. (2006). Laser Doppler Vibrometry: Development of advanced solutions answering to technology's needs. *Mechanical Systems and Signal Processing*, *20*(6), 1265–1285.

Chalaturnyk, R. J., Scott, J. D., & Özüm, B. (2007). MANAGEMENT OF OIL SANDS TAILINGS. *Http://Dx.Doi.Org/10.1081/LFT-120003695*, *20*(9–10), 1025–1046.

Chaudhary, M., & Gupta, A. (2009). Microcantilever-based sensors. *Defence Science Journal*, *59*(6), 634–641.

Cheaburu-Yilmaz, C. N., Lupuşoru, C. E., & Vasile, C. (2019). New Alginate/PNIPAAm Matrices for Drug Delivery. *Polymers 2019, Vol. 11, Page 366*, *11*(2), 366.

Cheaburu-Yilmaz, C. N., Lupuşoru, C. E., & Vasile, C. (2019). New Alginate/PNIPAAm Matrices for Drug Delivery. *Polymers 2019, Vol. 11, Page 366*, *11*(2), 366.

Chen, G. Y., Thundat, T., Wachter, E. A., & Warmack, R. J. (1995). Adsorption-induced surface stress and its effects on resonance frequency of microcantilevers. *Journal of Applied Physics*, *77*(8), 3618–3622.

Chen, G.Y.; Thundat, T.; Wachter, E.A.; Warmack. R.J. Adsorption-induced surface stress and its effects on resonance frequency of microcantilevers. Journal of Applied Physics 1995, 77, 3618.

Chen, T., Chiu, M. sen, & Weng, C. N. (2006). Derivation of the generalized Young-Laplace equation of curved interfaces in nanoscaled solids. *Journal of Applied Physics*, *100*(7).

Cheng, H., Shen, L., & Wu, C. (2006). LLS and FTIR Studies on the Hysteresis in Association and Dissociation of Poly(N-isopropylacrylamide) Chains in Water. *Undefined*, *39*(6), 2325–2329.

Cheri M. S.; Latifi H.; Sadeghi J.; Moghaddam M.S.; Shahraki H.; Hajghassem H. Real-time measurement of flow rate in microfluidic devices using a cantilever-based optofluidic sensor. Analyst 2014, 139, 431-438.

Cherian, S.; Thundat, T. Determination of adsorption-induced variation in the spring constant of a microcantilever. Applied Physics Letters 2002, 80, 2219.

Cho, E. C., Lee, J., & Cho, K. (2003). Role of bound water and hydrophobic interaction in phase transition of poly(N-isopropylacrylamide) aqueous solution. *Macromolecules*, *36*(26), 9929–9934.

Choi, A., Seo, K. D., Yoon, H., Han, S. J., & Kim, D. S. (2019). Bulk poly(N-isopropylacrylamide) (PNIPAAm) thermoresponsive cell culture platform: toward a new horizon in cell sheet engineering. *Biomaterials Science*, *7*(6), 2277–2287.

Choi, A., Seo, K. D., Yoon, H., Han, S. J., & Kim, D. S. (2019). Bulk poly(N-isopropylacrylamide) (PNIPAAm) thermoresponsive cell culture platform: toward a new horizon in cell sheet engineering. *Biomaterials Science*, *7*(6), 2277–2287.

Chu, W. H., Mehregany, M., & Mullen, R. L. (1993). Analysis of tip deflection and force of a bimetallic cantilever microactuator. *Journal of Micromechanics and Microengineering*, *3*(1), 4–7.

Coleman, M. M., Skrovanek, D. J., & Painter, P. C. (2016). A Simple Method for Determining the Lower Critical Solution Temperature of Polymer Blends Using a Raman Spectrometer, *38*(3), 448–450.

Cooper, A. (2005). Heat capacity effects in protein folding and ligand binding: A re-evaluation of the role of water in biomolecular thermodynamics. *Biophysical Chemistry*, *115*(2-3 SPEC. ISS.), 89–97.

Cossey, H. L., Batycky, A. E., Kaminsky, H., & Ulrich, A. C. (2021). Geochemical Stability of Oil Sands Tailings in Mine Closure Landforms. *Minerals 2021, Vol. 11, Page 830*, *11*(8), 830.

Dareing, D. W., & Thundat, T. (2005). Simulation of adsorption-induced stress of a microcantilever sensor. *Journal of Applied Physics*, *97*(4).

Datar, R.; Kim, S.; Jeon, S.; Hesketh, P.; Manalis, S.; Boisen, A.; Thundat, T. Cantilever Sensors: Nanomechanical Tools for Diagnostics. MRS Bulletin 2009, 34, 449.

dell'Isola, F.; Corte, A.D; Giorgio, I. Higher-gradient continua: The legacy of Piola, Mindlin, Sedov and Toupin and some future research perspectives. Math. Mech. Solids 2016, 22, 852–872.

dell'Isola, F.; Giorgio, I.; Pawlikowski, M.; N.L. Rizzi. Large deformations of planar extensible beams and pantographic lattices: heuristic homogenization, experimental and numerical examples of equilibrium. Proc R Soc A 2016, 472, 0790.

dell'Isola, F.; Seppecher, P.; Madeo, A. How contact interactions may depend on the shape of Cauchy cuts in Nth gradient continua: approach "à la D'Alembert". Z. Angew. Math. Phys 2012, 63, 1119–1141.

Digital, M., Digital Scholar, M., & Youn, S. (2017). *Quantitative Understanding of Nanoparticle Flocculation in Water Quantitative Understanding of Nanoparticle Flocculation in Water Treatment Treatment*.

Doberenz, F., Zeng, K., Willems, C., Zhang, K., & Groth, T. (2020). Thermoresponsive polymers and their biomedical application in tissue engineering-A review. *Journal of Materials Chemistry B*, *8*(4), 607–628.

Dorignac, J.; Kalinowski, A.; Erramilli, S.; Mohanty, P. Dynamical Response of Nanomechanical Oscillators in Immiscible Viscous Fluid for In Vitro Biomolecular Recognition. Physical Review Letters 2006, 96, 186105.

Effects of pH, salt, surfactant and composition on phase transition of poly(NIPAm/MAA) nanoparticles. (n.d.). Retrieved September 20, 2022, from https://onlinelibrary-wiley-com.login.ezproxy.library.ualberta.ca/doi/epdf/10.1002/%28SICI%291099-0518%2819990715%2937%3A14%3C2667%3A%3AAID-POLA42%3E3.0.CO%3B2-J

Ekinci, K. L., Yang, Y. T., & Roukes, M. L. (2004). Ultimate limits to inertial mass sensing based upon nanoelectromechanical systems. *Journal of Applied Physics*, *95*(5), 2682–2689.

Etayash, H., & Thundat, T. (2015). Microcantilever Chemical and Biological Sensors. *Encyclopedia of Nanotechnology*, 1–9.

Etayash, H.; Khan, M.F.; Kaur, K.; Thundat, T. Microfluidic cantilever detects bacteria and measures their susceptibility to antibiotics in small, confined volumes, Nature Communications 2016, 7, 1-9.

Faucher, M., Walter, B., Rollier, A. S., Seguini, K., Legrand, B., Couturier, G., Aimé, J. P., Bernard, C., Boisgard, R., & Buchaillot, L. (2007). Proposition of atomic force probes based on silicon ring-resonators. *TRANSDUCERS and EUROSENSORS '07 - 4th International Conference on Solid-State Sensors, Actuators and Microsystems*, 1529–1532.

French, P. J., Sarro, P. M., Mallée, R., Fakkeldij Elke, E. J. M., & Wolffenbuttel, R. F. (1997). Optimization of a low-stress silicon nitride process for surface-micromachining applications. *Sensors and Actuators A: Physical*, *58*(2), 149–157.

Gao, N., Zhao, D., Jia, R., & Liu, D. (2016). Microcantilever Actuation by Laser Induced Photoacoustic Waves. *Scientific Reports*, *6*.

Gao, X., Cao, Y., Song, X., Zhang, Z., Xiao, C., He, C., & Chen, X. (2013). pH- and thermo-responsive poly(N-isopropylacrylamide-co-acrylic acid derivative) copolymers and hydrogels with LCST dependent on pH and alkyl side groups. *Journal of Materials Chemistry B*, *1*(41), 5578–5587.

Gardeniers, J. G. E., Tilmans, H. A. C., & Visser, C. C. G. (1998). LPCVD silicon-rich silicon nitride films for applications in micromechanics, studied with statistical experimental design*. *Journal of Vacuum Science & Technology A: Vacuum, Surfaces, and Films*, *14*(5), 2879.

Gavoille, T., Pannacci, N., Bergeot, G., Marliere, C., & Marre, S. (2019). Microfluidic approaches for accessing thermophysical properties of fluid systems. In *Reaction Chemistry and Engineering* (Vol. 4, Issue 10, pp. 1721–1739). Royal Society of Chemistry.

Germain, P.; The Method of Virtual Power in Continuum Mechanics. Part 2: Microstructure. SIAM J Appl Math, 1973, 25, 556–575

Ghoraishi, M. S., Hawk, J. E., Phani, A., Khan, M. F., & Thundat, T. (2016). Clustering mechanism of ethanol- water mixtures investigated with photothermal microfluidic cantilever deflection spectroscopy. *Nature Publishing Group*, *December 2015*, 1–7.

Gimzewski, J.K.; Gerber, C.; Meyer, E.; Schlittler, R.R. Observation of a chemical reaction using a micromechanical sensor, Chemical Physics Letters 1994, 217, 589-594.

Godin, M., Tabard-Cossa, V., & Grutter, P. (2001). Quantitative surface stress measurements using a microcantilever. *American Institute of Physics*, *79*(4), 551–553.

Goeders, K.M.; Colton, J.S.; Bottomley, L.A. Microcantilevers: Sensing Chemical Interactions via Mechanical Motion. Chemical Reviews 2008, 108, 522-542.

Grigoryev, B.A.; Nemzer, B.V.; Kurumov, D.S. Surface tension of normal pentane, hexane, heptane, and octane, Int J Thermophys 1992,13,453-464.

Gurtin, M.E.; Markenscoff, X.; Thurston, R.N. Effect of surface stress on the natural frequency of thin crystals. Applied Physics Letters 1976, 29, 529.

Gurtin, M.E.; Murdoch, A.I. A continuum theory of elastic material surfaces, Arch. Rational Mech. Anal. 1975, 57,291–323.

Gurtin, M.E; Weissmuller, J.; Larche, F. A general theory of curved deformable interface in solids at equilibrium, Philos. Mag. A 1998, 78, 1093–1109.

Guruprasad, B., & Veena, M. G. (2022). Analysis of MEMS cantilever sensor for sensing volatile organic compounds. *Micro and Nano Engineering*, *16*, 100143.

Hajesfandiari, A.; Sukhotskiy, V.; Alodhayb, A.; Khan, F.; Thundat, T. Furlani, E.P. Microfluidic microcantilever as a sensitive platform to measure evaporation rate of picoliters of ethanol, Measurement 2020, in press.

Hansen, K. M., & Thundat, T. (2005). Microcantilever biosensors. *Methods*, *37*(1), 57–64.

He, J.; Lilley, C.M. Surface stress effect on bending resonance of nanowires with different boundary conditions. Applied Physics Letters 2008, 93, 263108.

Http://Orca.Phys.Uvic.ca/~tatum/Physopt/Physopt2.Pdf." n.d.

Https://Courses.Lumenlearning.Com/Physics/Chapter/13-2-Thermal-Expansion-of-Solids-and-Liquids/." n.d.

Https://Pressbooks.Bccampus.ca/Practicalphysicsphys1104/Chapter/13-2-Thermal-Expansion-of-Solids-and-Liquids/." n.d.

Https://Refractiveindex.Info/?Shelf=main&book=H2O&page=Hale." n.d.

Huang, G.Y.; Gao, W.; Yu, S.W.; Model for the adsorption-induced change in resonance frequency of a cantilever. Applied Physics Letters 2006, 89, 043506.

Hwang, K.S; Eom, K.; Lee, J.H.; Chun, D.W.; Cha, B.H.; Yoon, D.S.; Kim, T.S.; Park, J.H. Dominant surface stress driven by biomolecular interactions in the dynamical response of nanomechanical microcantilevers. Applied Physics Letters 2006, 89, 173905.

Inomata, N., Toda, M., Sato, M., Ishijima, A., & Ono, T. (2012). Pico calorimeter for detection of heat produced in an individual brown fat cell. *Applied Physics Letters*, *100*(15).

Javili, A.; dell'Isola, F.; Steinmann, P. Geometrically nonlinear higher-gradient elasticity with energetic boundaries. J. Mech.Phys. Solids 2013, 61, 2381–2401.

Jeuken, L. J. C. (2008). AFM Study on the Electric-Field Effects on Supported Bilayer Lipid Membranes. *Biophysical Journal*, *94*(12), 4711.

Jiang, K.; Khan, F.; Thomas, J.; Desai, P.R.; Phani, A.; Das, S.; Thundat, T. Thermomechanical responses of microfluidic cantilever capture DNA melting and properties of DNA premelting states using picoliters of DNA solution, Applied Physics Letters 2019, 114, 173703.

Khan, M. F., Miriyala, N., Lee, J., Hassanpourfard, M., Kumar, A., & Thundat, T. (2016). Heat capacity measurements of sub-nanoliter volumes of liquids using bimaterial microchannel cantilevers. *Applied Physics Letters*, *108*(21).

Khan, M. F., Schmid, S., Davis, Z. J., Dohn, S., & Boisen, A. (2011). Fabrication of resonant micro cantilevers with integrated transparent fluidic channel. *Microelectronic Engineering*, *88*(8), 2300–2303.

Khan, M. Faheem. (2012). *Microchannel resonators to characterize liquid samples : Ph. D. thesis*.

Khan, M.F.; Schmid, S.; Larsen, P.E.; Davis, Z.J.; Yan, W.; Stenby, E.H.; Boisen, A. Online measurement of mass density and viscosity of pL fluid samples with suspended microchannel resonator, Sensors and Actuators, B: Chemical 2013, 185, 456-461.

Kim, C.I. Strain-Gradient Elasticity Theory for the Mechanics of Fiber Composites Subjected to Finite Plane Deformations: Comprehensive Analysis. Multiscale Science and Engineering 2019, 1, 150-160

Kim, C.I. Superposed Incremental Deformations of an Elastic Solid Reinforced with Fibers Resistant to Extension and Flexure. Advances in Materials Science and Engineering 2018, 2018.

Kim, C.I; Islam, S. Mechanics of third-gradient continua reinforced with fibers resistant to flexure in finite plane elastostatics. Continuum Mechanics and Thermodynamics 2020, 32, 1-23

Kim, C.I; Zeidi. M. Gradient elasticity theory for fiber composites with fibers resistant to extension and flexure. International Journal of Engineering Science 2018, 131, 80-99.

Klaitabtim, D., & Tuantranont, A. (2005). Design consideration and finite element modeling of MEMS cantilever for nano-biosensor applications. *2005 5th IEEE Conference on Nanotechnology*, *1*, 311–314.

Kong, S.; Zhou, S.; Nie, Z.; Wang, K. The size-dependent natural frequency of Bernoulli–Euler micro-beams. International Journal of Engineering Science 2008, 46, 427-437.

Kurihara, K. (2012). Steady-State and Transient Performance Analysis of Permanent-Magnet Machines Using Time-Stepping Finite Element Technique. In *Finite Element Analysis - New Trends and Developments*. InTech.

Lachut, M.J.; Sader, J.E. Effect of Surface Stress on the Stiffness of Cantilever Plates. Physical Review Letters 2007, 99, 206102.

Lagowski, J.; Gatos, H.C.; Sproles, E.S. Surface stress and the normal mode of vibration of thin crystals: GaAs. Applied Physics Letters 1975, 26, 493.

Lai, J., Perazzo, T., Shi, Z., & Majumdar, A. (1997). Optimization and performance of high-resolution micro-optomechanical thermal sensors. *Sensors and Actuators, A: Physical*, *58*(2), 113–119.

Lavrik, N. v.; Sepaniak, M.J.; Datskos, P.G. Cantilever transducers as a platform for chemical and biological sensors. Review of Scientific Instruments 2004, 75, 2229.

Lee, I., & Lee, J. (2012). *Quality factor and vibration amplitude based viscosity measurements using suspended microchannel resonators*. 1–4.

Lee, I., Park, K., & Lee, J. (2013). Precision density and volume contraction measurements of ethanol-water binary mixtures using suspended microchannel resonators. *Sensors and Actuators, A: Physical*, *194*, 62–66.

Liu, C.; Rajapakse, N. Continuum Models Incorporating Surface Energy for Static and Dynamic Response of Nanoscale Beams. IEEE Transactions on Nanotechnology 2010, 9, 422 - 431.

Liu, J., Wang, X., & Zhang, W. (2018). Atomic Force Microscopy Imaging Study of Aligning DNA by Dumbbell-like Au-Fe 3 O 4 Magnetic Nanoparticles. *Langmuir*, *34*(49), 14875–14881.

Liu, Y., & Iqbal, S. M. (2009). Silicon-Based Novel Bio-Sensing Platforms at the Micro and Nano Scale. *ECS Transactions*, *16*(15), 25–45.

Longo, G., Alonso-Sarduy, L., Rio, L. M., Bizzini, A., Trampuz, A., Notz, J., Dietler, G., & Kasas, S. (2013). Rapid detection of bacterial resistance to antibiotics using AFM cantilevers as nanomechanical sensors. *Nature Nanotechnology*, *8*(7), 522–526.

Lu, J., Xu, M., Lei, Y., Gong, L., & Zhao, C. (2021). Aqueous Synthesis of Upper Critical Solution Temperature and Lower Critical Solution Temperature Copolymers through Combination of Hydrogen-Donors and Hydrogen-Acceptors. *Macromolecular Rapid Communications*, *42*(7).

Lu, P.; Lee, H.P.; Lu, C.; O'Shea, S.J. Surface stress effects on the resonance properties of cantilever sensors, Physical Review B 2005, 72, 085405.

Malvar, O.; Ruz, J. J.; Kosaka, P. M.; Domínguez, C. M.; Gil-Santos, E.; Calleja, M.; Tamayo, J. Mass and stiffness spectrometry of nanoparticles and whole intact bacteria by multimode nanomechanical resonators. Nat. Commun. 2016; 7: 13452.

Manzoor Bukhari, S.A.; Khan, M.F.; Goswami, A.; McGee, R.; Thundat, T. Thermomechanical analysis of picograms of polymers using a suspended microchannel cantilever. RSC Advances 2017, 7, 8415.

Marquez, S., Álvarez, M., Fariña Santana, D., Homs-Corbera, A., Domínguez, C., & Lechuga, L. M. (2017). Array of Microfluidic Beam Resonators for Density and Viscosity Analysis of Liquids. *Journal of Microelectromechanical Systems*, *26*(4), 749–757.

McFarland, A.W.; Poggi, M.A.; Doyle, M.J.; Bottomley, L.A.; Colton, J.S. Influence of surface stress on the resonance behavior of microcantilevers. Applied Physics Letters 2005, 87, 053505.

Minami, S., Watanabe, T., Suzuki, D., & Urayama, K. (2016). Rheological properties of suspensions of thermo-responsive poly(N-isopropylacrylamide) microgels undergoing volume phase transition. *Polymer Journal 2016 48:11*, *48*(11), 1079–1086.

Mindlin, R.D; Tiersten, H.F. Effects of couple-stresses in linear elasticity. Arch Ration Mech Anal 1962, 11, 415–448.

Mirasoli, M., Guardigli, M., Michelini, E., & Roda, A. (2014). Recent advancements in chemical luminescence-based lab-on-chip and microfluidic platforms for bioanalysis. *Journal of Pharmaceutical and Biomedical Analysis*, *87*, 36–52.

Miriyala, N. (n.d.). *Photothermal effects in micro/nano electromechanical systems*.

Morones-Ramirez, J. R. (2010). Environmentally responsive polymeric "intelligent" materials: The ideal components of non-mechanical valves that control flow in microfluidic systems. *Brazilian Journal of Chemical Engineering*, *27*(1), 1–14.

Mougin, Pascal.; Rasaolofosaon, Patrick.; Zinszer, Bernard. Petroacoustics of poorly consolidated reservoir rocks saturated with co2/methane/brine mixtures, SACS2 european research project 2002.

Mouro, J., Pinto, R., Paoletti, P., & Tiribilli, B. (2021). Microcantilever: Dynamical response for mass sensing and fluid characterization. In *Sensors (Switzerland)* (Vol. 21, Issue 1, pp. 1–35). MDPI AG.

Murthy, K. S. N., Prasad, G. R. K., Saikiran, N. L. N. V., & Manoj, T. V. S. (2016). Design and simulation of MEMS biosensor for the detection of tuberculosis. *Indian Journal of Science and Technology*, *9*(31).

Mutyala, M. S. K., Bandhanadham, D., Pan, L., Pendyala, V. R., & Ji, H. F. (2009). Mechanical and electronic approaches to improve the sensitivity of microcantilever sensors. *Acta Mechanica Sinica/Lixue Xuebao*, *25*(1), 1–12.

Najafi Sohi, A.; Nieva, P.M. Size-dependent effects of surface stress on resonance behavior of microcantilever-based sensor. Sensors and Actuators, A: Physical 2018, 269, 505.

Nakamura, A., Murakami, K., Nakamura, A., & Murakami, K. (2018b). The Aggregation of Bentonite Using Poly(N-isopropylacrylamide) as a Flocculant. *Journal of Materials Science and Chemical Engineering*, *6*(4), 94–108.

Narayanaswamy, A., & Gu, N. (2011). Heat transfer from freely suspended bimaterial microcantilevers. *Journal of Heat Transfer*, *133*(4).

Olcum, Selim.; Cermak, Nathan.; Wasserman, Steven C.; Christine, Kathleen S.; Atsumi, Hiroshi.; Payer, Kris R.; Shen, Wenjiang.; Lee, Jungchul.; Belcher, Angela M. .; Bhatia, Sangeeta N.; Manalis, Scott R. Weighing nanoparticles in solution at the attogram scale. Proceedings of the National Acacdemy of sciences 2014, 4, 1310-1315.

Öle Kiminta, D. M., Luckham, P. F., & Lenon, S. (1995). The rheology of deformable and thermoresponsive microgel particles. *Polymer*, *36*(25), 4827–4831.

optical and thermal imaging. (n.d.).

Park, S.J.; Seo, M.K. Solid-Liquid Interface in Interface Science and Technology 2011, 18, 147-252.

Patkar, R. S., Vinchurkar, M., Ashwin, M., Adami, A., Giacomozzi, F., Lorenzelli, L., Baghini, M. S., & Ramgopal Rao, V. (2020). Microcantilever Based Dual Mode Biosensor for Agricultural Applications. *IEEE Sensors Journal*, *20*(13), 6826–6832.

Payam, A. F., Trewby, W., & Voïtchovsky, K. (2017). Simultaneous viscosity and density measurement of small volumes of liquids using a vibrating microcantilever. *Analyst*, *142*(9), 1492–1498.

Prak ,Dianne J. Luning.; Cowart ,Jim S.; Trulove ,Paul C. Density, Viscosity, Speed of Sound, Bulk Modulus, and Surface Tension of Binary Mixtures of n-Heptane + 2,2,4-Trimethylpentane at (293.15 to 338.15) K and 0.1 MPa, J. Chem. Eng. Data 2014, 59, 11, 3842–3851

Prakash Gumfekar, S. (n.d.). *Multifunctional Water-Soluble Polymers for Dewatering of Oil Sands Tailings*.

Qiu, L., Zhu, N., Feng, Y., Michaelides, E. E., Żyła, G., Jing, D., Zhang, X., Norris, P. M., Markides, C. N., & Mahian, O. (2020). A review of recent advances in thermophysical properties at the nanoscale: From solid state to colloids. In *Physics Reports* (Vol. 843, pp. 1–81). Elsevier B.V.

R. B. Karabalin, L. G. Villanueva, M. H. Matheny, J. E. Sader, and M. L. Roukes. Stress-Induced Variations in the Stiffness of Micro- and Nanocantilever Beams. Phys. Rev. Lett. 108, 236101

Rahaeifard, M. (2016). Static behavior of bilayer microcantilevers under thermal actuation. *International Journal of Engineering Science*, *107*, 28–35.

Rahman, M., & Zhao, H. (2020). Temperature sensing performance and calibration of bi-material layer structure: role of material property variation. *Forces in Mechanics*, *1*, 100001.

Ramos, D., Mertens, J., Calleja, M., & Tamayo, J. (2007a). Study of the origin of bending induced by bimetallic effect on microcantilever. *Sensors*, *7*(9), 1757–1765. https://doi.org/10.3390/S7091757

Ren, H., Qiu, X. P., Shi, Y., Yang, P., Winnik, F. M., & Winnik, F. M. (2020). The Two Phase Transitions of Hydrophobically End-Capped Poly(N-isopropylacrylamide)s in Water. *Macromolecules*, *53*(13), 5105–5115.

Ren, Q.; Zhao, Y.; Influence of surface stress on frequency of microcantilever-based biosensors. Microsystem Technologies 2004, 10, 307-314.

Rivera, O., Pavez, O., Kao, J. L., & Nazer, A. (2016). Metallurgical characterization of kaolin from Atacama, Chile. *Revista Escola de Minas*, *69*(4), 473–478.

Ru, C. Q. (2016). A strain-consistent elastic plate model with surface elasticity. *Continuum Mechanics and Thermodynamics*, *28*(1–2), 263–273. https://doi.org/10.1007/s00161-015-0422-9

Ruz, J.J.; Pini, V.; Malvar, O.; Kosaka, P.M.; Calleja, M.; Tamayo, J. Effect of surface stress induced curvature on the eigenfrequencies of microcantilever plates. AIP Advances 2018, 8, 105213.

Sadat, S., Meyhofer, E., & Reddy, P. (2013). Resistance thermometry-based picowatt-resolution heat-flow calorimeter. *Applied Physics Letters*, *102*(16), 163110.

Sader, J.E. Surface stress induced deflections of cantilever plates with applications to the atomic force microscope: Rectangular plates. Journal of Applied Physics 2001, 89, 2911.

Schild, H. G. (1992). Poly(N-isopropylacrylamide): experiment, theory and application. *Progress in Polymer Science*, *17*(2), 163–249.

Senesac, L. R., Yi, D., Greve, A., Hales, J. H., Davis, Z. J., Nicholson, D. M., Boisen, A., & Thundat, T. (2009). Micro-differential thermal analysis detection of adsorbed explosive molecules using microfabricated bridges. *Review of Scientific Instruments*, *80*(3), 035102.

Senesac, L., & Thundat, T. (2007). Explosive Vapor Detection Using Microcantilever Sensors. *Counterterrorist Detection Techniques of Explosives*, 109–130.

Senff, H., & Richtering, W. (2000). Influence of cross-link density on rheological properties of temperature-sensitive microgel suspensions. *Colloid and Polymer Science 2000 278:9*, *278*(9), 830–840.

Senff, H., Richtering, W., Senff, H., & Richtering, W. (1999). Temperature sensitive microgel suspensions: Colloidal phase behavior and rheology of soft spheres. *JChPh*, *111*(4), 1705–1711.

Serrano, J. R., Phinney, L. M., & Rogers, J. W. (2009). Temperature amplification during laser heating of polycrystalline silicon microcantilevers due to temperature-dependent optical properties. *International Journal of Heat and Mass Transfer*, *52*(9–10), 2255–2264.

Seuring, J., & Agarwal, S. (2012). Polymers with Upper Critical Solution Temperature in Aqueous Solution. *Macromolecular Rapid Communications*, *33*(22), 1898–1920.

Seyed Bolouri, SE; Kim, C.I; Yang, S. Linear theory for the mechanics of third-gradient continua reinforced with fibers resistance to flexure. Mathematics and Mechanics of Solids 2019, 25, 937-960.

Sharma, P., Ganti, S., & Bhate, N. (2003). Effect of surfaces on the size-dependent elastic state of nano-inhomogeneities. *Applied Physics Letters*, *82*(4), 535–537.

Simmonds, M. J., Meiselman, H. J., & Baskurt, O. K. (2013). Blood rheology and aging. *Journal of Geriatric Cardiology : JGC*, *10*(3), 291–301.

Sohi, A.N.; Nieva, P.M. Frequency response of curved bilayer microcantilevers with applications to surface stress measurement. Journal of Applied Physics 2016, 119, 044503.

Sone, H., Fujinuma, Y., & Hosaka, S. (2004). Picogram mass sensor using resonance frequency shift of cantilever. *Japanese Journal of Applied Physics, Part 1: Regular Papers and Short Notes and Review Papers*, *43*(6 A), 3648–3651.

Spencer, A.J.M.; Soldatos, K.P. Finite deformations of fibre-reinforced elastic solids with fibre bending stiffness. Int J Nonlin Mech. 2007, 42, 355–368.

Spin Mill with Plasma FIB | NanoFAB." n.d. Accessed October 19, 2022.

Stachiv, I.; Fang, T.-H..; Chen, T.-H. Micro-/nanosized cantilever beams and mass sensors under applied axial tensile/compressive force vibrating in vacuum and viscous fluid. AIP Advances 2015,5, 117140

Stachiva, I. Impact of surface and residual stresses and electro-/magnetostatic axial loading on the suspended nanomechanical based mass sensors: A theoretical study, Journal of Applied Physics,2014, 115, 214310

Stachiv, I.; Gan, L.; Kuo, C.-Y.; Šittner P., Ševeček, O. Mass Spectrometry of Heavy Analytes and Large Biological Aggregates by Monitoring Changes in the Quality Factor of Nanomechanical Resonators in Air. A*CS Sens*. 2020, 5, 7, 2128–2135

Sun, B., Lin, Y., Wu, P., & Siesler, H. W. (2008). A FTIR and 2D-IR Spectroscopic Study on the Microdynamics Phase Separation Mechanism of the Poly(N-isopropylacrylamide) Aqueous Solution. *Undefined*, *41*(4), 1512–1520. https://doi.org/10.1021/MA702062H

Tam%, K. C., Wu, X. Y., & Pelton, R. H. (1991). *Viscometry-a useful tool for studying conformational changes of poly(N-isopropylacrylamide) in solutions*.

Tamayo, J.; Ramos, D.; Mertens, J.; Calleja, M. Effect of the adsorbate stiffness on the resonance response of microcantilever sensors. Applied Physics Letters 2006, 89, 224104.

Theses Dissertations, M., & Nayak, P. K. (2015). *Thermo-Responsive Poly(N-Isopropylacrylamide) and its Critical Solution Temperature Type Behavior in Presence of Hydrophilic Ionic Liquids*.

Thundat, T., & Senesac, L. (2007). Receptor-Free Detection of Chemicals and Biomolecules Using Nanomechanical Sensors. *Microscopy and Microanalysis*, *13*(S02), 696–697.

Thundat, T., Warmack, R. J., Chen, G. Y., & Allison, D. P. (1998a). Thermal and ambient-induced deflections of scanning force microscope cantilevers. *Applied Physics Letters*, *64*(21), 2894.

Thundat, T., Zheng, X.-Y., Chen, G. Y., & Warmack, R. J. (1993). Role of relative humidity in atomic force microscopy imaging. *Surface Science Letters*, *294*(1–2), L939–L943.

Tian, H. Y., Yan, J. J., Wang, D., Gu, C., You, Y. Z., & Chen, X. S. (2011). Synthesis of thermo-responsive polymers with both tunable UCST and LCST. *Macromolecular Rapid Communications*, *32*(8), 660–664.

Toda, M., Ono, T., Liu, F., & Voiculescu, I. (2010). Evaluation of bimaterial cantilever beam for heat sensing at atmospheric pressure. *Review of Scientific Instruments*, *81*(5).

Vajihinejad, V., & Soares, J. B. P. (2018). Monitoring polymer flocculation in oil sands tailings: A population balance model approach. *Chemical Engineering Journal*, *346*, 447–457.

Vajihinejad, V., Gumfekar, S. P., Bazoubandi, B., Najafabadi, Z. R., Soares, J. B. P., Vajihinejad, V., Gumfekar, S. P., Bazoubandi, B., Rostami, Z., & Soares, N. B. P. (2019). Water Soluble Polymer Flocculants: Synthesis, Characterization, and Performance Assessment. *Macromolecular Materials and Engineering*, *304*(2), 1800526.

van Duinen, D., Butt, H. J., & Berger, R. (2019). Two-Stage Collapse of PNIPAM Brushes: Viscoelastic Changes Revealed by an Interferometric Laser Technique. *Langmuir*.

Vančura, C., Dufour, I., Heinrich, S. M., Josse, F., & Hierlemann, A. (2007). Analysis of Resonating Microcantilevers Operating in a Viscous Analysis of Resonating Microcantilevers Operating in a Viscous Liquid Environment Liquid Environment Recommended Citation Recommended Citation Analysis of Resonating Microcantilevers Operating in A Viscous Liquid Environment. In *Sensors and Actuators A: Physical* (Vol. 141, Issue 1).

Vashist, S. K., & Holthofer, H. (2010). Microcantilevers for Sensing Applications. *Http://Dx.Doi.Org/10.1177/002029401004300305*, *43*(3), 84–88.

Vokoun, D., Samal, S., & Stachiv, I. (2022). Magnetic Force Microscopy in Physics and Biomedical Applications. In *Magnetochemistry* (Vol. 8, Issue 4). MDPI.

Voudouris, P., Florea, D., van der Schoot, P., & Wyss, H. M. (2013). Micromechanics of temperature sensitive microgels: Dip in the Poisson ratio near the LCST. *Soft Matter*, *9*(29), 7158–7166.

Vowell, S. (2009). Microfluidics: the effects of surface tension. *2009-03-19)[2010-09-21], Http://Www, Phys. ...*, 1–10.

Vyas, A., Staaf, H., Rusu, C., Ebefors, T., Liljeholm, J., Smith, A. D., Lundgren, P., & Enoksson, P. (2018). A Micromachined Coupled-Cantilever for Piezoelectric Energy Harvesters. *Micromachines*, *9*(5).

Wachter, E.A.; Thundat, T. Micromechanical sensors for chemical and physical measurements. Review of Scientific Instruments 1995, 66, 3662.

Wang, D.F.; Ono, T.; Esashi, M. Thermal treatments and gas adsorption influences on nano mechanics of ultra-thin silicon resonators for ultimate sensing. Nanotechnology 2004, 15, 1851.

Wang, G.F.; Feng, X.Q. Effects of surface elasticity and residual surface tension on the natural frequency of microbeams. Applied Physics Letters 2007, 90, 231904.

Wang, J., Huang, Z., Duan, H., Yu, S., Feng, X., Wang, G., Zhang, W., & Wang, T. (2011). Surface stress effect in mechanics of nanostructured materials. *Acta Mechanica Solida Sinica*, *24*(1), 52–82.

Wei, Y., Zeng, Q., Hu, Q., Wang, M., Tao, J., & Wang, L. (2018). Self-cleaned electrochemical protein imprinting biosensor basing on a thermo-responsive memory hydrogel. *Biosensors and Bioelectronics*, *99*, 136–141.

Werner, P., Münzberg, M., Hass, R., & Reich, O. (2017). Process analytical approaches for the coil-to-globule transition of poly(N-isopropylacrylamide) in a concentrated aqueous suspension. *Analytical and Bioanalytical Chemistry*, *409*(3), 807–819.

Wig, A., Arakawa, E. T., Passian, A., Ferrell, T. L., & Thundat, T. (2006). Photothermal spectroscopy of Bacillus anthracis and Bacillus cereus with microcantilevers. *Sensors and Actuators, B: Chemical*, *114*(1), 206–211.

Winnik, F. M. (1990). Fluorescence Studies of Aqueous Solutions of Poly(AT-isopropylacrylamide) below and above Their LCST. *Macromolecules*, *23*(1), 233–242.

Wu, C., & Wang, X. (1998). *Globule-to-Coil Transition of a Single Homopolymer Chain in Solution*.

Xu, X., Bizmark, N., Christie, K. S. S., Datta, S. S., Ren, Z. J., & Priestley, R. D. (2022). Thermoresponsive Polymers for Water Treatment and Collection. *Macromolecules*, *55*(6), 1894–1909.

Yang, J., & Paul, O. (2002). Fracture properties of LPCVD silicon nitride thin films from the load–deflection of long membranes. *Sensors and Actuators A: Physical*, *97–98*, 520–526.

Zapomel, J.; Stachiv, I.; Ferfecki, P. A novel method combining Monte Carlo–FEM simulations and experiments for simultaneous evaluation of the ultrathin film mass density and Young′s modulus. Mech Syst Signal Process 2016, 66-67, 223

Zeidi, M.; Kim, C.I. Finite plane deformations of elastic solids reinforced with fibers resistant to flexure: complete solution. Archive of Applied Mechanics 2018, 88, 819-835.

Zeidi, M.; Kim, C.I. Mechanics of an elastic solid reinforced with bidirectional fiber in finite plane elastostatics: complete analysis, Continuum Mechanics and Thermodynamics 2018, 30, 573-592.

Zeidi, M.; Kim, C.I. Mechanics of fiber composites with fibers resistant to extension and flexure. Mathematics and Mechanics of Solids 2017, 24, 3-17.

Zhang, D., Thundat, T., & Narain, R. (2017). Flocculation and dewatering of mature fine tailings using temperature-responsive cationic polymers. *Langmuir*, *33*(23), 5900–5909.

Zhang, J. Q., Yu, S. W., Feng, X. Q., & Wang, G. F. (2008). Theoretical analysis of adsorption-induced microcantilever bending. *Journal of Applied Physics*, *103*(9). https://doi.org/10.1063/1.2912727

Zhang, K., Zhu, Q., & Chen, Z. (2017). Effect of distributed mass on the node, frequency, and sensitivity of resonant-mode based cantilevers. *Sensors (Switzerland)*, *17*(7).

Zhang, N., Zheng, S., Pan, Z., & Liu, Z. (2018). Phase Transition Effects on Mechanical Properties of NIPA Hydrogel. *Polymers 2018, Vol. 10, Page 358*, *10*(4), 358. https://doi.org/10.3390/POLYM10040358

Zhang, Q., & Hoogenboom, R. (2015). Polymers with upper critical solution temperature behavior in alcohol/water solvent mixtures. *Progress in Polymer Science*, *48*, 122–142. https://doi.org/10.1016/J.PROGPOLYMSCI.2015.02.003

Zhang, Q., Ruan, W., Wang, H., Zhou, Y., Wang, Z., & Liu, L. (2010). A self-bended piezoresistive microcantilever flow sensor for low flow rate measurement. *Sensors and Actuators, A: Physical*, *158*(2), 273–279. https://doi.org/10.1016/j.sna.2010.02.002

Zhang, Y., Ren, Q., & Zhao, Y. P. (2004). Modelling analysis of surface stress on a rectangular cantilever beam. *Journal of Physics D: Applied Physics*, *37*(15), 2140–2145.

Zhang, Y., Zhuo, L. J. and H. S. Zhao. 2013. "Determining the Effects of Surface Elasticity and Surface Stress by Measuring the Shifts of Resonant Frequencies." *Proceedings of the Royal Society A: Mathematical, Physical and Engineering Sciences* 469 (2159). https://doi.org/10.1098/rspa.2013.0449.

Zhao, J.; Zhou, S.; Wang, B.; Wang, X. Nonlinear microbeam model based on strain gradient theory. Applied Mathematical Modelling 2012, 36,2674-2686.